In the Name of Allah, the Beneficent, the Merciful.

Modelling Nanostructures with Circularly Birefringent Materials

BY

ENTESAR ALI GANASH

A thesis submitted in partial fulfillment of
the requirement for the Philosophy Doctor's Degree
in Physics

Department of Physics and Astronomy
The University of Sheffield
Sheffield, United Kingdom

January 2014

To my lovely and amazing
mother and father

ABSTRACT

In this work, we have modelled multilayer magneto-photonic nanostructures in one dimension which display circular birefringence. Starting from Maxwell's equations, we have derived the 4×4 transfer matrix for these media. This is used to calculate optical and magneto-optical properties when the structure is deposited on an isotropic transparent substrate. For a transparent substrate it is important to include the effect of multiple incoherent back reflections in the substrate; therefore, the calculations were adapted to consider such reflections for both thick finite isotropic and circularly birefringent substrates. The results show the significant contribution of incoherent back reflections on the magneto-optical Kerr effects. We have reanalysed Sato's modulation method including incoherent back reflections in the substrate. We have derived exact and approximate Faraday rotation formulae for a circularly birefringent film on a circularly birefringent substrate; and a circularly birefringent cavity structure.

ACKNOWLEDGMENT

All praise is for ALLAH, Lord of the worlds, the Almighty, with whose gracious help it was possible to accomplish this task.

My sincere thanks and appreciation to all the people who had extended their valuable time, tireless efforts and their unswerving support that played a vital role in the fulfillment of my dream.

I would like to thank my supervisor Prof. David Whittaker for his valuable suggestions, guidance, assistance and patience during this work.

Thanks and gratitude is also given to Emeritus Prof. Gillian Gehring for her wonderful ideas and helpful suggestions. Thanks also go to Dr. Dominic Hosler and Dr. Marzook ALshammary for their helps and collaborating.

I am indebted to English Language Teaching Center (ELTC) for the Writing Advisory Service (WAS) especially Dr. James Foley for his advice and collaborating through thesis writing.

To King AbudlAziz University in KSA for a study scholarship and the University of Sheffield for giving me the chance to continue my higher education.

It is always pleasant to express my appreciation to those who gave me their life for building my life, to the warm embraces of love that knows no end, my parents for their prayers, overwhelming support, kindness and understanding, whom I considered an essential factor for the attainment of my goals.

Thanks a lot to my brothers and sisters who placed me in their hearts and prayers especially my dear sister Magdah who was beside me when I was in a serious condition. She made my life very smooth. No word can ever express my thanks to her. Special thanks also go to my younger brother Hassan for his helps.

Thanks also go to Dr. Reem Aboras for her continuous encouragement, support and prayers. Despite being far apart, she always stays close to me.

I also like to thank my friends either in KSA or here in the UK who were very helpful and supportive especially Dr. Nourah Alsenany, Dr. Hana Farhan, Mrs. Radia Alnahdi and Dr. Nada Alzarnogy; I wish you all long life, prosperity and happiness.

Thanks to everybody who has helped me by any way through this work.

LIST OF SYMBOLS

h	Thickness
n	Refractive index
$\tilde{n}$	Complex refractive index
κ	Extinction coefficient
α	Absorption coefficient
λ	Wavelength
c	Vacuum speed of light
ω	Frequency
q	Wave vector
$\boldsymbol{r}$	Position vector
$\varepsilon_0,\ \mu_0$	Vacuum permittivity and permeability
$\varepsilon(\mathbf{r}), \mu(\boldsymbol{r})$	Relative permittivity and magnetic permeability
ε, μ	Dielectric constant and magnetic permeability
$\underline{\underline{\varepsilon}}$	Dielectric matrix
B	Magnetic induction field
D	Electric displacement
E	Electric field
H	Magnetic field
J	Current density
ρ	Free charge density
E^0	Amplitude of the electric field
B^0	Amplitude of the magnetic field
χ	Ellipticity
ψ	Rotation
$\Delta\theta$	Change in the phase
S_0, S_1, S_2, S_3	Stokes' parameters
I_x, I_y	Intensity of linear polarised state(horizontal, *x*, and vertical, *y*,)
I_a, I_b	Intensity of linear diagonal polarised state (at $+45^o$, *a*, and at -45^o, *b*,)
I_+, I_-	Intensity of circularly polarised state (+, and, -,)
DP	Polarised degree
$q^{\pm}$	Two circularly wave vectors
$E_{x,y}^{0\pm}$	Circularly eigenvector components
$\boldsymbol{\sigma}^+,\ \boldsymbol{\sigma}^-$	Left and right circularly polarised lights
$R_{++},\ R_{--}$	Refractivity for left and right circularly polarised light
$r_{++}, r_{+-}, r_{-+}, r_{--}$	Circular reflection coefficients

$r_{xx}, r_{xy}, r_{yx}, r_{yy}$	Linear reflection coefficients
$\tilde{r}_{xx}, \tilde{r}_{xy}, \tilde{r}_{yx}, \tilde{r}_{yy}$	Linear reflection coefficients for the reverse direction
$r_{xx}^b, r_{xy}^b, t_{yx}^b, r_{yy}^b$	Linear reflection coefficients of the back of the substrate
$R_f,\ T_f$	Reflectivity and transmission of a structure
$\tilde{R}_f, \tilde{T}_f$	Reflectivity and transmission for the reverse direction.
R_b, T_b	Reflectivity and transmission of the back of the substrate
$\delta^{\pm}$	Two phase differences
2Δ	Small difference between two circular refractive indices
$\delta(t)$	Periodically changing retardation
δ_0	Retardation amplitude
Ω	Modulation frequency
$J_n(\delta_0)$	Bessel functions of integral order
$\underline{t},\ \underline{r}$	Amplitude coefficient matrices of transmission and reflection of the front of a structure
$\underline{\tilde{t}}, \underline{\tilde{r}}$	Coefficient matrices of transmission and reflection for the opposite direction
$\underline{t_b}, \underline{r_b}$	Coefficient matrices of transmission and reflection of the back substrate
$\underline{\varphi},\ \underline{\tilde{\varphi}}$	Rotation matrices in substrate for forward and reverse directions
φ	Rotation angle for substrate
FC	Finesse coefficient
$\mathcal{F}$	Finesse
Q	Resolving power or the quality factor of resonator
FSR	Free spectral range
$\mathbb{N}$	Number of bilayers

CONTENTS

ABSTRACT i
ACKNOWLEDGMENT ii
LIST OF SYMBOLS iii
CONTENTS v
LIST OF FIGURES viii

CHAPTER 1
INTRODUCTION 1
1.1 Background 1
1.2 Aims of Work 4
1.3 Plan of Research 5

CHAPTER 2
OVERVIEW OF PHOTONIC STRUCTURES 7
2.1 Maxwell's Equations 7
2.2 Photonic Band Gaps 9
2.3. Light Localisation 10
2.4 Applications of Photonic Crystals 11
2.5 Photonic Structures in Nature 16
2.6 Computational Techniques 17
2.6.1 Finite Difference Time Domain 17
2.6.2 Plane Wave Expansion 18
2.6.3 Multiple-Scattering Theory 18
2.6.4 Transfer Matrix 19

CHAPTER 3
MAGNETIC AND OPTICAL PROPERTIES 20
3.1 Light Polarisation 20
3.2 Birefringent Materials 21

3.3 Magneto-Optic Effects 23
3.4 Stokes' Parameters and Poincaré sphere 27

CHAPTER 4

TRANSFER MATRIX DERIVATION AND OPTICAL PROPERTY CALCULATIONS 30
4.1 Introduction 30
4.2 Non-Birefringent Materials at a Finite Angle 31
4.2.1 Theory and Calculations 31
4.2.2 Results and Discussion 38
4.3 Birefringent Materials at a Normal Incidence 43
4.3.1 Theory and Calculations 43
4.3.2 Results and Discussion 49
4.4 Conclusions 57

CHAPTER 5

EFFECT OF INCOHERENT BACK SUBSTRATE REFLECTIONS 58
5.1 Introduction 58
5.2 Theory and calculations 59
5.3 Results and Discussion 69
5.4 Conclusions 83

CHAPTER 6

MODULATION METHOD 84
6.1 Introduction 84
6.2 Theory and calculations 88
6.3 Numerical Calculations 92
6.4 Conclusions 96

CHAPTER 7

THEORETICAL ANALYSIS OF STRUCTURES ON A CIRCULARLY BIREFRINGENT SUBSTRATE 97

7.1 Theory and calculations 97

7.1.1 Required calculations for the rotation going through the circularly birefringent substrate 101

7.1.2 Required calculations for the forward propagation direction 103

7.1.3 Required calculations for the reverse propagation direction 104

7.1.4 Required calculations at circularly birefringent substrate-air interface 106

7.2 Results and Discussion 107

7.3 Faraday rotation theory of simple film with air on both sides 109

7.3.1 Exact formula of Faraday rotation 111

7.3.2 Approximate formula of Faraday 112

7.4 Results and Discussion 115

7.5 Faraday rotation theory of a simple film on a circularly birefringent substrate. 118

7.5.1 Exact formula of Faraday rotation 118

7.5.2 Approximate formula of Faraday rotation 120

7.6 Results and Discussion 123

7.7 Faraday rotation theory of a circularly birefringent cavity 125

7.7.1 Exact formula of Faraday rotation 126

7.7.2 Approximate formula of Faraday rotation 127

7.8 Results and Discussion 130

7.9 Conclusions 131

CHAPTER 8

CONCLUSIONS 133

8.1 Summary 133

8.1 Outlook to the Future 135

APPENDIX A 137

REFRENCES 138

LIST OF FIGURES

Figure 1.1: Schematic diagrams of one-, two-, and three-dimensional photonic crystals, taken from http://ab-initio.mit.edu/photons/index.html accessed on 11/1/2013, with permission from Prof. John D. Joannopoulos. 1
Figure 2.1: The wavelength in one-dimensional band gap (Yablonovitch, 2001), with permission from Andy Christie, Slims film, and courtesy for reuse from Karin Tucker. 9
Figure 2.2: The electric field distribution in a waveguide splitter (Fan *et al.*, 2001),with permission from Susannah Lehman, Authorized agent, the optical society. 14
Figure 3.1: A graphical illustration of the process of magneto-optical effects, where ψ is the rotation angle and χ is the ellipticity angle. Adapted from Mansuripur (2009). 24
Figure 3.2: Schematic diagrams of different magneto-optical Kerr effects. I and R are the incident and reflected waves, respectively. **H** is the magnetic field. Adapted from Reim and Schoenes (1990) 25
Figure 3.3: Schematic diagram of the Poincaré sphere and Stokes' parameters. Adapted from Born and Wolf (1999). 29
Figure 4.1: Schematic diagram of a quarter-wave stack model. n_s is the substrate refractive index, n_0 is the air refractive index. n_1, n_2, h_1 and h_2 are the refractive indices and thicknesses for each couple of layers, periodically. I, R and T are the incident, reflected and transmitted waves, respectively. θ is the incident angle. 32
Figure 4.2: Reflectivity spectra of Bragg mirror composed of 6 layers, for both types of polarisation at normal incidence. 38
Figure 4.3: Reflectivity spectra for both types of polarisation at finite angles, (a) $20°$ and (b) $30°$. 40
Figure 4.4: Reflectivity spectra at normal incidence for various numbers of layers (*N*). 41
Figure 4.5: Reflectivity spectra at normal incidence without and with absorption for (a) 6-layers (b)18-layers, (the extinction coefficients for Bragg stack were taken from Kato *et al.* (2003) as $\kappa_{SiO_2} \cong 0.0$, and $\kappa_{Ta_2O_5} = 7.47 \times 10^{-3}$ at $\approx 1.722\ eV$). 42
Figure 4.6: Reflectivity spectra at normal incidence for both right, R_{--}, and left, R_{++}, circularly polarised lights. The difference between them is shown by the green curve. 51
Figure 4.7: Reflectivity spectrum for linearly polarised light, R_{xy} at normal incidence. 52
Figure 4.8: Kerr and Faraday ellipticity spectra for a simple $Bi{:}YIG$ film. 53
Figure 4.9: Kerr and Faraday rotation spectra for a simple $Bi{:}YIG$ film. 53

Figure 4.10: Reflectivity spectrum of linearly polarised light, R_{xx} for $(Ta_2O_5/SiO_2)^6$ / $Bi{:}YIG/(SiO_2/Ta_2O_5)^6$ 54
Figure 4.11: Kerr ellipticity for $(Ta_2O_5/SiO_2)^6$ $/Bi{:}YIG/(SiO_2/Ta_2O_5)^6$ 55
Figure 4.12: Kerr rotation for $(Ta_2O_5/SiO_2)^6$ $/Bi{:}YIG/(SiO_2/Ta_2O_5)^6$ 55
Figure 4.13: Simulated spectra of reflectivity, transmittance and Faraday rotation for $(SiO_2/TiO_2)^6$ $/Co_6Ag_{94}/SiO_2$. The right figures (a) and (b) are reprinted with permission from [*Journal of Applied Physics* **107**, 093101. 'Enhancement of Faraday rotation effect in heterostructures with magneto-optical metals' Dong, L., Jiang, H., Chen, H., and Shi, Y.]. Copyright [2010], AIP Publishing LLC. http://dx.doi.org/10.1063/1.3406152 (courtesy of Dong, L). 56
Figure 5.1: Simulated reflectivity spectra result from coherent and incoherent treatments for $(SiO_2/TiO_2)^2$. For clarity, the insert displays a small energy range. 60
Figure 5.2: Illustrating the parameters used in equations 5.1 and 5.2. n_0 is the air refractive index, n_s is the substrate refractive index and h_s is the substrate thickness. Adapted from Whittaker and Gehring (2010). 62
Figure 5.3: Illustrating the three possible types of reflections. 65
Figure 5.4: Schematic diagram of multiple incoherent reflection and transmission amplitudes in a thick substrate. For clarity, the rays are drawn at small angles. 66
Figure 5.5: Comparison (a) reflectivity and (b) transmission spectra with and without incoherent reflections for the simple film, $Bi{:}YIG$. 71
Figure 5.6: (a) Comparison with and without incoherent back reflections in Kerr ellipticity spectra for $Bi{:}YIG$ film and (b) the green spectrum is plotted in the magnified scale. 73
Figure 5.7: Comparison with and without incoherent back reflections in Faraday ellipticity spectra for $Bi{:}YIG$ film. 74
Figure 5.8: Comparison with and without incoherent back reflections in Kerr rotation spectra for $Bi{:}YIG$ film. 75
Figure 5.9: Comparison with and without incoherent back reflections in Faraday rotation spectra for $Bi{:}YIG$ film. 75
Figure 5.10: The degree of depolarisation for $Bi{:}YIG$ film with incoherent back reflections situation with air and silver after the substrate. 76
Figure 5.11: Kerr effects for $Bi{:}YIG$ film with incoherent back reflections when thickness is equal to 10 $(\lambda/2\sqrt{\varepsilon_{xx}})$, where $\lambda = 720\ nm$. 77
Figure 5.12: Kerr (a) ellipticity and (b) rotation spectra with and without incoherent back reflections for $(Ta_2O_5/SiO_2)^6$ $/Bi{:}YIG/(SiO_2/Ta_2O_5)^6$, using $\varepsilon_{xy} = -0.00369$. 78
Figure 5.13: Kerr (a) ellipticity and (b) rotation spectra with and without incoherent back reflections for $(SiO_2/TiO_2)^6$ $/Co_6Ag_{94}/SiO_2$, using $\varepsilon_{xy} = -1.2$, which gives much larger magneto-optical effects. 80

Figure 5.14: Visualisation of the path of rotation on the Poincaré sphere. The red points are the positions of wavelength where the jump occurs between 625.7 *nm* and 625.8 *nm*. 81
Figure 5.15: the relation between Stokes' parameters S_1 and S_2. The green dotted line refers arbitrarily to zero longitude. The red squares are the positions of wavelength where the jump occurs between 625.7 *nm* and 625.8 *nm*. 81
Figure 5.16: The modified Kerr rotation spectrum without incoherent back reflections for $(SiO_2/TiO_2)^6\ /Co_6Ag_{94}/SiO_2,$ using $\varepsilon_{xy} = -1.2$ 82
Figure 6.1: Schematic diagram of fundamental components in the measuring method. Adapted from Sato (1981). 88
Figure 6.2: The unmodulated spectra both with and without incoherent back reflections using equation 6.23. The curves are identical to those obtained from Sato's method, equation 6.9 when $\Delta\theta$ is much smaller than one, in both cases. 93
Figure 6.3: (a) Kerr ellipticity and (b) Kerr rotation spectra for $Bi{:}YIG$ film both with and without incoherent back reflections using equations 6.19- 6.21. The curves are identical to those obtained from Sato's method, *i.e.*, $\frac{1}{4}\times$ (equation 6.12) and equation 6.13, respectively in both cases. 95
Figure 7.1: Schematic diagram of multiple incoherent reflections and transmission amplitudes in a thick circularly birefringent substrate. For clarity, the rays are drawn at small angles to the normal. 98
Figure 7.2: Numerical Faraday rotation spectra for the whole structure, $EuFeO_3/Bi{:}YIG$; for a thick substrate, $Bi{:}YIG$; for differences between the spectra of the whole structure and substrate alone and finally for the single pass in a thin film, $EuFeO_3$. 109
Figure 7.3: Schematic diagram of multiple passes in a simple film with air on both sides. For symbols see the text. For clarity, the rays are drawn at small angles to the normal. Adapted from Pedrotti and Pedrotti (1993). 110
Figure7.4: The exact, approximate analytical Faraday rotation results and the numerical result, for a thin film, $EuFeO_3$with air on both sides and has the multiple passes, are shown by the black curve. The single pass of light in the film is shown by the pink curve. The red point indicates Faraday rotation on resonance. 117
Figure7.5: Faraday rotations against the ε_{xy} values for a thin film, $EuFeO_3$ with air on both sides at $\lambda = 600\ nm$..... 117
Figure7.6: Schematic diagram of multiple passes inside a simple circularly birefringent film deposited on a circularly birefringent substrate. For symbols see the text. For clarity, the rays are drawn at small angles to the normal. 119
Figure7.7: The exact, approximate analytical Faraday rotation results and the numerical result, for a thin film, $EuFeO_3$ on a circularly birefringent substrate and has the multiple passes, are shown by the black curve. The difference between the spectra of the whole structure and substrate alone is shown by the green curve. 124

Figure7.8: Schematic diagram of a circularly birefringent cavity structure on a transparent isotropic substrate. Here, h is the cavity thickness. 125
Figure7.9: Numerical spectrum and analytical Faraday rotation spectra for a cavity structure $(Ta_2O_5/SiO_2)^6\ /Bi{:}YIG/(SiO_2/Ta_2O_5)^6$ are shown by the same black curve. The red point indicates Faraday rotation on resonance. 131

CHAPTER 1

INTRODUCTION

1.1 Background

In 1987, both Yablonovitch and John introduced the concept of photonic crystal, Yablonovitch (1987) was studying forbidden spontaneous emissions in three-dimensional periodic media, and in the same year John (1987) was investigating photon localisation in disordered microstructures.

A photonic crystal is a material patterned with a periodic variation of refractive index or dielectric constant, which can produce photonic band gaps (PBG's): ranges of frequencies in which photons can not propagate in the crystal (Joannopoulos *et al.*, 1997). This band gap plays a significant role in the study of photonic structures. These structures can be classified into one-, two-, and three-dimensional photonic crystals, see figure 1.1.

Figure 1.1: Schematic diagrams of one-, two-, and three-dimensional photonic crystals, taken from http://ab-initio.mit.edu/photons/index.html accessed on 11/1/2013, with permission from Prof. John D. Joannopoulos.

The multilayer film is the simplest photonic crystal. It is composed of periodic layers which have varied refractive indices or dielectric constants in one-dimension. A simple example is the quarter-wave stack, where each individual layer has a thickness equal to a quarter-wavelength, which means the thickness, *h*, is given by

$$h = \frac{\lambda}{4n}, \tag{1.1}$$

where λ is the vacuum wavelength and *n* is the refractive index. The waves from each layer boundary reflect in phase at the mid gap frequency, therefore, the band gap of the quarter-wave stack is maximised (Joannopoulos *et al.*, 2008).

We do not get 'direct' magneto-optical effects because the relative magnetic permeability $\mu(\boldsymbol{r}) \cong 1$ at optical frequencies, but in some materials the dielectric constant, ε, is affected by a magnetic field, which leads to magneto-optical effects. If the materials are used inside the photonic crystal, a magneto-photonic crystal results. This produces unique features in the optical and magneto-optical effects (Inoue *et al.*, 2006). These features (high value of the transmission and Faraday rotation) are a consequence of multiple reflections in the magnetic layer (Kato *et al.*, 2003). The large enhancement of magneto-optical properties can be understood in circularly birefringent terms as being due to slight differences in the behaviour of right and left circularly polarised light (Inoue *et al.*, 2006).

The study of magneto-optical effects helps in understanding the electronic structures of atomic and molecular systems (Pershan, 1967). Previous studies have suggested the magneto-optical Kerr effect in the ultra-violet region may be useful in high density magneto-optical data-storage (VanDrent and Suzuki, 1997; Wang *et al.*, 1999). A high Faraday rotation is helpful in magneto-optical imaging and in integrated

optics as an optical isolator (Kahl and Grishin, 2004). Magneto-photonic structures have applications for control of optical devices using a magnetic field. The motivation to apply these structures in photonic crystals arises from the ability to control the optical properties of the photonic crystal by reorienting the magnetisation. In addition, there is the ability to enhance the magneto-optical effect due to light confinement (Lourtioz *et al.*, 2008).

The rotation polarisation state of the light is known as optical activity. It requires a breaking of inversion symmetry, as, for example in chiral molecules. This effect has importance in different fields such as molecular biology and analytical chemistry. Moreover, it is considered a possible signature for life in space (Plum *et al.*, 2009). The idea of chirality has stimulated research in developing microwave and optical artificial chiral meta-materials, since they have been identified as negative refraction resources (Plum *et al.*, 2009).

The study of magneto-optical activity involves two problems: relating the measured quantities such as rotation and ellipticity to the dielectric or conductivity tensor; and then explaining these functions in terms of the characteristics of the band structure or estimating them from relativistic and spin-polarised band structure computations (Reim and Schoenes, 1990). The present thesis is concerned with the first step.

In the photonic field, computational methods have been used in a set of problems such as photonic band analysis and calculation of reflection, transmission or emission spectra. These methods include finite difference time domain (FDTD), plane wave expansion, multiple scattering theory and transfer matrix.

There are many different experimental methods to measure magneto-optical properties, including the polarisation modulation method using a Faraday cell and the superior spinning analyser approach. In addition, several experiments have used piezo-bifringent modulators for measuring magneto-optical parameters, Kerr rotation and reflectance magneto-circular dichroism (RMCD), which is related to Kerr ellipticity (Sato, 1981). This will be explained in detail in Chapter 6.

In this work, we give attention to theoretical modelling of photonic structures which have magneto-optical properties. The work is useful in analysing real experimental magneto-optic data, as well as in designing novel structures that utilise sensitivities of the optical properties of photonic crystal to tiny differences in the refractive index.

1.2 Aims of Work

The aim of this work is to derive a 4×4 Transfer matrix treatment for circularly birefringent nanostructures with light at normal incidence. A FORTRAN programme is used to evaluate the matrix and calculate optical and magneto-optical spectra. This model is first used for structures on an infinite substrate that is ignoring any reflection from the back of the substrate. Then, it is modified to address the issues arising from the contribution of multiple incoherent back reflections in finite transparent substrates, which may be isotropic materials or themselves circularly birefringent. The reflections may be incoherent for several reasons, including finite angular resolutions or a slight wedge in the substrate. We also re-analyse Sato's modulation method including incoherent reflections. In addition, we derive approximate analytical expressions for the

Faraday rotation of a circularly birefringent film and cavity structure. The Faraday rotation formula is used to drive an expression for the effective number of light passes.

1.3 Plan of Research

The rest of this thesis will be divided into seven chapters. Each one will investigate a special topic.

In Chapter 2, the main ideas about photonic structures which will be used in our simulation program will be outlined. These topics include Maxwell's equations, photonic band gaps, the localisation of light and computational techniques such as the transfer matrix.

Chapter 3 will be devoted to concepts in optics and magneto-optics. These concern the polarisation of light, birefringent properties, Stokes' parameters and the Poincaré sphere. In addition, a description of the magneto-optical effects, Kerr and Faraday ellipticity and rotation, will be presented.

We shall use computer codes, which are written using the FORTRAN language, to calculate reflectivity and magneto-optic spectra. For this purpose Chapter 4 will focus on the derivation of the transfer matrix method for circularly birefringent structures, which is used in our codes.

We have already mentioned the effect of using a finite transparent substrate instead of an infinite one on the optical and magneto-optical spectra. This is an important issue which will be discussed extensively in Chapter 5. The incoherent back reflections within the substrate will be taken into account.

Sato's modulation method is universally applied experimentally to obtain continuous magneto-optical spectra. In Chapter 6, we will re-analyse the modulated method and simulate magneto-optical spectra for circularly birefringent medium with treatments both of coherent and incoherent back reflections.

In Chapter 7 we will investigate the problem of a circularly birefringent film on a substrate which is itself circularly birefringent. We will discuss the question of how the film properties can be deduced by comparing the results for the whole structures with those for a bare substrate. In addition, exact and approximate analytical formulae of Faraday rotation will be found for the following cases: where a single circularly birefringent film has air on both sides; when it is deposited on circularly birefringent substrate; and for a cavity structure which has Bragg mirrors on both sides of cavity layer with a circularly birefringent medium.

The last chapter will be devoted to the conclusions and outlook to the future of this research.

CHAPTER 2

OVERVIEW OF PHOTONIC STRUCTURES

In this chapter, some topics in photonic structures will be investigated briefly. These topics include Maxwell's equations, photonic band gaps, the localisation of light, applications of photonic crystals and some examples of photonic structures in nature. In addition, various computational techniques will be discussed.

2.1 Maxwell's Equations

The propagation of electromagnetic waves within a photonic structure obeys Maxwell's equations:

$$\begin{aligned} \nabla . \mathbf{B} &= 0, \\ \nabla \times \mathbf{E} + \frac{\partial \mathbf{B}}{\partial \mathrm{t}} &= 0, \\ \nabla . \mathbf{D} &= \rho, \\ \nabla \times \mathbf{H} - \frac{\partial \mathbf{D}}{\partial \mathrm{t}} &= \mathbf{J}, \end{aligned} \tag{2.1}$$

where **B** is the magnetic induction field, **D** is the electric displacement, **E** is the electric field, **H** is the magnetic field, **J** is the current density, and ρ is the free charge density. By coupling the two curl equations of 2.1 in source free (ρ=0 and **J**=0) and using the constitutive relations, ($\mathbf{D} = \varepsilon \mathbf{E}$, $\mathbf{B} = \mu_0 \mathbf{H}$), for nonmagnetic materials (the relative magnetic permeability $\mu(\boldsymbol{r}) \cong 1$) these equations can be turned into eigenvalue problem, the master equation, in terms of **H**(**r**):

$$\nabla \times \left(\frac{1}{\varepsilon(\mathbf{r})} \nabla \times \mathbf{H}(\mathbf{r}) \right) = \left(\frac{\omega}{c} \right)^2 \mathbf{H}(\mathbf{r}), \tag{2.2}$$

Where $\mathbf{r}$ is the (Cartesian) position vector, ω is the frequency and c is the vacuum speed of light, (given by $c = 1/\sqrt{\varepsilon_0 \mu_0}$). ε_0 and μ_0 are the vacuum permittivity and the vacuum permeability, respectively. $\varepsilon(\mathbf{r})$ is the relative permittivity, which is taken to be spatially dependent for photonic crystals.

Assumming the relative permittivity is not frequency dependent, scale invariance is a fundamental property of the master equation, which means there is no fundamental length scale. In detail, the master equation in dielectric configuration $\varepsilon(\mathbf{r})$ is given by equation 2.2. Then, in dielectric configuration $\varepsilon'(\boldsymbol{r})$ is an enlarged or compressed version of $\varepsilon(\mathbf{r})$: $\varepsilon'(\mathbf{r}) = \varepsilon(\mathbf{r}/s)$. By using $\nabla' = \nabla/s$ and $\mathbf{r}' = s\mathbf{r}$ equation 2.2 becomes:

$$\nabla \times \left(\frac{1}{\varepsilon(\mathbf{r})} \nabla \times \mathbf{H}\left(\frac{\mathbf{r}}{s}\right) \right) = \left(\frac{\omega}{cs} \right)^2 \mathbf{H}\left(\frac{\mathbf{r}}{s}\right), \tag{2.3}$$

where s is a scale parameter. This is also the master equation with mode profile $\mathbf{H}'(\mathbf{r}') = \mathbf{H}(\mathbf{r}'/s)$ and frequency $\omega' = \omega/s$. By just rescaling the old mode and its frequency, the new mode and its frequency are produced. The solution of the equation at one length scale is the same as the solution at another length scale (Joannopoulos *et al.*, 2008).

2.2 Photonic Band Gaps

The band gap has had much attention from researchers in the study of photonic structures. Yablonovitch (2001) explained the wave behaviours in photonic crystals. In a band gap structure, incident electromagnetic waves reflect partially from individual layers. These waves reflect in phase and strengthen each other. Then, as a result of the interference of the reflected and incident waves, standing waves arise. These prohibit propagation across the media. Figure 2.1 illustrates the wave behaviour within the band gap of a one-dimensional photonic crystal. There are two polarisations: transverse-magnetic (TM) and transverse-electric (TE), the first one has the electric field in the plane and the second one has the electric field perpendicular to the plane (Hecht, 2002). They have an individual band structure (Johnson and Joannopoulos, 2003). When light is incident obliquely, these polarisations need to be considered separately. However, at normal incidence there is no distinction between them.

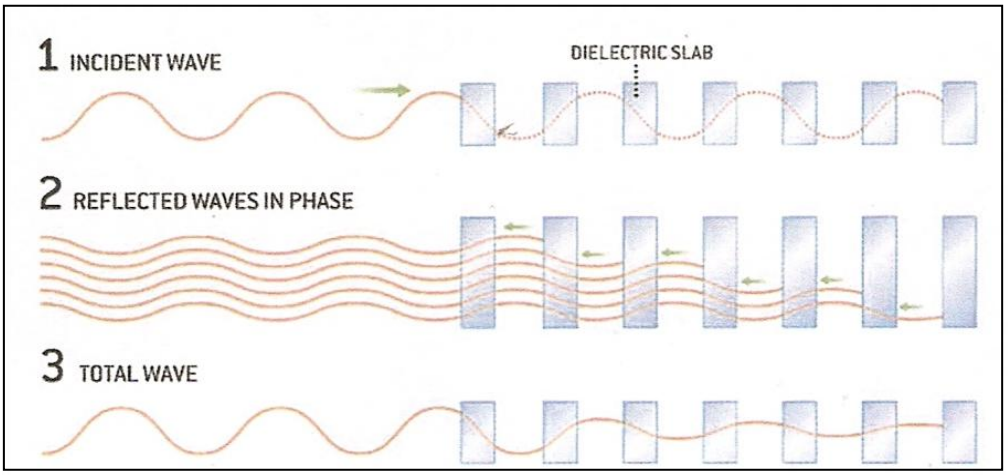

Figure 2.1: The wavelength in one-dimensional band gap (Yablonovitch, 2001), with permission from Andy Christie, Slims film, and courtesy for reuse from Karin Tucker.

The band gap may be easily calculated in the one-dimensional case. On the other hand, it is difficult in two-dimensions (Lourtioz *et al.*, 2008). This is not only because the wave propagates in two directions but also, because the polarisations are not generally separable. There are also two topologies: either holes with low index in the material with a high index or rods with a high index embedded in a low index material. The former, holes, may have a TE photonic band gap. The latter, rods, have a TM photonic band gap (Johnson and Joannopoulos, 2003). Since the study of three-dimensional photonic crystal is complicated, a photonic-crystal slab is used. This is the design of two-dimensional periodic structure with a finite height. It can confine the light vertically in the slab with index guiding (a general idea of total internal reflection) (Johnson and Joannopoulos, 2003).

2.3. Light Localisation

Defects in photonic crystals have received much attention in the study of photonic structures. Anything which causes a change in periodic structures is termed as a defect. There are two main types of defect: line and point defects. In the first one, waveguides are produced, while in the second one a cavity is produced. Modes associated with defects lie within the photonic band gap and are localised near the defects (Johnson and Joannopoulos, 2002). The modes in the gap have the complex wave vector, k, and decay exponentially away from the defect. Analytic continuation can be used to determine the explicit decay factor near to the gap edge. The quadratic approximation to the band structure is:

$$\omega = \omega_0 + \alpha(k - k_0)^2, \tag{2.4}$$

where α is constant and (k_0, ω_0) is a minimum location. So, the solution of equation 2.4 for frequency lower than ω_0 by small amount $\Delta\omega$ is:

$$k = k_0 + i\sqrt{\frac{\Delta\omega}{\alpha}}, \tag{2.5}$$

(Johnson and Joannopoulos, 2002). The power localisation in the high or low dielectric regions can distinguish the bands above and below a band gap. Because of that, the band above a photonic band gap is called the air band while the band below a photonic band gap is called the dielectric band (Joannopoulos *et al.*, 1997). Johnson and Joannopoulos (2002) mentioned that there are two methods to produce states within the photonic band gap: pulling a localised state down from the air band, by raising the dielectric constant in an area; and, pushing a localised state up from the dielectric band, by reducing the dielectric constant in an area.

2.4 Applications of Photonic Crystals

Introducing a point defect can localise or confine the light at one point inside the photonic crystal producing a cavity. These photonic structures can be designed to be used as filters, lasers and light emitting diodes (LEDs). Photonic crystals can be used to control spontaneous emission, which occurs naturally when an excited atom goes down to a lower energy state, and its energy is released as emitted radiation. Many light emitting devices in the optoelectronic industry depend on a spontaneous emission. Both

the density of allowed state and the coupling between the photon and the atom determine the rate of spontaneous emission (Joannopoulos *et al.,* 1997).

Photonic cavities have many applications. Typically, both a small volume, *V* and a high quality factor, Q are required in designing the cavities for these applications. The energy dissipated per cycle against the energy stored defines the cavity Q-factor. The loss on reflection at the interfaces between the inside and the outside of the cavity defines the Q-factor if the media have no absorption. The strength of the emitter-cavity interaction is determined by *V*. researchers often aim to maximise a ratio Q/*V* for a particular application (Akahane *et al.*, 2003a). L3 and L4 nano-cavities were introduced by Akahane *et al.* (2003b). These are types of photonic crystal nano-cavities that have three and four missing holes, respectively. A Q-factor of 45,000 and modal volume of 0.69 $(\lambda_0/n)^3$ (where λ_0 is the wavelength of light in air) in a nano-cavity based on silicon membrane were achieved by displacing air holes at both cavity ends (Akahane *et al.*, 2003a, 2005). Akahane *et al.* (2005) investigated experimentally and theoretically maximizing the quality factor Q of this cavity by displacing six air holes close to the end of the cavity.

Another form of cavity is a micro-cavity pillar. There is a long history on a micro-cavity pillar. Gérard *et al.* (1998) have enhanced the spontaneous emission using InAs quantum boxes which are put in a small volume GaAs/AlAs pillar micro-resonator. Sanvitto *et al.* (2005) have considered emission from a circular micro-pillar structure of 5-10 μm diameter. This pillar structure consisted of three layers of InAs quantum dots, which are formed a cavity. This cavity is surrounded by 27 alternating bilayers from AlAs/GaAs, in the bottom distributed Bragg reflector (DBR) and on the

top, 20 repeats. They recorded a Q factor equal to 30,000 approximately (but this is for large pillars, so Q/V is not good). Daraei *et al.* (2006) showed elliptical micro-cavity pillars have different values of Q-factor for modes polarised parallel to the long and the short pillar axes. The authors also controlled the polarisation of emission of quantum dots, which are inside the pillars, using the coupling between the photonic modes and the emission of the quantum dots.

As seen above, by introducing defects in photonic crystals, light can be localised. It can also be guided from one position to another by using a line defect. Electromagnetic waves with the frequencies inside the photonic band gap are restricted to the waveguide or can be guided within the waveguide (Joannopoulos *et al.*, 1997). Elimination of a single row from two-dimensional photonic crystals produces a single-mode waveguide, while increasing the number of removed rows produces multi-mode waveguides (Joannopoulos *et al.*, 2008). In conventional dielectric waveguides, for example, in optical fibres, electromagnetic waves can be guided with no losses, depending on the total internal reflection principle. However, when the optical fibre bends tightly, an incident angle becomes too big for the total internal reflection to happen. As a result, electromagnetic waves escape at the corners and then are lost (Joannopoulos *et al.*, 1997). However, in a theoretical study of photonic crystals, the electromagnetic waves can be transmitted through a waveguide with sharp corners without significant losses. Because of this, photonic crystal waveguides may have a practical significance in allowing miniaturisation of optoelectronic circuits and devices (Novotny and Hecht, 2006). Mekis *et al.* (1996) also showed a high transmission of electromagnetic waves around sharp corners in photonic crystal waveguides using

numerical simulations (the FDTD method). If the curvature radius of the right angle is zero, the power transmission still reaches 98%, compared with 30% for similar dielectric waveguides. High transmission, more than 80%, was measured experimentally by Lin *et al.* (1998) through a sharp 90° bend in a square lattice of alumina rods, which have radius equal to 0.20 a , where a is a lattice constant.

Another practical waveguide device is a splitter. This device splits the input power into two equal output waveguides (Joannopoulos *et al.*, 2008). Yonekura *et al.* (1999) estimated the reflection loss is from 0 to 4.6 dB at a 120° branching angle (Y-branch), which depends on the input wave frequency. Fan *et al.* (2001) have discussed theoretical considerations as well as the numerical simulations of T-shaped waveguide branches in photonic crystals. FDTD modelling of waveguide branches reveals almost full transmission. The result of such a transmission simulation is shown in figure 2.2.

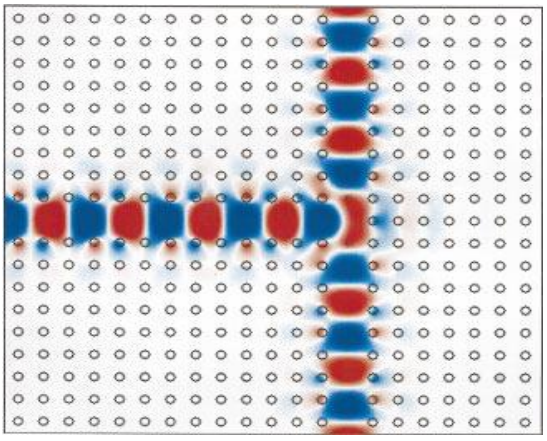

Figure 2.2: The electric field distribution in a waveguide splitter (Fan *et al.*, 2001),with permission from Susannah Lehman, Authorized agent, the optical society.

A photonic crystal slab, which is mentioned in section 2.2, is also known as photonic crystal waveguides (PCWs). This type of photonic and their implementation have received an increased interest from researchers. PCW may be broadly defined as the design of photonic crystals in two dimensions fabricated in the form of thin films with deep patterning. This design is useful in generating photonic band gap defined micro-lasers and in improving light extraction from LEDs (Astratov *et al.*, 2000a). Astratov *et al.* (2000b) used surface coupling techniques to investigate experimentally the band structure for two types of patterned waveguide structures: lattice of air stripes and honeycomb lattice of air cylinders. They studied a 'bulk' photonic crystal which is made of a core layer ($Al_{0.12}Ga_{0.88}$), a cladding layer ($Al_{0.35}Ga_{0.65}$) and a GaAs substrate. In the experimental investigation, the authors measured reflectivity spectra, the theoretical reflectivity spectra were calculated using a scattering matrix treatment to solve numerically the Maxwell equations for these structures. In both experimental and theoretical treatments, reflectivity spectra were obtained for different incidence angles. Resonant coupling arises if the energy and in-plan wave vector, k, of the incident light are equal to those in waveguide dispersion. The resonant coupling was shown as sharp feature in reflectivity spectra. k is determined by the incident angle θ using dispersion expression, $k = (\omega/c)\sin\theta$. Hence, via changing θ and observing the energy positions of the resonant features, the band structure of these types of photonic crystal were plotted.

2.5 Photonic Structures in Nature

There are many examples of photonic structures in nature. The sea mouse (*Aphrodite*) is an example of a living organism which produces a brilliant iridescence, colours which change with the angle of incident light and the view direction (Tayeb *et al.*, 2003). The colours are produced by structural properties; they are from interference or diffraction, not selective absorption in pigments. These effects are angle dependent, so iridescence distinguishes structure colours (Tayeb *et al.*, 2003). Parker *et al.* (2001) stated "The simple structure responsible for this effect is a remarkable example of photonic engineering by a living organism". The sea mouse has hexagonal close–packed (hcp) structures of holes with spacing about 0.5 μm in its spine and finer hairs. At the normal incidence of light, the spine exhibits a bright red colour. By increasing the incident angle of light, the red colour varies to green and blue. The finer hairs have gold colours which alter to green and blue (McPhedran *et al.*, 2003). Several studies have indicated that these two-dimensional structures have a partial photonic band gap (Tayeb *et al.*, 2003). The geometric parameters of the 88 layers forming the wall of the spine were computed by McPhedran *et al.* (2003), who also determined the reflectivity at normal incidence through these layer stacks of 88 gratings of the spine. Other examples of photonic crystals in nature are some butterflies such as *Morphorhetenor*, and the opal, which is formed of small silica spheres packed together (Tayeb *et al.*, 2003).

2.6 Computational Techniques

Computational methods have been used in a number of problems such as photonic band analysis, calculation of the reflection or the transmission spectra, and emission spectra. Methods include finite difference time domain (FDTD), plane wave expansion (PWE), multiple-scattering theory and transfer matrix. A large computer resource is required and a long time is spent during the computational process in both the FDTD and PWE methods (Yonekura *et al.*, 1999). These methods are briefly discussed below.

2.6.1 Finite Difference Time Domain

In 1966, the FDTD method was introduced by Yee (Yee, 1966). This is a popular numerical method in electromagnetism. In this technique, time and space are separated into a grid of discretised points (Joannopoulos *et al.*, 2008). The method provides a numerical solution to the two curls' Maxwell equations; see equation 2.1, in real space. The fields are propagated in a series of discrete time steps (Villeneuve *et al.*, 1996).

In the FDTD method, as mentioned, Maxwell equations are solved in a discretised domain where scales have to be controlled. Problems including open boundaries are treated by modifying the computational domain boundaries to absorb outgoing waves. The execution of the FDTD method uses an absorbing layer termed perfectly matched layer (PML). The matched medium is designed to absorb electromagnetic waves with no reflection (Berenger, 1994). Gedney (1996) introduced PML absorbing media based on uniaxial anisotropic media.

2.6.2 Plane Wave Expansion

The plane wave expansion method has been used to calculate band structure of photonic crystals. In this method, the electric or magnetic field is represented in terms of plane waves and given by the following:

$$\boldsymbol{u} = \exp(i\boldsymbol{k}.\boldsymbol{r}) \sum_{\boldsymbol{G} \in G} \boldsymbol{V}(\boldsymbol{G}) \exp(i\boldsymbol{G}.\boldsymbol{r}), \qquad (2.6)$$

where $\boldsymbol{u}$ denotes the electric or magnetic field, $\boldsymbol{k}$ is the wave vector, $\boldsymbol{r}$ is an arbitrary spatial vector, $\boldsymbol{G}$ is a linear combination of the reciprocal lattice vectors and $\boldsymbol{V}$ is the electric or magnetic vector. Limitations in numerical accuracy result from the discontinuity of the permittivity between two media, which means that the electromagnetic field components are also discontinuous (Lourtioz *et al.*, 2008).

2.6.3 Multiple-Scattering Theory

Classical wave studies are the origin of the multiple scattering theory (MST). The theory gives a united theoretical method to treat ordered and disordered dielectric systems, when the vector nature of waves is taken into account (Wang *et al.*, 1993). These authors gave an expression of multiple-scattering for electromagnetic waves. They also applied it to three-dimensional structures. The fundamental nature of multiple scattering theory is to divide the scattering potential into non overlapped districts. Every district can be treated as a single scatterer and the incident waves on this scatterer consist of the scattered waves from other scatterers, along with the incident waves itself. Its scattered waves become components of the incident waves for other scatterers (Chen and Li, 2003). Multiple scattering theory can be used to find the photonic band for dielectric and metallic systems (Zhang *et al.*, 2001).

2.6.4 Transfer Matrix

The transfer matrix is the main computational tool used in this thesis. In this section, a brief introduction to the general idea of the transfer matrix is given. The transfer matrix (T-matrix) connects the waves in different layers of the structure, *i.e.*, the forward, *a*, and backward, *b*, waves in the layer *N* connect to the forward and backward waves in layer *0* (Whittaker and Culshaw, 1999). It is defined by the following equation:

$$\begin{pmatrix} a_N \\ b_N \end{pmatrix} = \begin{pmatrix} M_{11} & M_{12} \\ M_{21} & M_{22} \end{pmatrix} \begin{pmatrix} a_0 \\ b_0 \end{pmatrix}. \tag{2.7}$$

The T-matrix can also be written in terms of the electric, *E*, and magnetic, *B*, fields, which is the form we actually use. This is given by the following equation:

$$\begin{pmatrix} E_N \\ B_N \end{pmatrix} = \begin{pmatrix} M_{11} & M_{12} \\ M_{21} & M_{22} \end{pmatrix} \begin{pmatrix} E_0 \\ B_0 \end{pmatrix}. \tag{2.8}$$

For a set of layers, the T- matrix is produced as the result of the product of each matrix in every layer, which means,

$$\mathrm{M} = \mathrm{M}_{N-1} \times \mathrm{M}_{\mathrm{N}-2} \times \ldots . \mathrm{M}_1, \tag{2.9}$$

Reflectivity and transmission spectra can be calculated using T-matrix method (Hecht, 2002). Details of this matrix will be given in Chapter 4.

CHAPTER 3

MAGNETIC AND OPTICAL PROPERTIES

In this chapter, some background about the polarisation of light and birefringent materials will be discussed. Magneto-optics effects, Kerr and Faraday ellipticity and rotation, will also be examined. In addition, Stokes' parameters and their geometric representation, the Poincaré sphere, will be introduced.

3.1 Light Polarisation

Most text books in optics have studied polarisation, for example Hecht (2002) and Smith *et al.,* (2007). The polarisation of light in free space may be broadly defined as the behaviour of an electric field in the polarisation plane perpendicular to the propagation vector. There are three types of polarisation depending on amplitude and phase difference: linear or plane; circular; and elliptical polarisation. In linear polarisation, the electric field remains in a fixed direction although its magnitude and sign are time dependent. However, in a circular polarisation type, the electric field rotates uniformly with time in the polarisation plane. This polarisation is important in considering light propagation through birefringent materials. The last type, elliptical polarisation emerges from a combination of the linear and circular polarisations. The elliptical polarisation is a general case of the polarisation. The linear and circular polarisations are just special cases.

3.2 Birefringent Materials

In anisotropic materials, the refractive index changes with crystal orientation. The refractive index light experiences depend on the polarisation state. Thus two ray components refracted in different directions result when a randomly polarised ray passes through a crystal. A material which has this characteristic is called doubly refracting or more precisely birefringent material (Smith *et al.*, 2007).

The eigenvector components represent linear and circular polarised states for linearly and circularly birefringent materials, respectively. These are given by Jones vectors. In a linearly birefringent material, two refracted beams, called the ordinary and extraordinary rays, emerge linearly polarised in orthogonal directions. The ordinary ray obeys Snell's law (law of refraction) while the extraordinary ray does not obey this law. There are two refractive indices correspond to these beams. In a circularly birefringent material, the two refractive indices are known as right and left according to the rotation direction of circularly polarised light. The difference between these refractive indices is smaller (Pedrotti and Pedrotti, 1993). A change from one polarisation state to another can be produced using linearly birefringent media such as calcite, quartz and ice. Chiral or optically active materials have the property of circular birefringence. There are different examples of these media in nature such as DNA, hormones, vitamins, proteins and sugar solutions. Waves with right and left circular polarisation states propagate without change in these substances at different speeds. As a result of this, the polarisation plane of linearly polarised waves rotates, and this phenomenon is called natural optical rotation (Orfanidis, 2008). Optically activity media have different refractive index for the two hands of circular polarisation (Smith *et al.*, 2007). These

refractive indices distinguish circularly birefringent material from ordinary birefringent materials. In order to explain the reason of existing different velocities for left and right circularly modes the following clarification is mentioned. The optical activity media have molecules or crystalline structures which are chiral, such as spiral forms that have left- or right-handed screw shapes. The linear polarised light propagated through a group of these molecules produces forced vibrations of electrons. These move along and around a spiral. Then the effect of left circularly polarised light on a left-handed spiral differs from the effect of right circularly polarised light on a right-handed spiral (Pedrotti and Pedrotti, 1993).

Birefringence can be induced by applying an external electric or magnetic field to an isotropic medium. In the case of an applied electric field transverse to a ray of light the effect is known as the Kerr effect (Smith *et al.,* 2007). This Kerr effect is often denoted as the quadratic electro-optic effect because it is proportional to the square of electric field (Hecht, 2002). A longitudinal-magnetic field can induce optical activity (difference between dielectric constants for two circular polarisations); this is known as the Faraday effect (Smith *et al.*, 2007). Alternatively, by applying mechanical stress on a transparent isotropic medium, optical anisotropy can be produced. This effect is known as the photo-elastic effect or stress birefringence. Birefringence can originate from anisotropy on a length scale much bigger than molecular dimensions. This situation is known as 'form birefringence' (Born and Wolf, 1999).

Birefringent layered structures have a highly significant role in many different devices such as narrow-band birefringent filters, multistage electro-optic modulators, and polarisers (Yeh, 1979).

3.3 Magneto-Optic Effects

As a result of the interaction between light and magnetisation, either internal magnetisation or using an external magnetic field, magneto-optical effects are produced. The effect on the optical properties is characterised by the dielectric matrix, $\underline{\underline{\varepsilon}}$. In a circular birefringent material or in the case of applying the magnetic field on a medium in the *z*-direction, this takes the form

$$\underline{\underline{\varepsilon}} = \begin{pmatrix} \varepsilon_{xx} & i\varepsilon_{xy} & 0 \\ -i\varepsilon_{xy} & \varepsilon_{xx} & 0 \\ 0 & 0 & \varepsilon_{zz} \end{pmatrix} \tag{3.1}$$

The diagonal elements are the same in isotropic media and the off diagonal element ε_{xy} is finite due to the magnetic field (Mansuripur, 2009). Precise values for diagonal and off-diagonal elements of the dielectric matrix provide important information about the band structure of the medium (Gao *et al.*, 1999).

Mansuripur (2009) attempted to explain the basis of magneto-optical effects: linearly polarised light can be expressed as a superposition of right and left circularly polarised components. The propagation of polarised light inside a magnetic material or along the applied magnetic field direction leads to the right and left circularly polarised components experiencing different refractive indices. They undergo a relative phase shift, which is equivalent to a rotation of polarisation plan; as in an optically active medium. There may also be a change in amplitude, which produces elliptically polarised light. Figure 3.1 illustrates this graphically. The phase change leads to a rotation. While the amplitude change gives rise to the ellipticity. This is described as either Kerr or Faraday rotation and ellipticity, depending on whether reflection or

transmission is measured (Reim and Schoenes, 1990). It should be pointed out the Kerr effect here is produced as a result of using magnetic media or applying the magnetic field, not to be confused with the Kerr effect or the quadratic electro-optic effect which is produced by applying electric field transverse to a light ray. It should be pointed out in this thesis when we refer to the Kerr and Faraday effects, we mean the magneto-optical Kerr and Faraday effects.

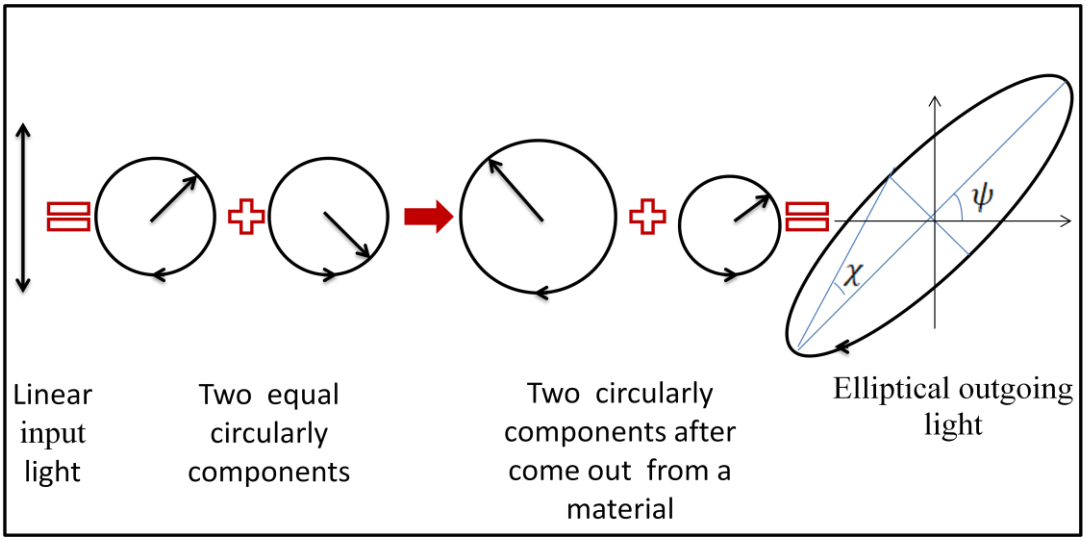

Figure 3.1: A graphical illustration of the process of magneto-optical effects, where ψ is the rotation angle and χ is the ellipticity angle. Adapted from Mansuripur (2009).

In the magneto-optical Kerr effect, as mentioned above, the input linear polarised light reflects from the medium and the polarisation changes to a rotated, elliptically polarised state. In order to measure the polarisation states, photometric and ellipsometric techniques can be used (Finazzi *et al.*, 2009).

The magneto-optical Kerr effect (*i.e.*, when dealing with the reflection measurements) can be classified into three types according to magnetic field directions relative to the incidence plane and the direction of propagation. These are the polar, longitudinal (meridional) and transverse (equatorial) magneto-optical Kerr effects. The first one is similar to the Faraday effect in transmission measurements since a propagation direction is parallel or anti-parallel to the applied magnetic field direction (Reim and Schoenes, 1990). This first type, the polar Kerr effect, is proportional to the out-of-plane magnetisation component. The longitudinal magneto-optical Kerr effect is produced by the in-plane magnetisation component parallel to the incidence plane, whereas the transverse magneto-optical Kerr effect is produced by the component of in-plane magnetisation perpendicular to the incidence plane (Hamrle *et al.*, 2007), see figure 3.2.

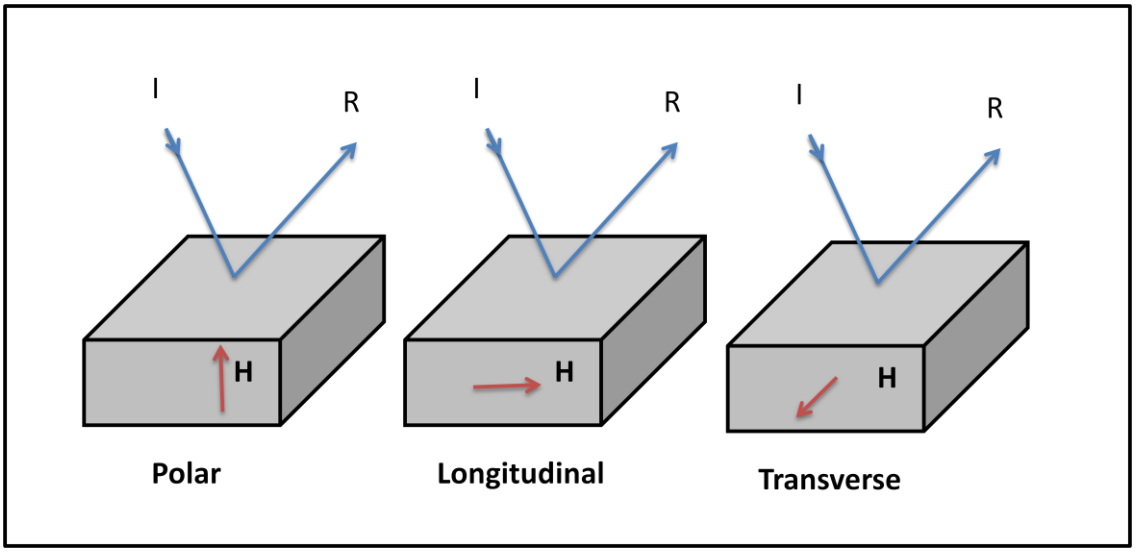

Figure 3.2: Schematic diagrams of different magneto-optical Kerr effects. I and R are the incident and reflected waves, respectively. **H** is the magnetic field. Adapted from Reim and Schoenes (1990).

The magneto-optical effects can be used to monitor optically the magnetisation state of a medium since changes to the ellipticity and rotation indicate the magnetisation direction is changed within the material (Mansuripur, 2009). In 1999, Sakaguchi and Sugimoto used multilayer films, which have periodic magnetic and dielectric materials, as Faraday rotators in optical isolators. The rotation was controlled either by changing the intensity of the magnetic field or increasing the number of magneto-optical layers.

The Kerr ellipticity (χ) and rotation (ψ) are defined by Sato (1981) as:

$$\chi = \frac{1}{4}\left(\frac{\Delta R}{R}\right) = \frac{1}{2}\left(\frac{R_+ - R_-}{R_+ + R_-}\right), \tag{3.2}$$

$$\psi = -\frac{1}{2}\Delta\theta = -\frac{1}{2}(\theta_+ - \theta_-) \tag{3.3}$$

where R_+ and R_- are the reflectivity for right and left circularly polarised light, respectively (as they are called in Sato's article) . $\Delta\theta$ refers to the change in the phase. More details of Sato's experiment will be given later in Chapter 6. A similar definition can be used in the transmission case.

In 1999, Sakaguchi and Sugimoto also gave a mathematical definition of ellipticity (χ) and rotation (ψ) that is adapt for reflection as follows:

$$\chi = \tan\left(\frac{1}{2}\sin^{-1}\left(\frac{-2\,\mathrm{Im}\left(\frac{r_{xy}}{r_{xx}}\right)}{1+\left|\frac{r_{xy}}{r_{xx}}\right|^2}\right)\right), \tag{3.4}$$

$$\psi = \frac{1}{2}\tan^{-1}\left(\frac{2\,\mathrm{Re}\left(\frac{r_{xy}}{r_{xx}}\right)}{1-\left[\frac{r_{xy}}{r_{xx}}\right]^2}\right), \tag{3.5}$$

where *r* is the complex reflectivity amplitude, and the first and second subscripts refer to incoming and outgoing waves, respectively. Re and Im denote the real and the imaginary part of a complex number, respectively. It should be pointed out that both rotation definitions depend on amplitude and phase information. The two definitions are, in fact, identical, as is shown in appendix A.

3.4 Stokes' Parameters and Poincaré sphere

In 1852, Stokes introduced a set of parameters which are used to describe the polarisation states of light. Stokes' parameters are properties of observed light beams and can represent either partial or full polarisation Hecht (2002).

Stokes' parameters are given in terms of intensity, which may be determinted experimentally or theoretically as will be seen later, by Born and Wolf (1999) as:

$$\begin{aligned} S_0 &= I_x + I_y, \\ S_1 &= I_x - I_y, \\ S_2 &= I_a - I_b, \\ S_3 &= I_+ - I_-, \end{aligned} \tag{3.6}$$

where S_0 is the total intensity, S_1, S_2 and S_3 are the differences in intensities (*I's*) between two linear polarised state (horizontal, *x*, and vertical, *y*,), two linear diagonal polarised state (at $+45^o$, *a*, and at -45^o, *b*,) and two circularly polarised state (right, +, and left, -,), respectively as they are called in Born and Wolf 's book.

Other studies (Born and Wolf, 1999; Smith, 1997) considered the relationship between Stokes' parameters and ellipticity, χ, or rotation angle, ψ, (see figure 3.3) as the following:

$$S_1 = S_0 \cos 2\chi \cos 2\psi, \tag{3.7 a}$$

$$S_2 = S_0 \cos 2\chi \sin 2\psi, \tag{3.7 b}$$

$$S_3 = S_0 \sin 2\chi. \tag{3.7 c}$$

These equations are equivalent to equations 3.2-3.5 as will be discussed, in detail, in Chapter 5. For a total polarised state of light beam

$$S_0^2 = S_1^2 + S_2^2 + S_3^2, \tag{3.8}$$

whereas for a partial polarised state of light

$$S_0^2 > S_1^2 + S_2^2 + S_3^2, \tag{3.9}$$

and the polarised degree, DP, is given by:

$$DP = \frac{\sqrt{S_1^2 + S_2^2 + S_3^2}}{S_0} \tag{3.10}$$

The polarisation state of a plane monochromatic wave can be represented by a point on or inside a sphere, known as the Poincaré sphere, see figure 3.3. In the Poincaré sphere, Stokes' parameters S_1, S_2 and S_3 are the Cartesian coordinates and S_0 indicates the distance between the origin and the point. If the point is on the sphere's surface, the state is fully polarised, otherwise is partially polarised. The north pole of the sphere corresponds to right circularly polarised light while the south pole is left circular polarisation. Linear polarised states are represented by points in the equatorial plane (Born and Wolf, 1999). The Poincaré sphere was used by Suits (1992) to give an obvious demonstration of the change in polarisation where the action of a photo-

elastic modulator, which is experimentally useful in measuring Kerr magneto-optic effects, is represented by the motion of points on the sphere, and the output intensity is given as the projection onto an axis. As shown in figure 3.3, ellipticity, χ, and rotation angle, ψ, can be interpreted as, respectively, latitude and longitude, on the sphere (Smith, 1997).

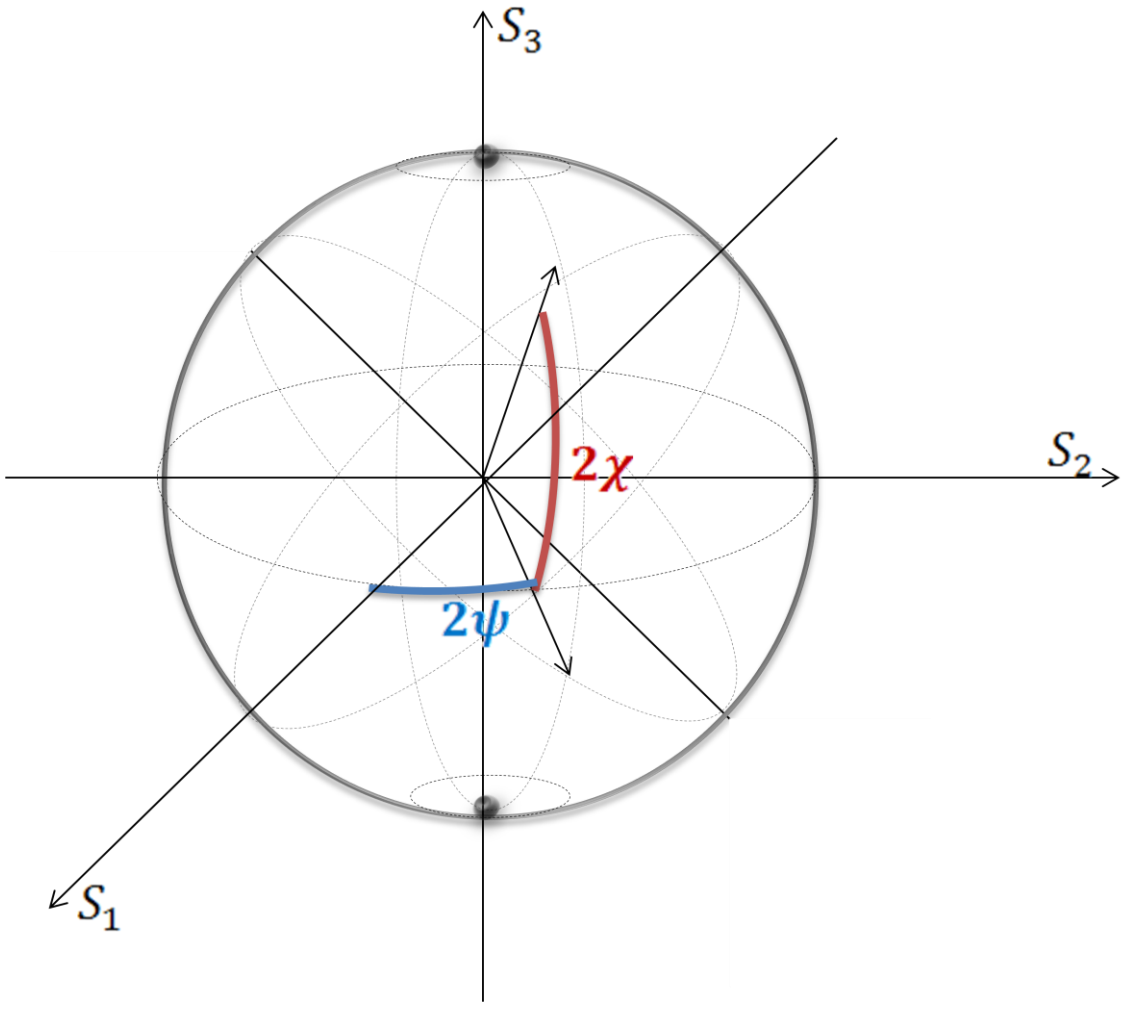

Figure 3.3: Schematic diagram of the Poincaré sphere and Stokes' parameters. Adapted from Born and Wolf (1999).

CHAPTER 4

TRANSFER MATRIX DERIVATION AND OPTICAL PROPERTY CALCULATIONS

As discussed in Chapter 2, many computational techniques have been used in the photonics field. In this chapter, we concentrate on the transfer matrix method for both isotropic and anisotropic media. This method was used to calculate reflectivity spectra using computational codes, which were written using the FORTRAN programme.

4.1 Introduction

In this section, some previous investigations about using a 4×4 transfer matrix in anisotropic materials are cited. Berreman (1972) developed a 4×4 differential matrix approach, starting from Maxwell's equations, to find the reflection and transmission of light by liquid crystals. The propagation of electromagnetic waves in periodic stratified structures was described in a general theoretical method by Yeh *et al.* (1977). They used a diagonalisation of the unit cell translation operator to find the Bloch wave solutions, the dispersion relations, and the band structure. This theory was utilised in the problems of birefringence and group velocity by Yariv and Yeh (1977). Yeh (1979) extended the theory of wave propagation into periodic birefringent layered materials. The author used a 4×4 transfer matrix technique to find the reflection and transmission coefficients in these media in the case of linear polarisation. The formulae of reflection and transmission amplitudes were produced explicitly by Lekner (1991) for different polarisations when waves are incident on an arbitrary uniaxial crystal face. These

formulae were found in terms of optical constants as well as the direction cosines of the optical axis relative to the laboratory axes.

4.2 Non-Birefringent Materials at a Finite Angle

4.2.1 Theory and Calculations

Hecht (2002) started from boundary conditions of fields to find expression for 2×2 transfer matrices for a multilayer structure and used it to calculate reflectivity and transmission. In isotropic materials, TE and TM polarisations are independent of each other (Yeh, 1979) so, the transfer matrix calculations can be treated for each polarisation separately as 2×2 matrices or for both polarisations together as 4×4 matrix. We do 4×4 matrix calculations to build up the theory for 4×4 matrices. In this section, we follow a similar procedure; starting from Maxwell's equations to derive an expression in terms of 4×4 matrices. Then we use our matrix to calculate reflectivity and transmission spectra. At normal incidence there is no distinction between TM and TE polarisations of light. However, when light incidents with an oblique angle, the polarisations need to be considered.

A wave with frequency ω was considered to be incident at a finite angle on a multilayer structure of non-birefringent materials, for example, a quarter-wave stack. The electric $\boldsymbol{E}$ and magnetic $\boldsymbol{B}$ fields are

$$\boldsymbol{E} = \begin{pmatrix} E_x^0 \\ E_y^0 \\ E_z^0 \end{pmatrix} e^{ikx} e^{iqz} e^{-i\omega t}, \tag{4.1}$$

$$\boldsymbol{B} = \begin{pmatrix} B_x^0 \\ B_y^0 \\ B_z^0 \end{pmatrix} e^{ikx} e^{iqz} e^{-i\omega t}, \tag{4.2}$$

where E_i^0 and B_i^0 are the amplitudes of the electric and magnetic fields, respectively, (i=x,y,z). q is the wave vector in the z-direction and k is the wave vector in the x-direction and is the same in each layer given by ($k = \omega\, sin\theta/c$), see figure 4.1.

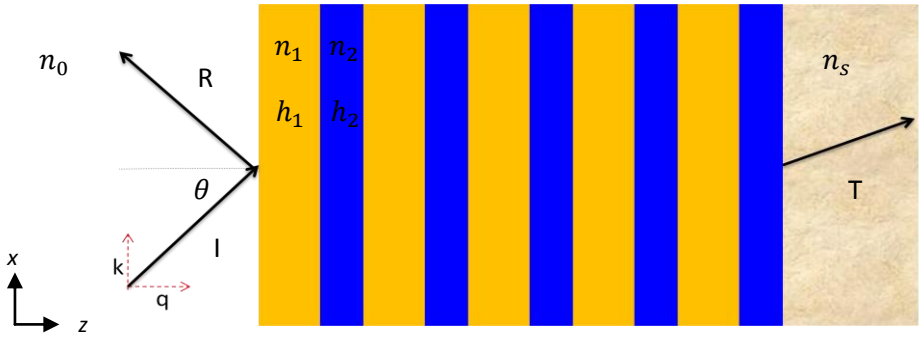

Figure 4.1: Schematic diagram of a quarter-wave stack model. n_s is the substrate refractive index, n_0 is the air refractive index. n_1, n_2, h_1 and h_2 are the refractive indices and thicknesses for each couple of layers, periodically. I, R and T are the incident, reflected and transmitted waves, respectively. θ is the incident angle.

The propagation of electromagnetic waves obeys Maxwell's equations. For nonmagnetic materials, the two curl equations of Maxwell's equations are

$$\nabla \times \boldsymbol{E} = -\frac{\partial \boldsymbol{B}}{\partial t}, \tag{4.3}$$

$$\nabla \times \boldsymbol{B} = \frac{\varepsilon(\boldsymbol{r})}{c^2}\frac{\partial \mathbf{E}}{\partial \mathrm{t}}, \tag{4.4}$$

where c is the vacuum speed of light and $\varepsilon(\boldsymbol{r})$ is the relative permittivity (related with the refractive index, n, by $\varepsilon = n^2$). From equation 4.3, we obtain the following relations:

$$\left.\begin{aligned} -iqE_y^0 &= i\omega B_x^0 && (a)\\ i(q^2 + k^2/q)\,E_x^0 &= i\omega B_y^0 && (b)\\ ikE_y^0 &= i\omega B_z^0 && (c) \end{aligned}\right\} \tag{4.5}$$

Similary, from equation 4.4, we get:

$$\left.\begin{aligned} -iqB_y^0 &= -i\frac{n^2}{c^2}\omega E_x^0 && (a)\\ (q^2 + k^2/q)\,B_x^0 &= -i\frac{n^2}{c^2}\omega E_y^0 && (b)\\ ikB_y^0 &= -i\frac{n^2}{c^2}\omega E_z^0 && (c) \end{aligned}\right\} \tag{4.6}$$

It should be pointed out using the two divergence equations of Maxwell's equations gives $B_z^0 = -k\,B_x^0/\,q$ and $E_z^0 = -k\,E_x^0/\,q$. Substituting those B_z^0 and E_z^0 in equations 4.5, 6-c leads to equations 4.5, 6-a. By substituting E_y^0 from equation 4.5-a in 4.6-b or substituting B_y^0 from equation 4.5-b in 4.6-a, we can find the magnitude of the total wave vectors as given by:

$$q^2 + k^2 = \frac{n^2\omega^2}{c^2}, \tag{4.7}$$

There are two solutions of wave equation, the first one corresponds to TM polarisation and is given by:

$$\left.\begin{aligned} E_x\,(z) &= ae^{iqz}e^{ikx} + be^{-iqz}e^{-ikx}, \\ \tilde{B}_y\,(z) &= \frac{n^2\omega}{cq}\left(ae^{iqz}e^{ikx} - be^{-iqz}e^{-ikx}\right), \\ E_y\,(z) &= 0, \\ \tilde{B}_x\,(z) &= 0, \end{aligned}\right\} \tag{4.8}$$

the second solution corresponds to TE polarisation and is given by:

$$\left.\begin{aligned} E_y\,(z) &= a'e^{iqz}e^{ikx} + b'e^{-iqz}e^{-ikx} \\ \tilde{B}_x\,(z) &= \frac{-cq}{\omega}\left(a'e^{iqz}e^{ikx} - b'e^{-iqz}e^{-ikx}\right), \\ E_x\,(z) &= 0, \\ \tilde{B}_y\,(z) &= 0, \end{aligned}\right\} \tag{4.9}$$

where a, a' are the amplitudes of forward waves, b, b' are the amplitudes of backward waves and $\tilde{B}_{x,y}(z) = cB_{x,y}$. The forward and backward amplitudes can be found in term of $E_x\,(0)$, $E_y\,(0)$, $\tilde{B}_x\,(0)$ and $\tilde{B}_y\,(0)$ with setting $z=0$ into equations 4.8 and 4.9. Then substituting the results in the same equations with $z=h$, we find the following equation. It should be pointed that out we just need the relationships between the fields on either side of structure. So, if we call them $z=z_0$, and $z= z_0 + h$, we get the same matrix:

$$\begin{pmatrix} E_x(h) \\ \tilde{B}_y(h) \\ E_y(h) \\ \tilde{B}_x(h) \end{pmatrix} = \underbrace{\begin{pmatrix} \cos qh & \frac{cq}{n^2\omega} i \sin qh & 0 & 0 \\ \frac{n^2\omega}{cq} i \sin qh & \cos qh & 0 & 0 \\ 0 & 0 & \cos qh & \frac{-\omega}{cq} i\ \sin qh \\ 0 & 0 & \frac{-cq}{\omega} i\ \sin qh & \cos qh \end{pmatrix}}_{M} \begin{pmatrix} E_x(0) \\ \tilde{B}_y(0) \\ E_y(0) \\ \tilde{B}_x(0) \end{pmatrix}, \tag{4.10}$$

M is called the 4×4 transfer matrix of a single layer, and includes the two block diagonal matrices, which can be used to solve TM and TE patterns separately. The transfer matrix depends on the refractive index, *n*, and the thickness, *h*, of the layer. From the last equation and as Hecht (2002) mentioned , this matrix connects the fields at the interface between two layers. For multilayer structures such as a quarter wave stack, let us write $u^l \equiv u^l(0)$, in layer *l*, where *u* is a vector given as $\begin{pmatrix} E_x \\ \tilde{B}_y \\ E_y \\ \tilde{B}_x \end{pmatrix}$. We apply the boundary conditions at an interface between two layers, which means $E_x, \tilde{B}_y, E_y,$ and $\tilde{B}_x$ are continuous, so $u^{l+1} = u^l(h)$. Equation 4.10 can be written as:

$$u^{l+1} = M_l u^l \ , \tag{4.11}$$

and

$$u^l \ = M_{l-1} u^{l-1}, \tag{4.12}$$

So equation 4.11 can be written as:

$$u^{l+1} = M_l \, M_{l-1} u^{l-1}. \tag{4.13}$$

Hence, as mentioned previously, the T-matrix is computed as the product of the matrix for each layer. So for *N* layers, equation 4.10 can be written as:

$$\begin{pmatrix} E_x^N \\ \tilde{B}_y^N \\ E_y^N \\ \tilde{B}_x^N \end{pmatrix} = \underbrace{M_{\mathrm{N}-1} M_{\mathrm{N}-2} \ldots . M_1}_{M} \begin{pmatrix} E_x^1 \\ \tilde{B}_y^1 \\ E_y^1 \\ \tilde{B}_x^1 \end{pmatrix}, \tag{4.14}$$

here the superscripts *1* and *N* refer to the initial and final layers, respectively. The resultant matrix *M* is 4×4 matrix. In calculating the reflectivity and transmission, there are two reflection coefficients, r_{TM}, r_{TE} and two transmission coefficients, t_{TM}, t_{TE} for TM and TE polarisations. From equation 4.14 and using the relation between the fields, equations 4.5 and 4.6, we get:

$$\begin{pmatrix} t_{TM} \\ f_{s_{TM}} t_{TM} \\ t_{TE} \\ f_{s_{TE}} t_{TE} \end{pmatrix} = \begin{pmatrix} m_{11} & m_{12} & 0 & 0 \\ m_{21} & m_{22} & 0 & 0 \\ 0 & 0 & m_{33} & m_{34} \\ 0 & 0 & m_{43} & m_{44} \end{pmatrix} \begin{pmatrix} 1 + r_{TM} \\ f_{0_{TM}}(1 - r_{TM}) \\ 1 + r_{TE} \\ f_{0_{TE}}(1 - r_{TE}) \end{pmatrix}, \tag{4.15}$$

where

$$f_{0_{TM}} = \frac{n_0^2 \omega}{c q_0}, \qquad f_{s_{TM}} = \frac{n_s^2 \omega}{c q_s},$$

$$f_{0_{TE}} = \frac{-c q_0}{\omega}, \qquad f_{s_{TE}} = \frac{-c q_s}{\omega},$$

here, the index *s* refers to the substrate layer, while the index *0* refers to the surface (air).The value of q can be found from equation 4.7. Solving equation 4.15 for r_{TM}, t_{TM}, r_{TE} and t_{TE}, we find for TM polarisation:

$$r_{TM} = \frac{-f_{s_{TM}} m_{11} - f_{0_{TM}} f_{s_{TM}} m_{12} + m_{21} + f_{0_{TM}} m_{22}}{f_{s_{TM}} m_{11} - f_{0_{TM}} f_{s_{TM}} m_{12} - m_{21} + f_{0_{TM}} m_{22}}, \tag{4.16}$$

$$t_{TM} = \frac{2 f_{0_{TM}} (m_{11} m_{22} - m_{12} m_{21})}{f_{s_{TM}} m_{11} - f_{0_{TM}} f_{s_{TM}} m_{12} - m_{21} + f_{0_{TM}} m_{22}}, \tag{4.17}$$

and for TE polarisation:

$$r_{TE} = \frac{-f_{s_{TE}} m_{33} - f_{0_{TE}} f_{s_{TE}} m_{34} + m_{43} + f_{0_{TE}} m_{44}}{f_{s_{TE}} m_{33} - f_{0_{TE}} f_{s_{TE}} m_{34} - m_{43} + f_{0_{TE}} m_{44}}, \tag{4.18}$$

$$t_{TE} = \frac{2f_{0_{TE}}(m_{33}m_{44} - m_{34}m_{43})}{f_{s_{TE}}m_{33} - f_{0_{TE}}f_{s_{TE}}m_{34} - m_{43} + f_{0_{TE}}m_{44}}. \tag{4.19}$$

The power fraction in the incident wave which is reflected or transmitted is known as reflectance, R and transmittance, T respectively. It is obtained from the squared modulus of the amplitudes ratio (Pedrotti and Pedrotti, 1993). R and T are calculated for both types of polarisation by the following relations:

$$\begin{aligned} R_{TM} &= |r_{TM}|^2, \\ T_{TM} &= \frac{f_{s_{TM}}}{f_{0_{TM}}}|t_{TM}|^2, \\ R_{TE} &= |r_{TE}|^2, \\ T_{TE} &= \frac{f_{s_{TE}}}{f_{0_{TE}}}|t_{TE}|^2, \end{aligned} \tag{4.20}$$

where the factors $\frac{f_{s_{TM}}}{f_{0_{TM}}}$ and $\frac{f_{s_{TE}}}{f_{0_{TE}}}$ refer to the flow of power in a material. At normal incidence, the 2×2 transfer matrices for TM and TE are identical. It is given as the following:

$$\begin{pmatrix} E_x(h) \\ \tilde{B}_y(h) \end{pmatrix} = \begin{pmatrix} \cos qh & \frac{i}{n}\sin qh \\ i\,n\sin qh & \cos qh \end{pmatrix} \begin{pmatrix} E_x(0) \\ \tilde{B}_y(0) \end{pmatrix}, \tag{4.21}$$

where the magnitude of wave vector now is $q = \pm n\omega/c$. The reflectivity and transmission coefficients are calculated as:

$$r = \frac{-n_s m_{11} - n_o n_s m_{12} + m_{21} + n_o m_{22}}{n_s m_{11} - n_o n_s m_{12} - m_{21} + n_o m_{22}}, \tag{4.22}$$

$$t = \frac{2n_o(m_{11}m_{22} - m_{12}m_{21})}{n_s m_{11} - n_o n_s m_{12} - m_{21} + n_o m_{22}}, \tag{4.23}$$

these equations will be used again in Chapter 7.

4.2.2 Results and Discussion

In the special case of normal incidence of light, as mentioned above, there is no difference between TM and TE polarisations. Reflectivity spectra for a quarter wave stack consisted of $(SiO_2/Ta_2O_5)^3$ on a glass substrate were calculated at normal incidence is shown in figure 4.2. The air refractive index was n_0 =1.0. Ignoring absorption for simplicity, the parameters of the dielectric layers and the refractive index of the glass substrate were taken from Kato *et al.*,(2003) as the following: $n_1 = n_{SiO_2} = 1.47$ and $n_2 = n_{Ta_2O_5} = 2.18$, periodically at $\lambda = 720\, nm \approx 1.722\, eV$ and the layer thickness was equal to $\lambda/4n_{1,2}$. The refractive index of the glass substrate was $n_s = 1.52$. Kato *et al.*,(2003) pointed out these dielectric multilayers are being exploited in optical communication as narrow band pass filters.

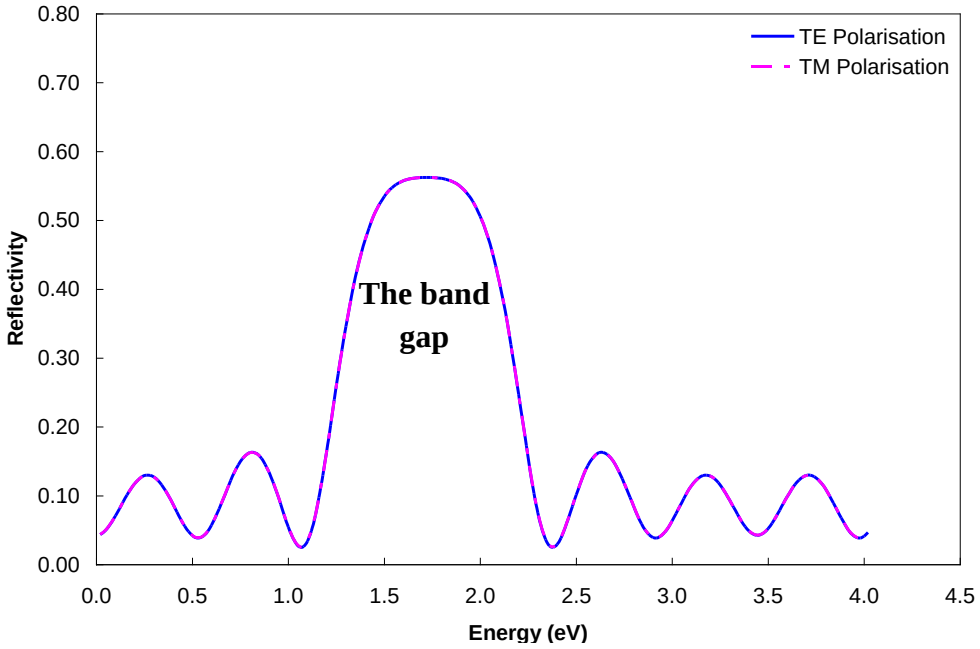

Figure 4.2: Reflectivity spectra of Bragg mirror composed of 6 layers, for both types of polarisation at normal incidence.

Reflectivity spectra for $(SiO_2/Ta_2O_5)^3$ on a glass substrate were also calculated for both TM and TE polarised light at incident angles equal to $20^\circ$and 30°. The difference between polarisations is represented in figure 4.3-a, b. It is clear from this figure that the reflectivity values for TM polarised light are lower than those for TE polarised light; this is connected to the disappearance of TM reflectivity at Brewster's angle (Brewster's angle is the incident angle where the reflection coefficient of TM polarisation reaches zero when the sum of incident and refracted angles is equal to $\pi/2$, (Smith *et al*., 2007)). In addition, the reflectivity values for TE polarised light increase as the incident angle is increased, while for TM they decrease, until the incident angle is close to Brewster's angle, then they increase again. The external Brewster's angle at the interface between air and the first layer (*i.e.,* SiO_2 layer) is $\sim 56^\circ$ and the internal angle corresponding to this external angle $\sim 34^\circ$. In addition, reflectivity spectra for a quarter-wave stack were calculated at a normal incidence of light for different numbers of layers. In figure 4.4, the number of nodes increases as the number of layers is increased owing to an increase in the number of reflected waves from each interface. There are wave oscillations at both sides of the band gap, due to the constructive or destructive interference of waves between the top and bottom of structure leading to the formation of Fabry-Perot fringes. The band diagram of structures can be found from analysis of these oscillation points (Labilloy *et al.*, 1999). The figure also illustrates that when the number of layers is increased, the reflectivity peak at the band gap feature becomes flatter and the reflectivity values at the gap become closer to unity (Hecht, 2002).

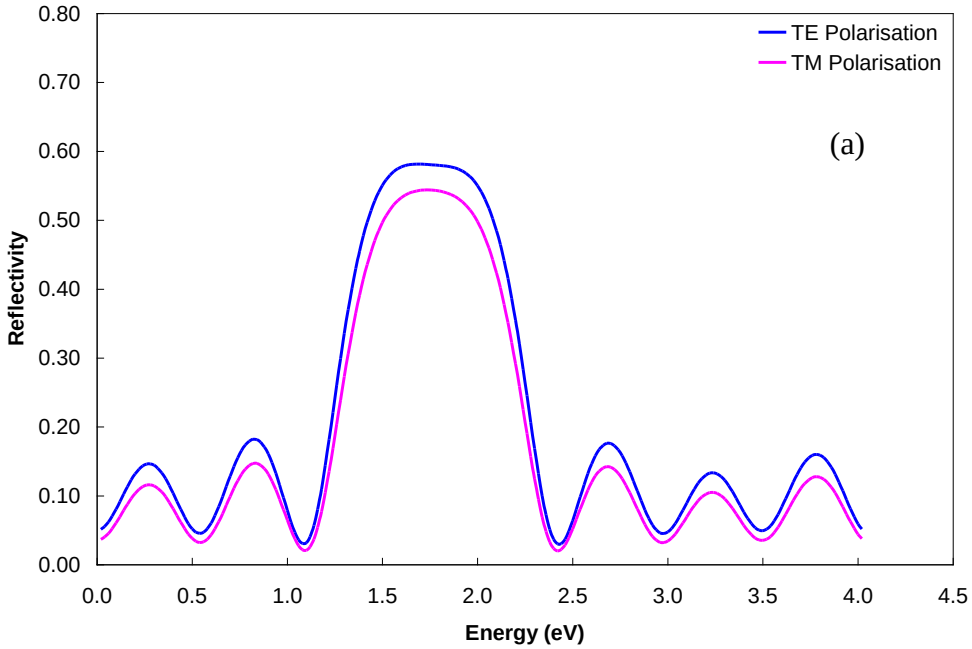

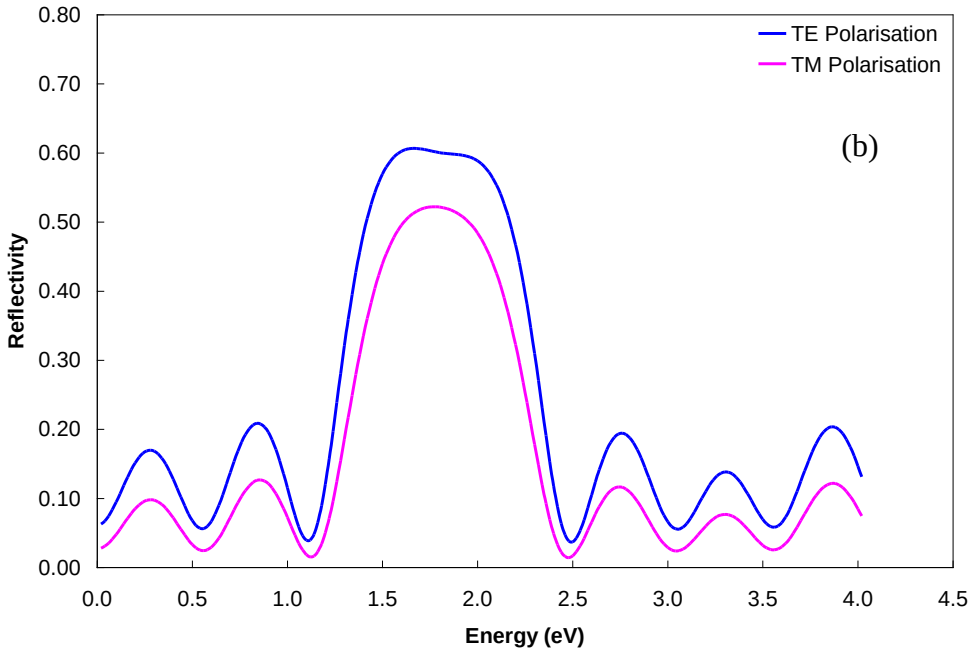

Figure 4.3: Reflectivity spectra for both types of polarisation at finite angles, (a) 20˚and (b) 30˚.

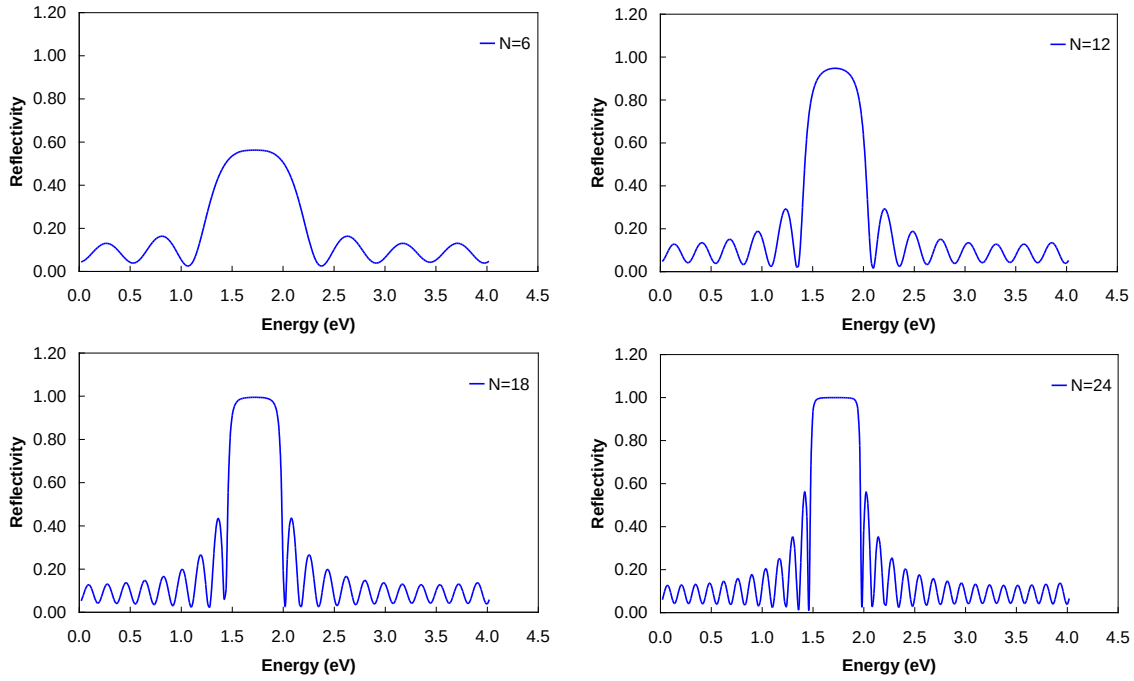

Figure 4.4: Reflectivity spectra at normal incidence for various numbers of layers (*N*).

Next, we consider the reflectivity spectra calculated for the Bragg stack consisted of six and eighteen layers, when absorption is included. In absorbing media, the refractive index becomes a complex number, $\tilde{n}$. It is given by:

$$\tilde{n} = n + i\kappa, \tag{4.24}$$

where n is the real refractive index and κ is the imaginary part and called the extinction coefficient, which determines the absorption rate (Pedrotti and Pedrotti, 1993). The extinction coefficients were taken from Kato *et al.* (2003) as $\kappa_{SiO_2} \cong 0.0$ and $\kappa_{Ta_2O_5} = 7.47 \times 10^{-3}$ at $\approx 1.722\, eV$. The absorption effect on reflectivity spectra is shown in figure 4.5-a, b. The reflectivity values decreased when the absorption was taken in our account. The extent of the decrease depends on the extinction coefficient. The asymmetry in the photonic band gap, which appears clearly in figure 4.5-b can tell

that the material with absorption (here Ta_2O_5) is the one which the mode has the field peak on the low energy side of the gap.

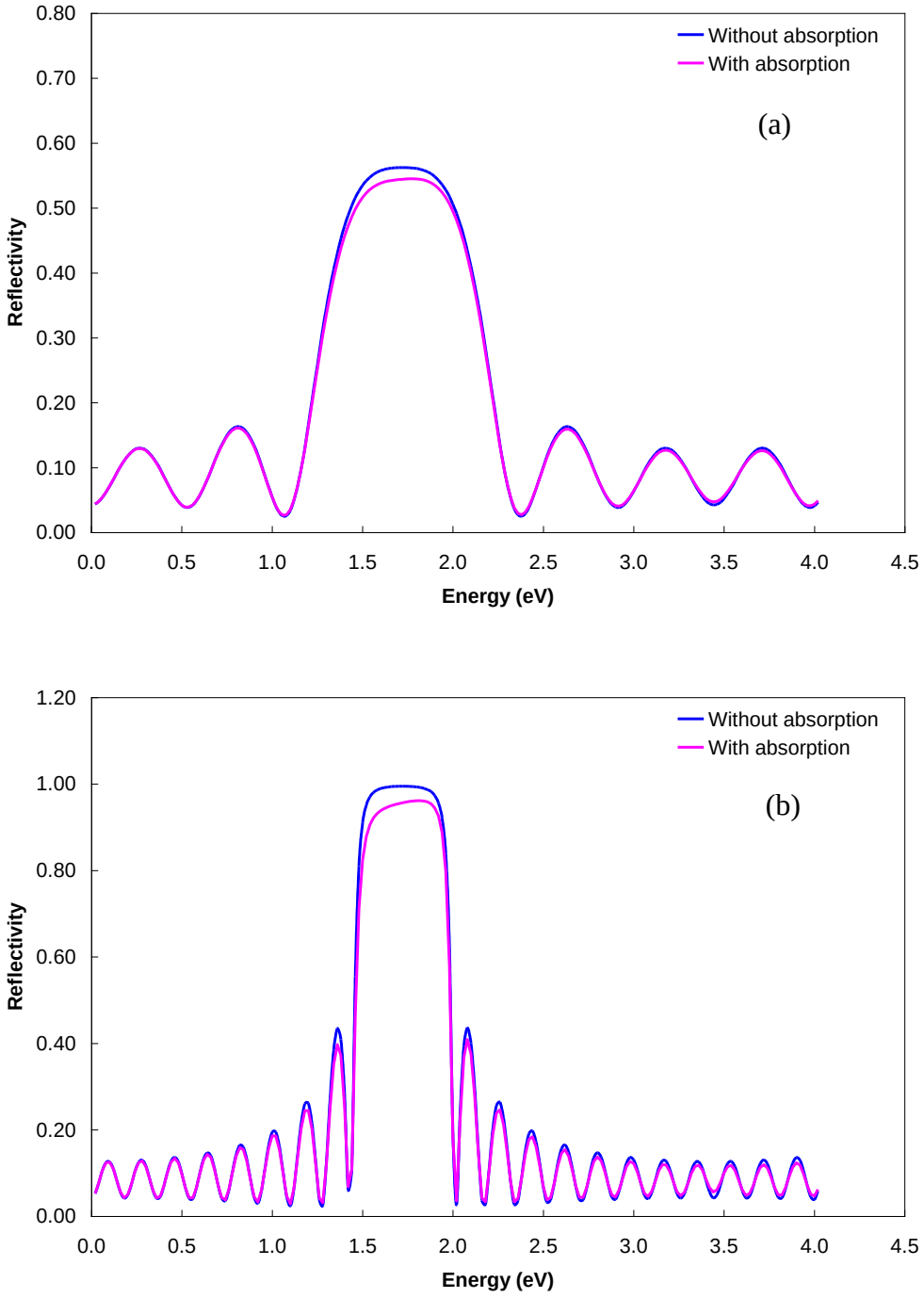

Figure 4.5: Reflectivity spectra at normal incidence without and with absorption for (a) 6-layers (b)18-layers, (the extinction coefficients for Bragg stack were taken from Kato *et al.* (2003) as $\kappa_{SiO_2} \cong 0.0$, and $\kappa_{Ta_2O_5} = 7.47 \times 10^{-3}$ at $\approx 1.722\ eV$).

4.3 Birefringent Materials at a Normal Incidence

4.3.1 Theory and Calculations

In isotropic materials, the two modes of polarisation (*i.e.*, TE and TM) are independent of each other. However, in birefringent materials because of the anisotropy of the media, coupled modes occur at an interface where an incident wave generates waves which have different states of polarisation (Yeh, 1979). In this section, we develop the mathematical treatments of the T-matrix to include anisotropic, circularly birefringent materials in the case of normal incidence of light.

The constitutive relation at a normal incidence for lossless media which display a circular birefringence in an applied magnetic field in *z*-direction is given in matrix form by:

$$\begin{pmatrix} D_x \\ D_y \\ D_z \end{pmatrix} = \begin{pmatrix} \varepsilon_{xx} & i\varepsilon_{xy} & 0 \\ -i\varepsilon_{xy} & \varepsilon_{xx} & 0 \\ 0 & 0 & \varepsilon_{zz} \end{pmatrix} \begin{pmatrix} E_x \\ E_y \\ E_z \end{pmatrix}, \tag{4.25}$$

where the permittivity matrix $\underline{\underline{\varepsilon}}$ has the quantities of $\varepsilon_{xx}, \varepsilon_{xy}, \varepsilon_{zz}$, which are real in our work, and $\varepsilon_{xx}, \varepsilon_{zz} > 0$, also $|\varepsilon_{xy}| \leq \varepsilon_{xx}$. So, it is a hermitian and positive-definite. ε_{xy} is proportional to the applied magnetic field and inverts sign with the field direction (Orfanidis, 2008).

Let us consider a wave with frequency ω incident on a multilayer structure of birefringent media on a transparent isotropic substrate, for simplicity, at normal incidence of light. An anisotropic substrate case will be considered in Chapter 7. The electric $\boldsymbol{E}$ and magnetic $\boldsymbol{B}$ fields of the waves propagating with wave vector q in the *z*-direction are

$$\boldsymbol{E} = \begin{pmatrix} E_x^0 \\ E_y^0 \\ E_z^0 \end{pmatrix} e^{iqz}, \tag{4.26}$$

$$\boldsymbol{B} = \begin{pmatrix} B_x^0 \\ B_y^0 \\ B_z^0 \end{pmatrix} e^{iqz}, \tag{4.27}$$

where $E_z^0 = B_z^0 = 0,$ since $\nabla.\boldsymbol{B} = 0$ and $\nabla.\boldsymbol{D} = 0$ with choosing this particular form of the permittivity matrix (see equation 4.25).

For our purpose, the two curl Maxwell's equations are used in the following form:

$$\nabla \times \boldsymbol{E} = i\,\omega\,\boldsymbol{B}, \tag{4.28}$$

$$\nabla \times \boldsymbol{B} = -i\,\mu\,\omega\,\underline{\underline{\varepsilon}}\,\boldsymbol{E}. \tag{4.29}$$

From equation 4.28, we obtain the following relations:

$$\left.\begin{aligned} B_x^0 &= \frac{-q}{\omega}\ E_y^0\,, && (a) \\ B_y^0 &= \frac{q}{\omega}\ E_x^0\,. && (b) \end{aligned}\right\} \tag{4.30}$$

Similarly, from equation 4.29, we find:

$$\left.\begin{aligned} \frac{q}{\mu\omega} B_y^0 &= \varepsilon_{xx}E_x^0 + i\varepsilon_{xy}E_y^0, && (a) \\ \frac{-q}{\mu\omega} B_x^o &= -i\varepsilon_{xy}E_x^0 + \varepsilon_{xx}E_y^0. && (b) \end{aligned}\right\} \tag{4.31}$$

To find the magnitude of the wave vector q, substituting equation 4.30-b into 4.31-a and equation 4.30-a into 4.31-b, we get:

$$\left.\begin{aligned} \omega^2\mu(\ \varepsilon_{xx}E_x^0 + i\varepsilon_{xy}E_y^0\ ) &= q^2\ E_x^0, && (a) \\ \omega^2\mu(-i\varepsilon_{xy}E_x^0 + \varepsilon_{xx}E_y^0\ ) &= \ q^2\ E_y^0. && (b) \end{aligned}\right\} \tag{4.32}$$

These last equations can be rewritten in matrix notation as:

$$\omega^2\mu\begin{pmatrix}\varepsilon_{xx} & i\varepsilon_{xy}\\ -i\varepsilon_{xy} & \varepsilon_{xx}\end{pmatrix}\begin{pmatrix}E_x^0\\ E_y^0\end{pmatrix} = q^2\begin{pmatrix}E_x^0\\ E_y^0\end{pmatrix}. \tag{4.33}$$

Solving equation 4.33 for q, we get

$$q^{\pm} = \omega\sqrt{\mu(\varepsilon_{xx} \pm \varepsilon_{xy})}, \tag{4.34}$$

the superscripts $\pm$ indicate two values of q. The eigenvector components which correspond to these values are found as:

$$\begin{pmatrix}E_x^{0+}\\ E_y^{0+}\end{pmatrix} = \begin{pmatrix}1\\ -i\end{pmatrix} \quad (a), \quad \begin{pmatrix}E_x^{0-}\\ E_y^{0-}\end{pmatrix} = \begin{pmatrix}1\\ i\end{pmatrix} \quad (b), \tag{4.35}$$

which represent circular polarised states. In these numerical calculations, the linearly polarised bases were chosen rather than circularly polarised bases. Using circularly polarised bases can simplify the calculations (because the two polarisations are decouple) and giving the same final results. However, our formalisim could be applied to different types of birefringent materials such as linear or linear together with circular birefringence just by changing those eigenvector components to suitable eigenvectors for the material used.

The general solutions for the electric and magnetic fields in circularly birefringent media, including both polarisations, are:

$$\left.\begin{aligned} E_x\,(z) &= aE_x^{0+}e^{iq^+z} + cE_x^{0+}e^{-iq^+z} + bE_x^{0-}e^{iq^-z} + dE_x^{0-}e^{-iq^-z},\\ B_y\,(z) &= f^+\left(aE_x^{0+}e^{iq^+z} - cE_x^{0+}e^{-iq^+z}\right) + f^-(bE_x^{0-}e^{iq^-z} - dE_x^{0-}e^{-iq^-z}),\\ E_y\,(z) &= aE_y^{0+}e^{iq^+z} + cE_y^{0+}e^{-iq^+z} + bE_y^{0-}e^{iq^-z} + dE_y^{0-}e^{-iq^-z},\\ B_x\,(z) &= -f^+\left(aE_y^{0+}e^{iq^+z} - cE_y^{0+}e^{-iq^+z}\right) - f^-\left(bE_y^{0-}e^{iq^-z} - dE_y^{0-}e^{-iq^-z}\right), \end{aligned}\right\} \tag{4.36}$$

where $f^{\pm}$, are given by:

$$f^{\pm} = \frac{q^{\pm}}{\omega}, \tag{4.37}$$

here *a, b* are the amplitudes of the forward waves, *c, d* are the amplitudes of backward waves. The forward and backward amplitudes can be found with setting *z=0,* in equation 4.36. Then substituting the results in the same equation with *z=h*, we find in matrix form:

$$\begin{pmatrix} E_x(h) \\ B_y(h) \\ E_y(h) \\ B_x(h) \end{pmatrix} = \underbrace{\begin{pmatrix} M_{11} & M_{12} \\ M_{21} & M_{22} \end{pmatrix}}_{M} \begin{pmatrix} E_x(0) \\ B_y(0) \\ E_y(0) \\ B_x(0) \end{pmatrix}, \tag{4.38}$$

where M is a 4×4 transfer matrix of a single layer, and includes 2×2 block matrices $M_{11}, M_{12}, M_{21},$ and M_{22}, are given by:

$$M_{11} = \begin{pmatrix} \frac{1}{2}\left(\frac{-E_y^{0-}}{E_y^{0+}}\cos q^+h + \frac{E_x^{0-}}{E_x^{0+}}\cos q^-h\right) & \frac{i}{2}\left(\frac{-E_y^{0-}}{f^+E_y^{0+}}\sin q^+h + \frac{E_x^{0-}}{f^-E_x^{0+}}\sin q^-h\right) \\ \frac{i}{2}\left(\frac{-f^+E_y^{0-}}{E_y^{0+}}\sin\ q^+h + \frac{f^-E_x^{0-}}{E_x^{0+}}\sin q^-h\right) & \frac{1}{2}\left(\frac{-E_y^{0-}}{E_y^{0+}}\cos q^+h + \frac{E_x^{0-}}{E_x^{0+}}\cos q^-h\right) \end{pmatrix},$$

$$M_{12} = \begin{pmatrix} -\frac{1}{2}\left(\frac{-E_x^{0-}}{E_y^{0+}}\cos q^+h + \frac{E_x^{0-}}{E_y^{0+}}\cos q^-h\right) & \frac{i}{2}\left(\frac{-E_x^{0-}}{f^+E_y^{0+}}\sin q^+h + \frac{E_x^{0-}}{f^-E_y^{0+}}\sin q^-h\right) \\ -\frac{i}{2}\left(\frac{-f^+E_x^{0-}}{E_y^{0+}}\sin q^+h + \frac{f^-E_x^{0-}}{E_y^{0+}}\sin q^-h\right) & \frac{1}{2}\left(\frac{-E_x^{0-}}{E_y^{0+}}\cos q^+h + \frac{E_x^{0-}}{E_y^{0+}}\cos q^-h\right) \end{pmatrix},$$

$$M_{21} = \begin{pmatrix} -\frac{1}{2}\left(\frac{E_y^{0-}}{E_x^{0+}}\cos q^+h - \frac{E_y^{0-}}{E_x^{0+}}\cos q^-h\right) & \frac{i}{2}\left(\frac{-E_y^{0-}}{f^+E_x^{0+}}\sin q^+h + \frac{E_y^{0-}}{f^-E_x^{0+}}\sin q^-h\right) \\ -\frac{i}{2}\left(\frac{-f^+E_y^{0-}}{E_x^{0+}}\sin q^+h + \frac{f^-E_y^{0-}}{E_x^{0+}}\sin q^-h\right) & \frac{1}{2}\left(\frac{E_y^{0-}}{E_x^{0+}}\cos q^+h - \frac{E_y^{0-}}{E_x^{0+}}\cos q^-h\right) \end{pmatrix}, \tag{4.39}$$

$$M_{22} = \begin{pmatrix} \frac{1}{2}\left(\frac{E_x^{0-}}{E_x^{0+}}\cos q^+h - \frac{E_y^{0-}}{E_y^{0+}}\cos q^-h\right) & \frac{i}{2}\left(\frac{-E_x^{0-}}{f^+E_x^{0+}}\sin q^+h + \frac{E_y^{0-}}{f^-E_y^{0+}}\sin q^-h\right) \\ \frac{i}{2}\left(\frac{-f^+E_x^{0-}}{E_x^{0+}}\sin q^+h + \frac{f^-E_y^{0-}}{E_y^{0+}}\sin q^-h\right) & \frac{1}{2}\left(\frac{E_x^{0-}}{E_x^{0+}}\cos q^+h - \frac{E_y^{0-}}{E_y^{0+}}\cos q^-h\right) \end{pmatrix},$$

where h is the layer thickness. By applying the boundary conditions at an interface between couple of layers for multilayer structures such as the quarter wave stack, for N layers equation 4.38 can be written as:

$$\begin{pmatrix} E_x^N \\ B_y^N \\ E_y^N \\ B_x^N \end{pmatrix} = \underbrace{M_{N-1}M_{N-2}\ldots.M_1}_{M} \begin{pmatrix} E_x^1 \\ B_y^1 \\ E_y^1 \\ B_x^1 \end{pmatrix}, \tag{4.40}$$

here the superscripts *1* and *N* refer to the initial and final layers, respectively. The resultant M is a 4×4 matrix.

When calculating the reflectivity and transmission, we require four linear reflection and four transmission coefficients as a result of coupling of modes in the anisotropic media (Yeh, 1979). Using equation 4.40 and the relation between the fields (equations 4.30-a, b), we get for linearly incoming *x*-polarised wave:

$$\begin{pmatrix} t_{xx} \\ f_s t_{xx} \\ t_{xy} \\ -f_s t_{xy} \end{pmatrix} = \begin{pmatrix} m_{11} & m_{12} & m_{13} & m_{14} \\ m_{21} & m_{22} & m_{23} & m_{24} \\ m_{31} & m_{32} & m_{33} & m_{34} \\ m_{41} & m_{42} & m_{43} & m_{44} \end{pmatrix} \begin{pmatrix} 1 + r_{xx} \\ f_0(1 - r_{xx}) \\ r_{xy} \\ f_0 r_{xy} \end{pmatrix}, \tag{4.41}$$

where $f_0 = q_0/\omega$, and $f_s = q_s/\omega$, here, the index *s* denotes the substrate layer, while the index *0* denotes the surface (air). The values of $q_{s,0}$ for the substrate layer and the surface are given by ($q_{s,0} = \omega n_{s,0}\ /c$). Solving equation 4.41 gives r_{xx}, r_{xy}, t_{xx} and t_{xy}. The first and second subscripts of the amplitudes refer to incoming and outgoing waves, respectively.

Similarly, for linearly incoming y-polarised wave we get:

$$\begin{pmatrix} t_{yx} \\ f_s t_{yx} \\ t_{yy} \\ -f_s t_{yy} \end{pmatrix} = \begin{pmatrix} m_{11} & m_{12} & m_{13} & m_{14} \\ m_{21} & m_{22} & m_{23} & m_{24} \\ m_{31} & m_{32} & m_{33} & m_{34} \\ m_{41} & m_{42} & m_{43} & m_{44} \end{pmatrix} \begin{pmatrix} r_{yx} \\ -f_0 r_{yx} \\ 1 + r_{yy} \\ -f_0(1 - r_{yy}) \end{pmatrix}, \tag{4.42}$$

solving equation 4.42 gives r_{yy}, r_{yx}, t_{yy} and t_{yx}.

The linearly polarised light can decompose into right, $\boldsymbol{\sigma}^{-}$, and left, $\boldsymbol{\sigma}^{+}$, circularly polarised lights which are given by the following expressions:

$$\left.\begin{aligned} \boldsymbol{\sigma}^{+} &= E^0(\hat{\mathbf{x}} + i\hat{\mathbf{y}})/\sqrt{2}, \\ \boldsymbol{\sigma}^{-} &= E^0(\hat{\mathbf{x}} - i\hat{\mathbf{y}})/\sqrt{2}, \end{aligned}\right\} \tag{4.43}$$

where E^0 is the amplitude of the electric field. Now we can work out circular reflection coefficients (r_{++}, r_{+-}, r_{-+} and r_{--}) in terms of linear reflection coefficients. For left incoming circularly polarised light, $\boldsymbol{\sigma}^{+}$, the outgoing wave can be written from the above analysis of linearly polarised light as:

$$\boldsymbol{E}^{out} = \left(r_{xx} + i r_{yx}\right)\frac{E^0}{\sqrt{2}}\hat{\mathbf{x}} + \left(r_{xy} + i r_{yy}\right)\frac{E^0}{\sqrt{2}}\hat{\mathbf{y}}. \tag{4.44}$$

Also, the outgoing wave can be written in terms of circularly polarised light as:

$$\boldsymbol{E}^{out} = r_{++}\frac{E^0}{\sqrt{2}}(\hat{\mathbf{x}} + i\hat{\mathbf{y}}) + r_{+-}\frac{E^0}{\sqrt{2}}(\hat{\mathbf{x}} - i\hat{\mathbf{y}}). \tag{4.45}$$

By solving the last two equations for r_{++} and r_{+-}, we find

$$r_{++} = \frac{1}{2}\left[r_{xx} + r_{yy} + i\left(-r_{xy} + r_{yx}\right)\right] \tag{4.46}$$

and

$$r_{+-} = \frac{1}{2}\left[r_{xx} - r_{yy} + i\left(r_{xy} + r_{yx}\right)\right]. \tag{4.47}$$

Similarly, for right incoming circularly polarised light circularly polarised light, $\boldsymbol{\sigma}^{-}$, we get:

$$r_{-+} = \frac{1}{2}\left[r_{xx} - r_{yy} - i\left(r_{xy} + r_{yx}\right)\right] \tag{4.48}$$

and

$$r_{--} = \frac{1}{2}\left[r_{xx} + r_{yy} + i\left(r_{xy} - r_{yx}\right)\right]. \tag{4.49}$$

The reflectivities for circular polarisations are calculated by the following relations:

$$\begin{aligned} R_{++} &= |r_{++}|^2, \\ R_{+-} &= |r_{+-}|^2, \\ R_{-+} &= |r_{-+}|^2, \\ R_{--} &= |r_{--}|^2. \end{aligned} \tag{4.50}$$

In this work, we choose to deal with circularly birefringent materials. In this type of material, the circularly polarised eigenstates propagate through the medium without any change or mixing in the eigenstates. This fact means r_{+-} and r_{-+} must be zero, and that implies the following relationships for linear polarisation $r_{xx} = r_{yy}$ and $r_{xy} = -r_{yx}$.

4.3.2 Results and Discussion

Reflectivity spectra, shown in figure 4.6, were calculated for both right, R_{--}, and left, R_{++}, circularly polarised light at a normal incidence of light for a single circularly birefringent layer, bismuth-substituted yttrium iron garnet ($Bi{:}YIG$), on a glass

substrate, ignoring absorption for simplicity. To provide a general idea about how our code worked, the parameters of this simple film and the refractive index of glass substrate were taken from Kato *et al.*,(2003) as the following: for $Bi{:}YIG$, $\varepsilon_{xx} = 5.59$; $\varepsilon_{xy} = -0.00369$; at $\lambda = 720\,nm$, its thickness was equal to $\lambda/2\sqrt{\varepsilon_{xx}}$ and the refractive index of the glass substrate was $n_s = 1.52$. For a given ω, the left $(\boldsymbol{\sigma}^{+})$ circularly polarised light has a lower value of wave vector q^{-}, and hence a higher speed than that of the right. The difference between the spectra of left and right circularly polarised light is very small, as is apparent in figure 4.6, because the value of ε_{xy} is small in a real medium. This means the waves propagate with only slightly different speeds. We know physically that the use of circularly birefringent materials implies $r_{+-} = r_{-+} = 0$. The reflectivity values of R_{+-} and R_{-+} were found to be equal to approximately zero with numerical errors, so that confirmed the calculations have worked as we expected. In addition, since, on this scale, there is negligible difference between the two circularly polarised lights, the reflectivity spectrum of *x*-polarised light, R_{xx} is also identical.

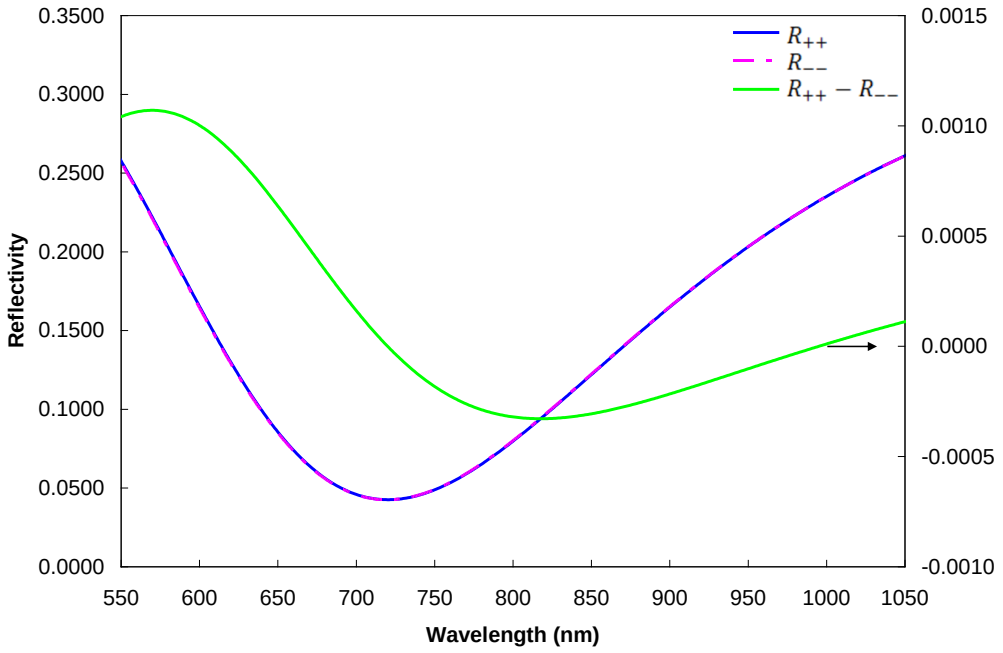

Figure 4.6: Reflectivity spectra at normal incidence for both right, R_{--}, and left, R_{++}, circularly polarised lights. The difference between them is shown by the green curve.

For the purpose of studying the Kerr rotation, the reflectivity spectrum, R_{xy} for linearly incoming *x*-polarised and outgoing y-polarised light was also calculated using $R_{xy} = |r_{xy}|^2$. As shown in figure 4.7, these reflectivity values are very small of order $\sim 10^{-7}$, because of the small value of ε_{xy}.

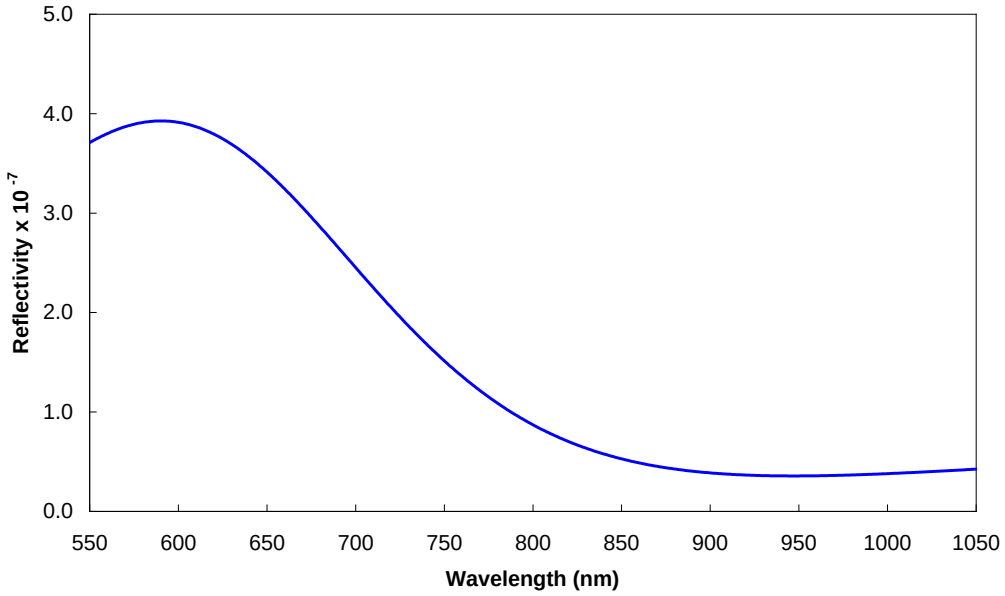

Figure 4.7: Reflectivity spectrum for linearly polarised light, R_{xy} at normal incidence.

Figure 4.8 shows Kerr and Faraday ellipticity spectra that are calculated using equation 3.2 in the reflectivity and transmission terms, respectively. Figure 4.9 shows the corresponding rotation spectra for $Bi{:}YIG$ on a glass transparent substrate using equation 3.3. It should be pointed out because there is no absorption in this calculation, we can only see the Kerr rotation because the reflection from the back of the film (the multiple reflections). Clearly, from figure 4.8, the Kerr ellipticity is zero approximately at the resonant wavelength, $\lambda = 720\, nm$, where the reflectivity value has a minimum (see figure 4.6). However, as shown in figure 4.9, the rotation has a maximum at that wavelength. Figure 4.9 shows small rotation angles for this simple layer. To obtain high Kerr rotation angles, a cavity structure will be investigated below.

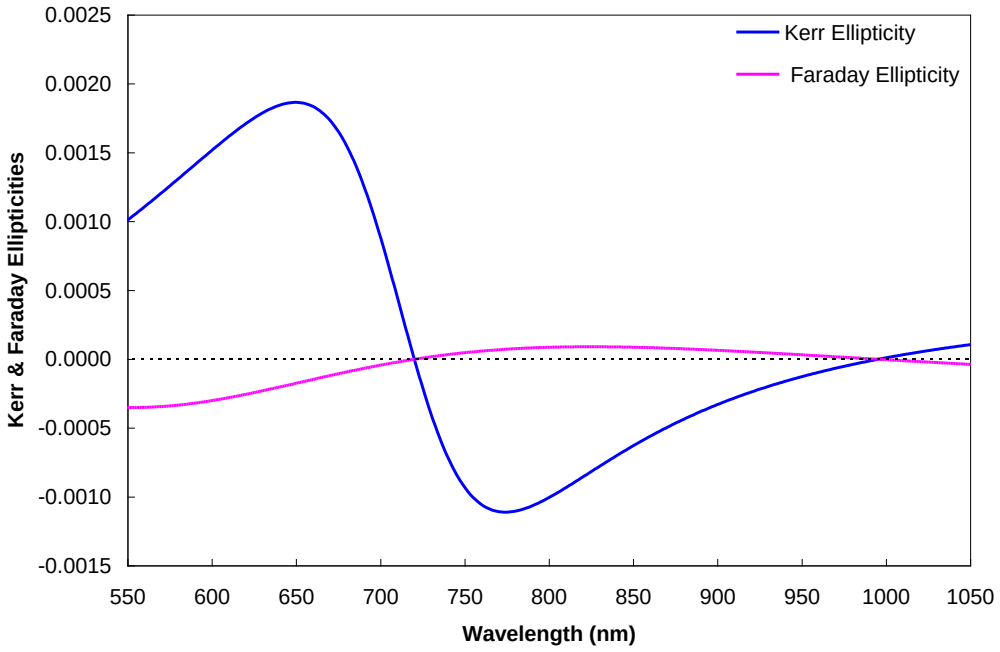

Figure 4.8: Kerr and Faraday ellipticity spectra for a simple $Bi{:}YIG$ film.

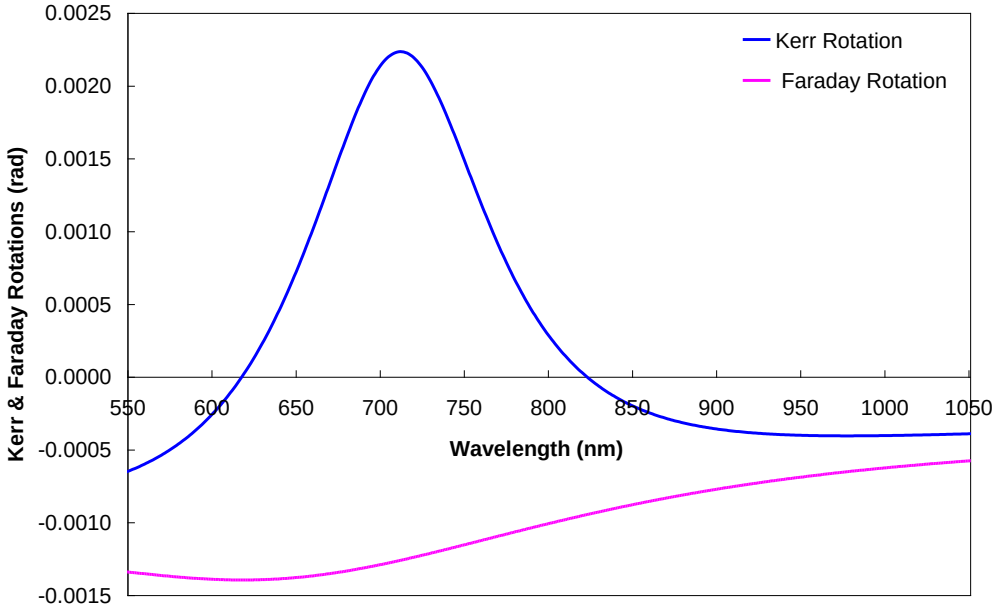

Figure 4.9: Kerr and Faraday rotation spectra for a simple $Bi{:}YIG$ film.

We studied a cavity structure $(Ta_2O_5/SiO_2)^6\ /Bi{:}YIG/(SiO_2/Ta_2O_5)^6$ which was taken from Kato *et al.*,(2003). This structure consists of a circularly birefringent thin film, $Bi{:}YIG,$ with the dielectric Bragg mirrors on each side. Ignoring absorption, the parameters of this cavity structure were taken from Kato *et al.*,(2003) as mentioned above. Reflectivity spectrum shown in figure 4.10 was calculated for linearly *x*-polarised light, R_{xx}, at normal incidence. Figure 4.10 shows high reflectivity values in the stop-band of the dielectric Bragg mirrors. A sharp dip is also apparent because of the cavity layer.

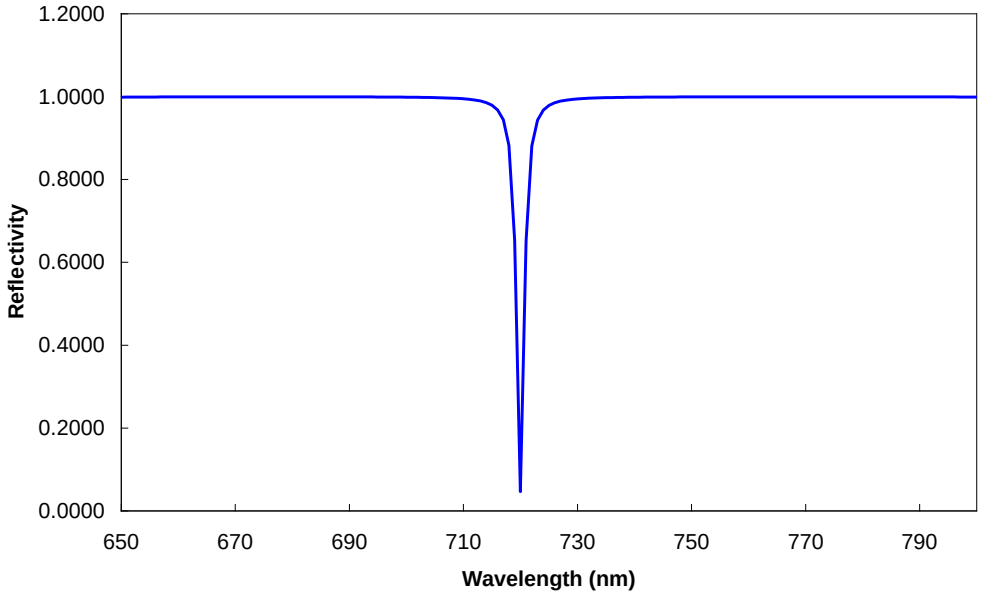

Figure 4.10: Reflectivity spectrum of linearly polarised light, R_{xx} for $(Ta_2O_5/SiO_2)^6\ /Bi{:}YIG/(SiO_2/Ta_2O_5)^6$.

Figure 4.11 shows the Kerr ellipticity spectrum of the structure. This was calculated using Sato's definition of ellipticity (see equation 3.2). The Kerr rotation spectrum in the cavity region, is shown in figure 4.12. At the resonant wavelength,

$\lambda = 720\ nm$ the maximum Kerr rotation is ~ 0.380 *rad* compared with 0.0022 *rad* for a simple film. Hence, the cavity structure enhances the magneto-optical rotation effect.

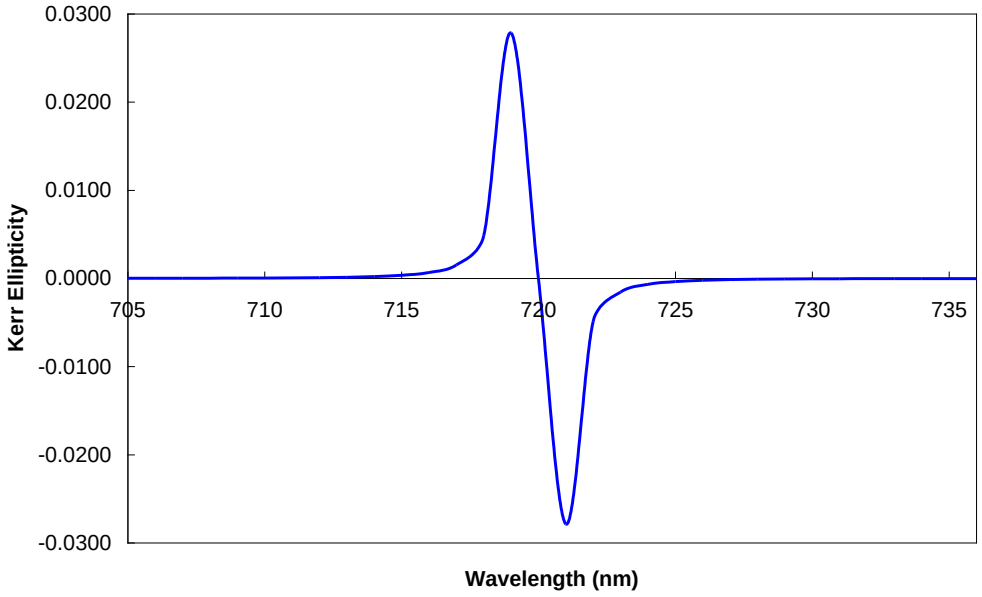

Figure 4.11: Kerr ellipticity for $(Ta_2O_5/SiO_2)^6\ /Bi{:}YIG/(SiO_2/Ta_2O_5)^6$.

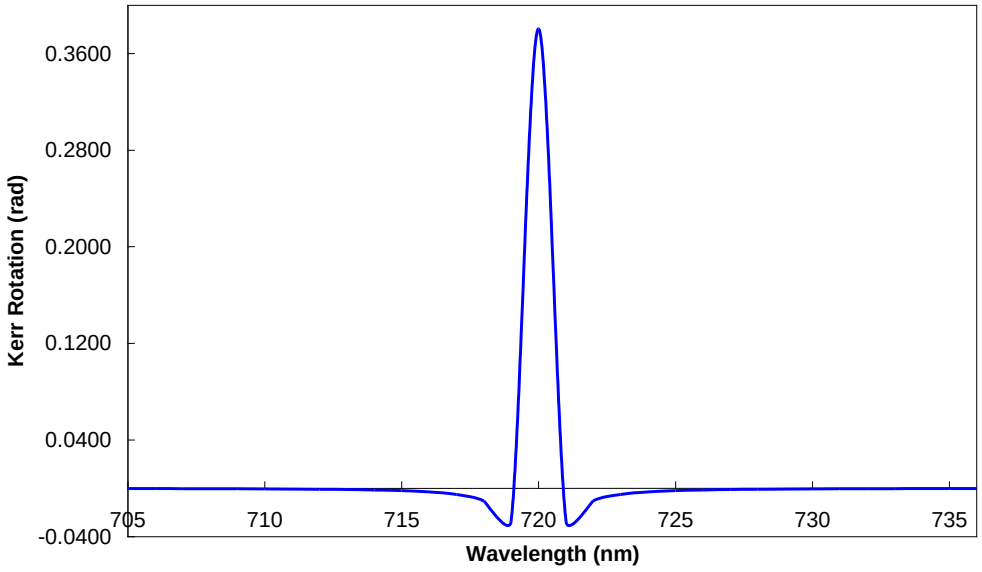

Figure 4.12: Kerr rotation for $(Ta_2O_5/SiO_2)^6\ /Bi{:}YIG/(SiO_2/Ta_2O_5)^6$.

In 2010, Dong *et al.* pointed out that the enhancement of the Faraday rotation could be valuable in the design of sensitive magneto-optical filters and optical isolators. To check our calculations against previous work, our numerical results were compared with those of Dong *et al.* (2010). The reflectivity, transmission and Faraday rotation spectra were calculated for the cavity structure, $(SiO_2/TiO_2)^6\ /Co_6Ag_{94}/SiO_2$, which was taken from Dong *et al.* (2010). The cavity mode is confined between the Bragg mirrors and the Co_6Ag_{94} magnetic metal layer.

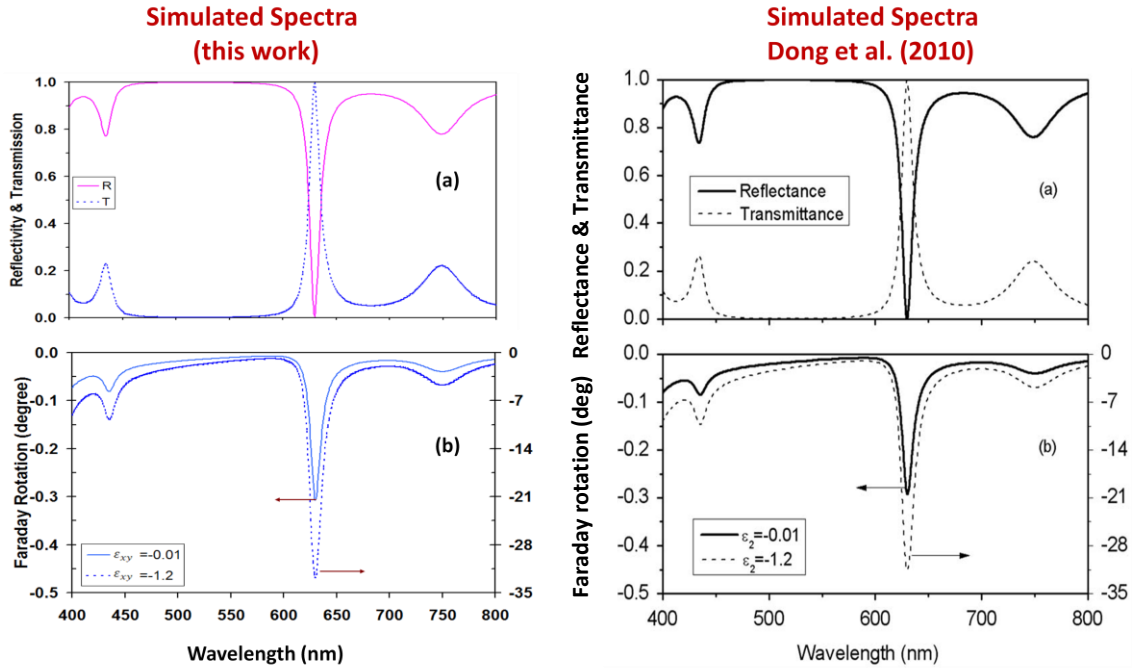

Figure 4.13: Simulated spectra of reflectivity, transmittance and Faraday rotation for $(SiO_2/TiO_2)^6\ /Co_6Ag_{94}/SiO_2$. The right figures (a) and (b) are reprinted with permission from [*Journal of Applied Physics* **107**, 093101. 'Enhancement of Faraday rotation effect in heterostructures with magneto-optical metals' Dong, L., Jiang, H., Chen, H., and Shi, Y.]. Copyright [2010], AIP Publishing LLC. http://dx.doi.org/10.1063/1.3406152 (courtesy of Dong, L).

The parameters of the cavity structure were taken from Dong *et al*. (2010) as the following: $n_{SiO_2} = 1.443$, $n_{Ta_2O_5} = 2.327$, and the layer thicknesses are 90 *nm* and 59.5 *nm* respectively, while for the last layer of SiO_2 the thickness is 20 *nm*. For the metallic Co_6Ag_{94}, ε_{xx} is a function of ω given by $\varepsilon_{xx} = 1 - \left(\omega_p^2/\omega^2 + i\,\omega\,\gamma\right)$; where $\omega_p = 9.9 \times 10^{15}$ Hz is the electronic plasma frequency and $\gamma = 0$ is the damping. The Faraday rotation calculations are performed for weak and strong birefringence $\varepsilon_{xy} = -0.01$; or $\varepsilon_{xy} = -1.2$, in both cases the maximum Faraday rotation occurs at $631\ nm$. The layer thickness was equal to 50.8 *nm*. We set the substrate refractive index as $n_s = 1.0$. Very good agreement is obtained for the reflectivity and transmission spectra, shown in figure 4.13-a. Figure 4.13-b shows similarly good agreement for the Faraday rotations at both small and large ε_{xy} values.

4.4 Conclusions

In this chapter, a multilayer structure of photonic crystal, such as the quarter-wave stack, was modelled for isotropic and anisotropic materials which display circular birefringence. Maxwell's equations were used to derive the transfer matrices for these media. These matrices were used to calculate the reflectivity spectra of isotropic media at a finite incident angle. In circularly birefringent media, the reflectivity spectra for both right and left circularly polarised lights were calculated at normal incidence of light. Magneto-optical spectra were calculated for a simple layer and cavity structure. The cavity structure enhanced magneto-optical effects and this result agreed well with previous work.

CHAPTER 5

EFFECT OF INCOHERENT BACK SUBSTRATE REFLECTIONS

The previous chapter has investigated a single layer and a cavity structure with circularly birefringent materials, when those were deposited on an infinite substrate. Major issue raised in this chapter is the consequence of using a thick but finite transparent substrate in place of an infinite one, on the optical and magneto-optical properties of circularly birefringent structures. The contribution of the incoherent back reflections within such a substrate will be considered.

5.1 Introduction

The interference fringes of transmission spectra have been used by Swanepoel (1983) to determine the thickness and optical constants of a thin absorbing film on a thick transparent substrate. He studied the contribution of incoherent multiple reflections from the back of this substrate. In 1986, Harbecke published a paper in which he considered a method that included coherent and incoherent multiple reflections concepts to calculate the transmission and reflectivity spectra for multilayer structures. A recent study of transmission and reflection by Whittaker and Gehring (2010), for both a multilayer micro-cavity and an opal structure, involved the contributions of multiple incoherent reflections from a finite substrate, more details will be given in section 5.2. Numerous studies have revealed that a thick substrate layer leads to unrealistic fine Fabry-Perot fringes in the spectra if reflections within the substrate are

treated coherently (for example, Harbecke, 1986 ; Whittaker and Gehring, 2010). To address this issue a formulism using incoherent multiple reflections in the substrate was applied in those studies. The existent of incoherent reflections can be ascribed to several possible reasons: the finite angular resolution of the measurement, since a slight change in the angle leads to differences in path lengths and consequently different fringes. Whittaker and Gehring (2010) speculated that due to in-homogeneities in the substrate, the light will be scattered at different angles. A possible explanation could also be related to experimental procedures, either the limitation of measurement resolution or the source bandwidth. Another factor is the non parallel surfaces of the thick layer (Katsidis and Siapkas, 2002).

5.2 Theory and calculations

Before describing our theory and to illustrate the problem, let us assume light is incident in the normal direction on a multilayer $(SiO_2/Ta_2O_5)^2$, placed on a thick finite transparent substrate. Initially, consider the multiple reflections within this substrate to be coherent. As a consequence, closely spaced Fabry-Perot fringes occur, shown by the blue curve in figure 5.1, which are not observed experimentally. However, by modifying our treatment with incoherent multiple back reflections the spectrum became more realistic as shown in the same figure by the pink curve.

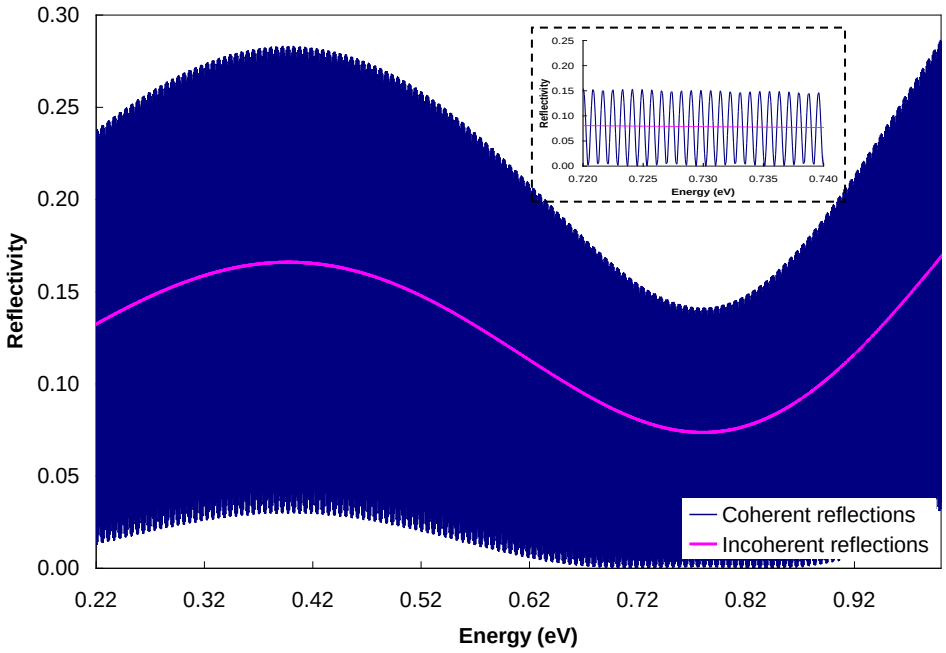

Figure 5.1: Simulated reflectivity spectra result from coherent and incoherent treatments for $(SiO_2/Ta_2O_5)^2$. For clarity, the insert displays a small energy range.

As mentioned above, Whittaker and Gehring (2010) calculated the transmission and reflection including the multiple incoherent reflections in substrate for a multilayer micro-cavity and an opal structure, which are not circularly birefringent materials. Here, we follow their method but for circularly birefringent materials where the polarisation properties for each of the multiply reflected beams are important and also calculate the magneto-optical effects. The total reflectivity is explained by Whittaker and Gehring (2010) as the reflectivity from the film plus the summation of an unlimited number of incoherent reflections from the substrate surfaces. Attenuation also occurs on each reflection from the substrate if an absorbing substrate is used. The expression for total reflectivity given by those authors, for a structure on a transparent isotropic substrate is the following:

$$R = R_f + T_f \left[1 + R_b \tilde{R}_f \, e^{-2\alpha h_s} + (R_b \tilde{R}_f \, e^{-2\alpha h_s})^2 + \cdots \right] R_b \tilde{T}_f \, e^{-2\alpha h_s},$$

$$= R_f + T_f \, (1 - e^{-2\alpha h_s} R_b \tilde{R}_f \,)^{-1} R_b \tilde{T}_f \, e^{-\alpha h_s}, \tag{5.1}$$

Similarly the transmission, T, is:

$$T = T_f \left[1 + R_b \tilde{R}_f \, e^{-2\alpha h_s} + (R_b \tilde{R}_f \, e^{-2\alpha h_s})^2 + \cdots \right] T_b e^{-\alpha h_s}$$

$$= T_f \, (1 - e^{-2\alpha h_s} R_b \tilde{R}_f)^{-1} T_b e^{-\alpha h_s}, \tag{5.2}$$

In equations 5.1 and 5.2 and as used in figure 5.2, R_f and T_f are the reflectivity and transmission of a structure, when waves travel from air into the transparent substrate going through this structure. $\tilde{R}_f$ and $\tilde{T}_f$ are the reflectivity and transmission for the reverse direction. The transfer matrix is used to find these front coefficients. R_b and T_b are the reflectivity and transmission of the back of the substrate, *i.e.*, from the substrate to air. These coefficients are found from the Fresnel expressions. α and h_s are the absorption coefficient and thickness of substrate, respectively. These expressions for *R* and *T* are fine if the polarisation does not change or mix when waves propagate through the medium. If the changing or mixing of polarisations occur, we should deal with reflectivities and transmissions in these expressions as matrices (Whittaker and Gehring, 2010), we could do this with any pair of orthogonal polarisation states as a basis, and we chose *x* and *y* linear states for example, T_f is replaced by 2×2 matrix $\begin{pmatrix} T_{fxx} & T_{fyx} \\ T_{fxy} & T_{fyy} \end{pmatrix}$ and similar for others reflectivities and transmissions. These are obtained from matrices for amplitudes such as $\begin{pmatrix} t_{xx} & t_{yx} \\ t_{xy} & t_{yy} \end{pmatrix}$. This choice then implies

we do the transfer matrix calculation with basis $\begin{pmatrix} E_x^0 \\ E_y^0 \end{pmatrix}$. The amplitude coefficient matrices are defined as the following:

$$\underline{t} = \begin{pmatrix} t_{xx} & t_{yx} \\ t_{xy} & t_{yy} \end{pmatrix}, \qquad \underline{r} = \begin{pmatrix} r_{xx} & r_{yx} \\ r_{xy} & r_{yy} \end{pmatrix},$$
$$\underline{\tilde{t}} = \begin{pmatrix} \tilde{t}_{xx} & \tilde{t}_{yx} \\ \tilde{t}_{xy} & \tilde{t}_{yy} \end{pmatrix}, \qquad \underline{\tilde{r}} = \begin{pmatrix} \tilde{r}_{xx} & \tilde{r}_{yx} \\ \tilde{r}_{xy} & \tilde{r}_{yy} \end{pmatrix}, \tag{5.3}$$
$$\underline{t_b} = \begin{pmatrix} t^b & 0 \\ 0 & t^b \end{pmatrix}, \qquad \underline{r_b} = \begin{pmatrix} r^b & 0 \\ 0 & r^b \end{pmatrix},$$

The first and second subscripts of the matrix elements refer to incoming and outgoing waves, respectively.

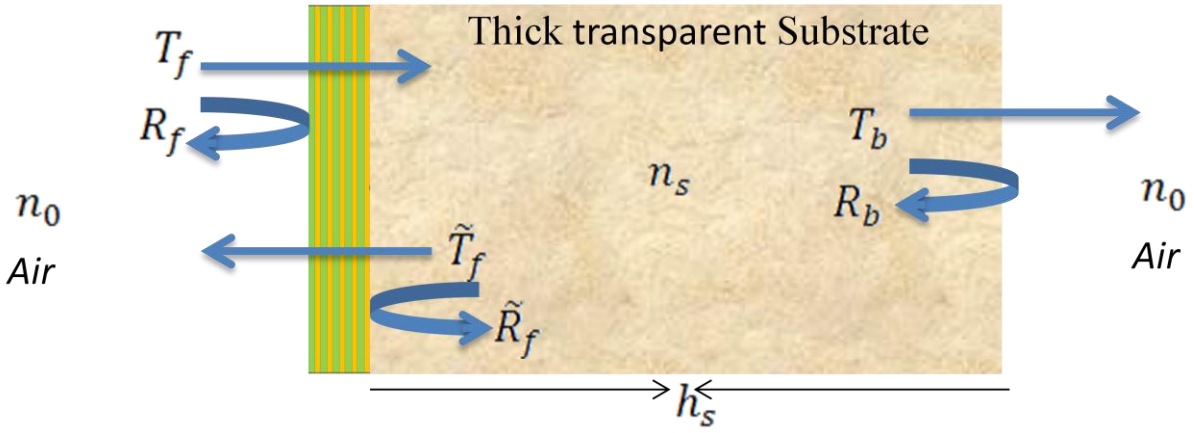

Figure 5.2: Illustrating the parameters used in equations 5.1 and 5.2. n_0 is the air refractive index, n_s is the substrate refractive index and h_s is the substrate thickness. Adapted from Whittaker and Gehring (2010).

Here $\underline{t}$ and $\underline{r}$ are the amplitude coefficient matrices of transmission and reflection of the front of a structure, *i.e.*, wave travelling from air into the substrate

going through the structure. The matrix elements are calculated as explained for the forward direction in Chapter 4 (see equations 4.41 and 4.42).

$\underline{\tilde{t}}$ and $\underline{\tilde{r}}$ are the amplitude coefficient matrices of transmission and reflection for the opposite direction, *i.e.*, wave travelling from the substrate into air going through the structure. To calculate the elements for these matrices, we follow the same calculations, which were described for the forward direction in Chapter 4 but now for the reversed direction, we get for linearly incoming *x*-polarised wave:

$$\begin{pmatrix} \tilde{t}_{xx} \\ f_0\tilde{t}_{xx} \\ \tilde{t}_{xy} \\ -f_0\tilde{t}_{xy} \end{pmatrix} = \begin{pmatrix} \widetilde{m}_{11} & \widetilde{m}_{12} & \widetilde{m}_{13} & \widetilde{m}_{14} \\ \widetilde{m}_{21} & \widetilde{m}_{22} & \widetilde{m}_{23} & \widetilde{m}_{24} \\ \widetilde{m}_{31} & \widetilde{m}_{32} & \widetilde{m}_{33} & \widetilde{m}_{34} \\ \widetilde{m}_{41} & \widetilde{m}_{42} & \widetilde{m}_{43} & \widetilde{m}_{44} \end{pmatrix} \begin{pmatrix} 1+\tilde{r}_{xx} \\ f_s(1-\tilde{r}_{xx}) \\ \tilde{r}_{xy} \\ f_s\tilde{r}_{xy} \end{pmatrix}, \tag{5.4}$$

where $\widetilde{M}$ is the 4×4 transfer matrix of the circularly birefringent structure for a reverse direction. $f_0 = q_0/\omega$, and $f_s = q_s/\omega$, here, the index s denotes the substrate layer, while the index *0* denotes the surface (air). Solving equation 5.4 gives $\tilde{r}_{xx}, \tilde{r}_{xy}, \tilde{t}_{xx}$ and $\tilde{t}_{xy}$. Similarly, for linearly incoming *y*-polarised wave we get:

$$\begin{pmatrix} \tilde{t}_{yx} \\ f_0\tilde{t}_{yx} \\ \tilde{t}_{yy} \\ -f_0\tilde{t}_{yy} \end{pmatrix} = \begin{pmatrix} \widetilde{m}_{11} & \widetilde{m}_{12} & \widetilde{m}_{13} & \widetilde{m}_{14} \\ \widetilde{m}_{21} & \widetilde{m}_{22} & \widetilde{m}_{23} & \widetilde{m}_{24} \\ \widetilde{m}_{31} & \widetilde{m}_{32} & \widetilde{m}_{33} & \widetilde{m}_{34} \\ \widetilde{m}_{41} & \widetilde{m}_{42} & \widetilde{m}_{43} & \widetilde{m}_{44} \end{pmatrix} \begin{pmatrix} \tilde{r}_{yx} \\ -f_s\tilde{r}_{yx} \\ 1+\tilde{r}_{yy} \\ -f_s(1-\tilde{r}_{yy}) \end{pmatrix}, \tag{5.5}$$

solving equation 5.5 gives $\tilde{r}_{yy}, \tilde{r}_{yx}, \tilde{t}_{yy}$ and $\tilde{t}_{yx}$. In the same way, as in Chapter 4, we can find the circular reflection coefficients, $\tilde{r}_{\pm\pm}$.

$\underline{t_b}$ and $\underline{r_b}$ are the amplitude coefficient matrices of transmission and reflection of the back substrate, *i.e.*, from the substrate to air. Fresnel's equations at a normal incidence are used to calculate the elements of both matrices $\underline{t_b}$ and $\underline{r_b}$, as the following:

$$t^b = \frac{2n_0}{n_s + n_0}, \qquad r^b = \frac{n_s - n_0}{n_s + n_0}, \tag{5.6}$$

It should be pointed out in the special case of circular polarised bases, because there is no polarisation mixing, the situation becomes simple and the matrix treatment is not needed. We could use equation 5.1 or 5.2 separately for left and right polarised light, *i.e*. we can adapted equation 5.1 for example, as $R_{\pm\pm}$ corresponding either dealing with left or right circularly polarised light.

Using equation 5.1, the reflectivity spectra for both left and right circularly polarised light can be found (case of adding the incoherent back reflections within the substrate). To calculate the magneto-optic effect, we need to re-work the calculations of Chapter 4 according for the incoherent contributions. Since now only the reflected intensities are known and the phase information is not defined, we cannot use Sato's (1981) definition for Kerr rotation, *i.e.*, equation 3.3. Each reflection term in equation 5.1 itself is coherent, but relative to the others is incoherent, see figure 5.3. To define fully the polarisation, we need the three Stokes' parameters, $S_1, S_2,$ and S_3, corresponding to linear polarisation, linear diagonal polarisation and circular polarisation as was mentioned in Chapter 3.

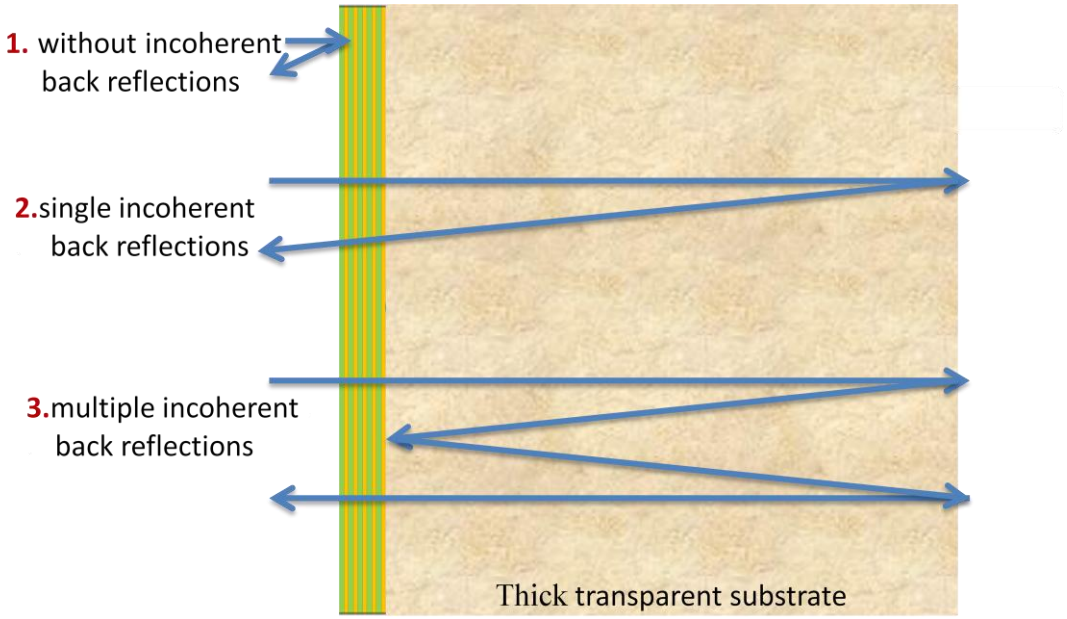

Figure 5.3: Illustrating the three possible types of reflections.

Let us consider a linearly incoming wave, *x*-polarised incident normally on a structure with circularly birefringent properties. Suppose the structure is deposited on a thick but finite substrate. There are multiple coherent reflections inside the thin film as well as multiple incoherent reflections within the substrate (Johs *et al.*, 1994). Because we need to know the polarisation properties for each of the multiply reflected beams, *i.e.* Stokes' parameters, we will need to do three basses, and then reset the transfer matrix in them. Therefore, we will deal with the reflectivities and transmissions in equations 5.1 and 5.2 as matrices but with the following treatment. The analysis of matrix treatment is illustrated schematically in figure 5.4 for multiple reflection and transmission amplitudes within the substrate. Here the basis of *x*- polarised wave, $\binom{1}{0}$, is used.

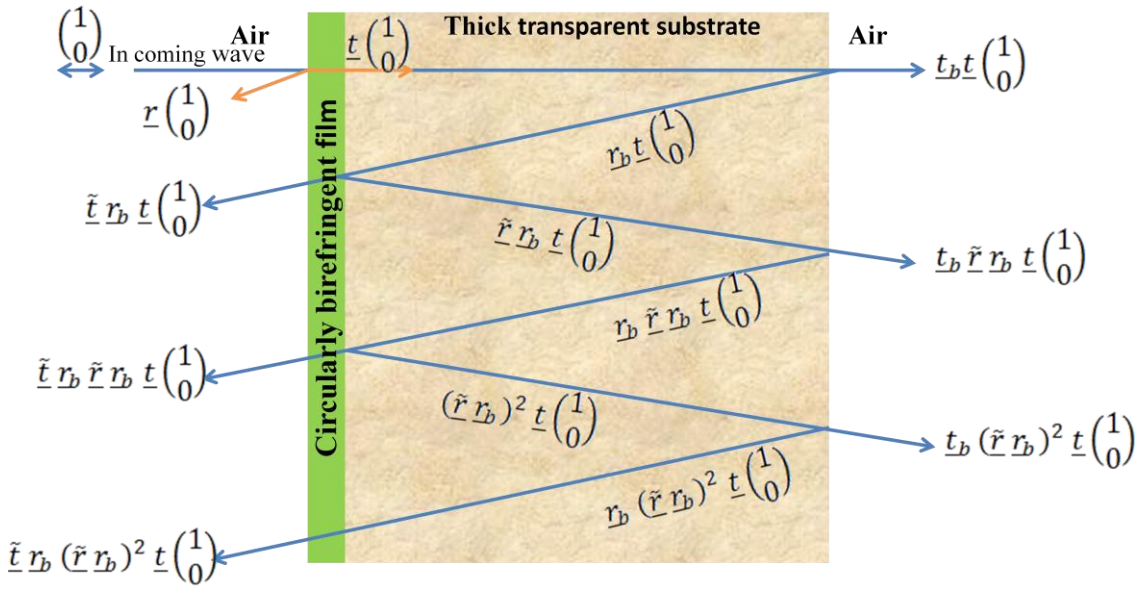

Figure 5.4: Schematic diagram of multiple incoherent reflection and transmission amplitudes in a thick substrate. For clarity, the rays are drawn at small angles.

In general, the amplitude of the n^{th} reflection term can be written as

$$\underline{\tilde{t}}\,\underline{r_b}\,(\underline{\tilde{r}}\,\underline{r_b})^n\,\underline{t}\begin{pmatrix}1\\0\end{pmatrix}. \tag{5.7}$$

Similarly, the amplitude of the n^{th} transmission term can be written as

$$\underline{t_b}\,(\underline{\tilde{r}}\,\underline{r_b})^n\,\underline{t}\begin{pmatrix}1\\0\end{pmatrix}, \tag{5.8}$$

where the amplitude coefficient matrices are defined by equation 5.3 and used in figure 5.4

Following this, the projection matrix, for example, $\underline{P_x}$, of linear *x*-polarisation is acted on amplitude expressions (5.7 and 5.8). To find the intensity in that projection, we take the modulus square and use the fact for any projection matrix, $\underline{P}^2 = \underline{P}$. We get the intensity in *x*-polarisation of the n^{th} reflection term as:

$$(1 \quad 0)\, \underline{t}^{\dagger}\, (\underline{r_b}^{\dagger}\underline{\tilde{r}}^{\dagger})^{n}\, \underline{r_b}^{\dagger}\, \underline{\tilde{t}}^{\dagger}\, \underline{P_x}\, \underline{\tilde{t}}\, \underline{r_b}\, (\underline{\tilde{r}}\, \underline{r_b})^{n}\, \underline{t} \begin{pmatrix} 1 \\ 0 \end{pmatrix}, \tag{5.9}$$

Similarly, the intensity in *x*-polarisation of the n^{th} transmission term is:

$$(1 \quad 0)\, \underline{t}^{\dagger}\, (\underline{r_b}^{\dagger}\underline{\tilde{r}}^{\dagger})^{n}\, \underline{t_b}^{\dagger}\, \underline{P_x}\, \underline{t_b}\, (\underline{\tilde{r}}\, \underline{r_b})^{n}\, \underline{t} \begin{pmatrix} 1 \\ 0 \end{pmatrix}. \tag{5.10}$$

After that, we add the intensity of all different numbers of reflections to obtain a suitable formula for the total reflectivity and transmission intensities in *x*-polarisation. For outgoing *x*-polarised light, these total intensities are found as:

$$R_{xx} = (1 \quad 0) \left[\underline{r}^{\dagger} \underline{P_x}\, \underline{r} + \underline{t}^{\dagger} \left(\sum_{n=0}^{\infty} (\underline{r_b}^{\dagger}\underline{\tilde{r}}^{\dagger})^{n}\, \underline{r_b}^{\dagger}\, \underline{\tilde{t}}^{\dagger} \underline{P_x}\, \underline{\tilde{t}}\, \underline{r_b}\, (\underline{\tilde{r}}\, \underline{r_b})^{n} \right) \underline{t} \right] \begin{pmatrix} 1 \\ 0 \end{pmatrix}, \tag{5.11}$$

$$T_{xx} = (1 \quad 0)\, \underline{t}^{\dagger} \left(\sum_{n=0}^{\infty} (\underline{r_b}^{\dagger}\underline{\tilde{r}}^{\dagger})^{n}\, \underline{t_b}^{\dagger}\, \underline{P_x}\, \underline{t_b}\, (\underline{\tilde{r}}\, \underline{r_b})^{n} \right) \underline{t} \begin{pmatrix} 1 \\ 0 \end{pmatrix}. \tag{5.12}$$

In equation 5.11, the term $(1 \quad 0)\, \underline{r}^{\dagger} \underline{P_x}\, \underline{r} \begin{pmatrix} 1 \\ 0 \end{pmatrix}$ refers to the reflectivity from the film. To calculate the infinite sums, we define the following matrices. $A = \underline{r_b}^{\dagger}\, \underline{\tilde{r}}^{\dagger}$, $B = \underline{r_b}^{\dagger} \underline{\tilde{t}}^{\dagger} \underline{P_x} \underline{\tilde{t}}\, \underline{r_b}$ for equation 5.11 or $B = \underline{t_b}^{\dagger} \underline{P_x} \underline{t_b}$ for equation 5.12 and C= $\underline{\tilde{r}}\, \underline{r_b}$. Then, the expansion of the infinite summations can be rewritten as:

$$\mathcal{S} = A^0 B C^0 + A^1 B C^1 + A^2 B C^2 + \cdots \quad , \tag{5.13}$$

where the superscripts are integers , by multiplying equation 5.13 by *A* from the left and by *C* from the right, we obtain:

$$A\mathcal{S}C = A^1 B C^1 + A^2 B C^2 + \cdots \quad . \tag{5.14}$$

Subtracting the last two equations gives rise to:

$$\mathcal{S} - A\mathcal{S}C = B, \tag{5.15}$$

in matrix elements notation for $\mathcal{S}$, *A*, *B* and *C* this gives:

$$\mathcal{S}_{11} - A_{11}\mathcal{S}_{11}C_{11} - A_{12}\mathcal{S}_{21}C_{11} - A_{11}\mathcal{S}_{12}C_{21} - A_{12}\mathcal{S}_{22}C_{21} = B_{11}, \quad (5.16)$$

$$\mathcal{S}_{21} - A_{21}\mathcal{S}_{11}C_{11} - A_{22}\mathcal{S}_{21}C_{11} - A_{21}\mathcal{S}_{12}C_{21} - A_{22}\mathcal{S}_{22}C_{21} = B_{21}, \quad (5.17)$$

$$\mathcal{S}_{12} - A_{11}\mathcal{S}_{11}C_{12} - A_{12}\mathcal{S}_{21}C_{12} - A_{11}\mathcal{S}_{12}C_{22} - A_{12}\mathcal{S}_{22}C_{22} = B_{12}, \quad (5.18)$$

$$\mathcal{S}_{22} - A_{21}\mathcal{S}_{11}C_{12} - A_{22}\mathcal{S}_{21}C_{12} - A_{21}\mathcal{S}_{12}C_{22} - A_{22}\mathcal{S}_{22}C_{22} = B_{22}, \quad (5.19)$$

by solving those four simultaneous equations for $\mathcal{S}_{11}$, $\mathcal{S}_{21}$, $\mathcal{S}_{12}$ and $\mathcal{S}_{22}$ the total reflectivity and transmission which are given by equations 5.11 and 5.12 respectively, can be found.

For different polarisation states, similar reflectivity and transmission expressions can be obtained just by changing the projection matrix: for outgoing y-linear polarised light, R_{xy}, outgoing a-linear diagonal polarised light at $+45^{\circ}$, R_{xa}, outgoing b-linear diagonal polarised light at -45°, R_{xb}, outgoing left circularly polarised light , R_{x+}, and outgoing right circularly polarised light , R_{x-}. These projection matrices are given by Hecht (2002) as the following:

$$\begin{aligned} \underline{P_x} &= \begin{pmatrix} 1 & 0 \\ 0 & 0 \end{pmatrix}, \qquad \underline{P_y} = \begin{pmatrix} 0 & 0 \\ 0 & 1 \end{pmatrix}, \\ \underline{P_a} &= \frac{1}{2}\begin{pmatrix} 1 & 1 \\ 1 & 1 \end{pmatrix}, \qquad \underline{P_b} = \frac{1}{2}\begin{pmatrix} 1 & -1 \\ -1 & 1 \end{pmatrix}, \\ \underline{P_+} &= \frac{1}{2}\begin{pmatrix} 1 & -i \\ +i & 1 \end{pmatrix}, \qquad \underline{P_-} = \frac{1}{2}\begin{pmatrix} 1 & +i \\ -i & 1 \end{pmatrix}. \end{aligned} \quad (5.20)$$

From the foregoing treatment, the reflected or transmitted intensities for each polarisation can be computed as is measured experimentally. As mentioned above, since the phase information can not be identified in this case, the definitions of rotation angle, ψ, which are given by Sato (1981) or Sakaguchi and Sugimoto (1999),

see equations 3.3 and 3.5 are not helpful. In contrast, equations 3.7- a, b, c can be manipulated to obtain the ellipticity, χ and rotation angle, ψ in the terms of Stokes' parameters, S_1, S_2 and S_3, which can simply be found in terms of either the reflected or transmitted intensity for each polarisation. These are (Born and Wolf, 1999):

$$\chi = \frac{1}{2}\sin^{-1}\left(\frac{S_3}{\sqrt{S_1^2 + S_2^2 + S_3^2}}\right), \tag{5.21}$$

$$\psi = \frac{1}{2}\tan^{-1}\left(\frac{S_2}{S_1}\right). \tag{5.22}$$

The Stokes' parameters can be written in term of reflectivites as:

$$\begin{aligned} S_0 &= R_{xx} + R_{xy}, \\ S_1 &= R_{xx} - R_{xy}, \\ S_2 &= R_{xa} - R_{xb}, \\ S_3 &= R_{x+} - R_{x-}. \end{aligned} \tag{5.23}$$

Equations 5.21 and 5.22 are suitable for both cases with and without incoherent back reflections. Similar procedures can be applied in dealing with transmissions.

5.3 Results and Discussion

Optical and magneto-optical effects were calculated for a simple film, $Bi{:}YIG$, ignoring the absorption of the film for simplicity. Its parameters and the refractive index of glass substrate were taken from Kato *et al.*,(2003) as mentioned in Chapter 4. Figure 5.5-a show the reflectivity spectrum for left circularly polarised light with incoherent back reflections along with that without incoherent back reflections, similarly figure 5.5-b shows the transmission spectra. We also calculated Kerr ellipticity with incoherent back

reflections by using the reflectivity results from equation 5.1 and Sato's definition (1981) of Kerr ellipticity (see equation 3.2) supposing there was air after the substrate. The results are shown in figure 5.6-a. The pink curve shows Kerr ellipticity with incoherent back reflections; and the blue curve shows Kerr ellipticity without incoherent back reflections for comparison. Inclusion of incoherent back reflections in our calculations showed a significant effect on spectra; therefore, as argued by Whittaker and Gehring (2010), ignoring the contribution of incoherent back reflections from substrate might be incorrect and this should be included in any realistic system if the substrate is transparent.

In the same way, figure 5.7 shows Faraday ellipticity spectra with and without incoherent back reflections. As can be seen from the figure, there is little effect when taking the incoherent back reflections into account. It happens because the transmission of film (in both directions) is high. Hence, most of the incident light passes through the film, and significant amount gets reflected back from the near of the substrate. Most of this passes through the film, contributing to the Kerr, with little being reflected back through the substrate to provide a contribution to the Faraday.

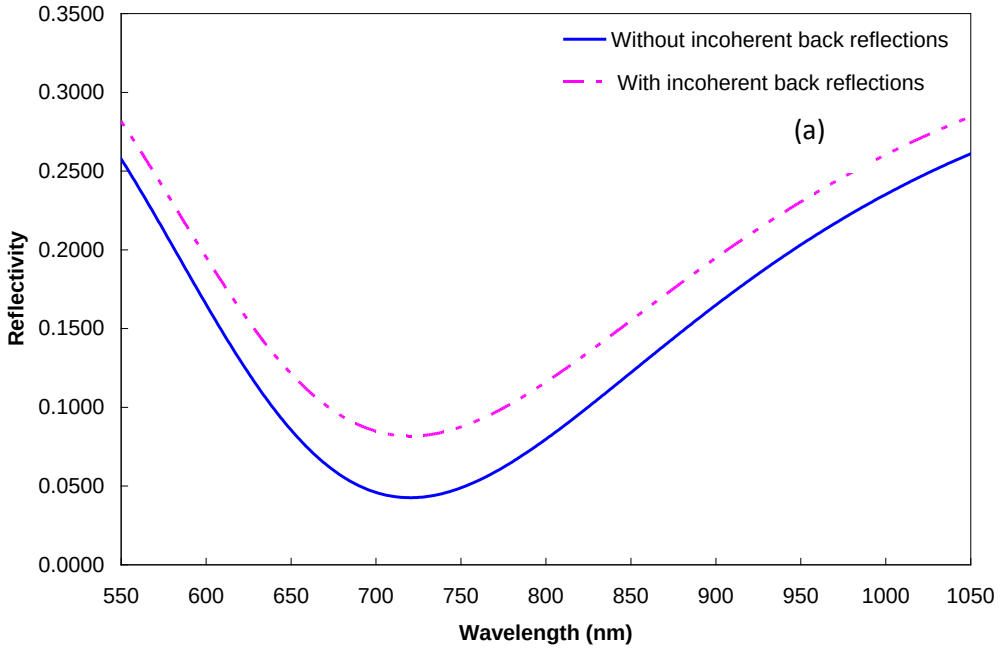

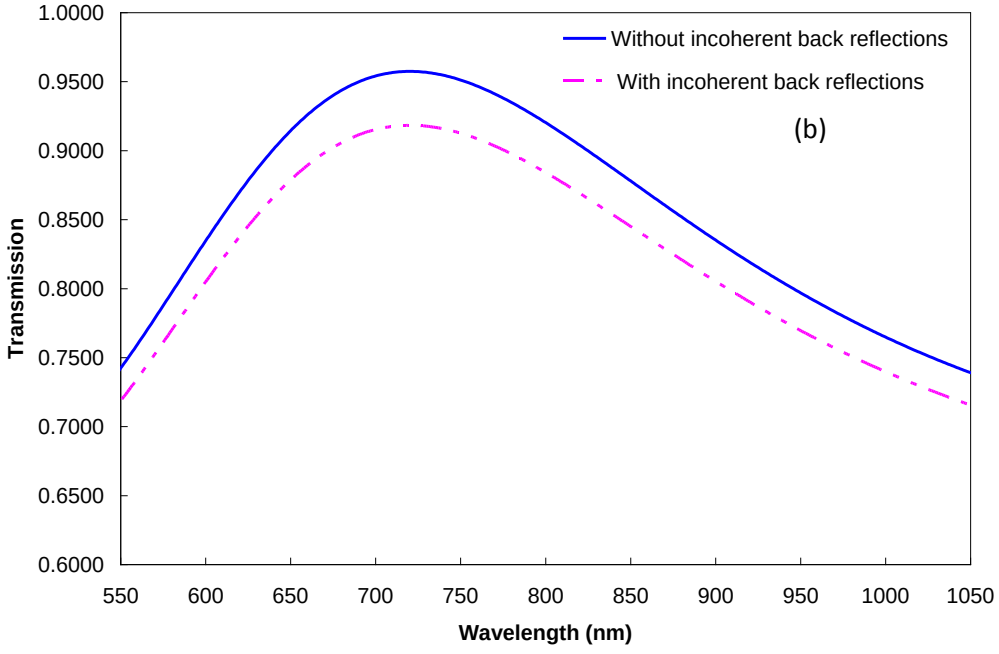

Figure 5.5: Comparison (a) reflectivity and (b) transmission spectra with and without incoherent reflections for the simple film, $Bi{:}YIG$.

To obtain stronger incoherent back reflections, a shiny metal such as silver and gold could be coated on the back of the substrate. In this case, most of the light is reflected back at the interface of the glass substrate and metal. Kerr ellipticity with incoherent back reflections was calculated, supposing there was silver after the substrate. The available value of the silver refractive index $\tilde{n} = 0.148 + i4.74$ was taken at $\lambda = 729.3\ nm$ from Palik (1998). In figure 5.6-a, the green curve shows Kerr ellipticity values. These values are very small $\sim 10^{-7}$. Figure 5.6-b shows the green curve in the magnified scale. If there is no absorption and perfect reflection from the metal, $R_{++} = R_{--}$=1, then from the definition see equation 3.2; the Kerr ellipticity is zero.

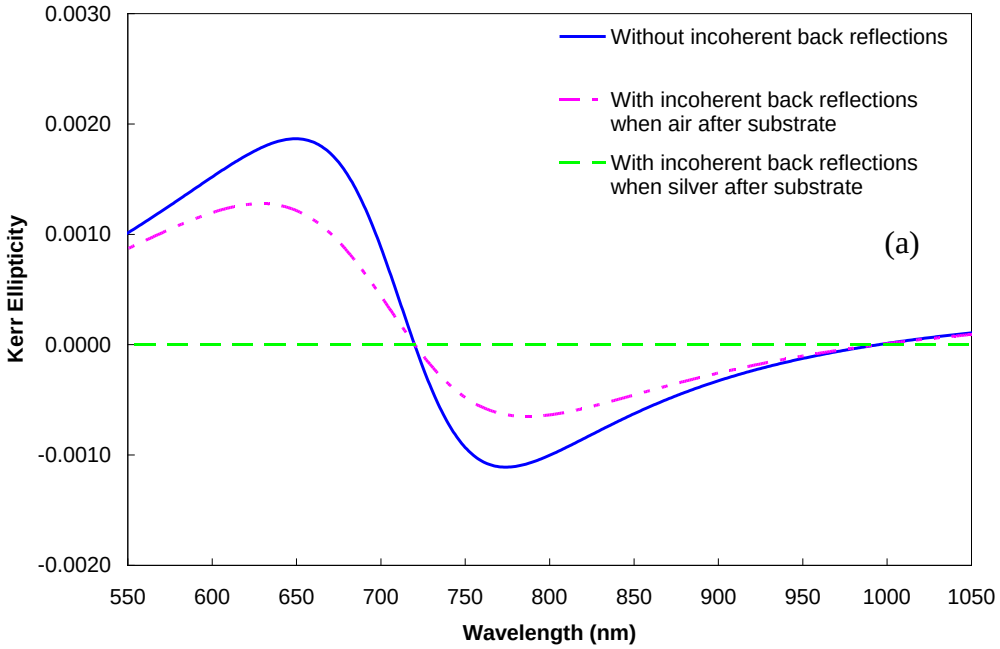

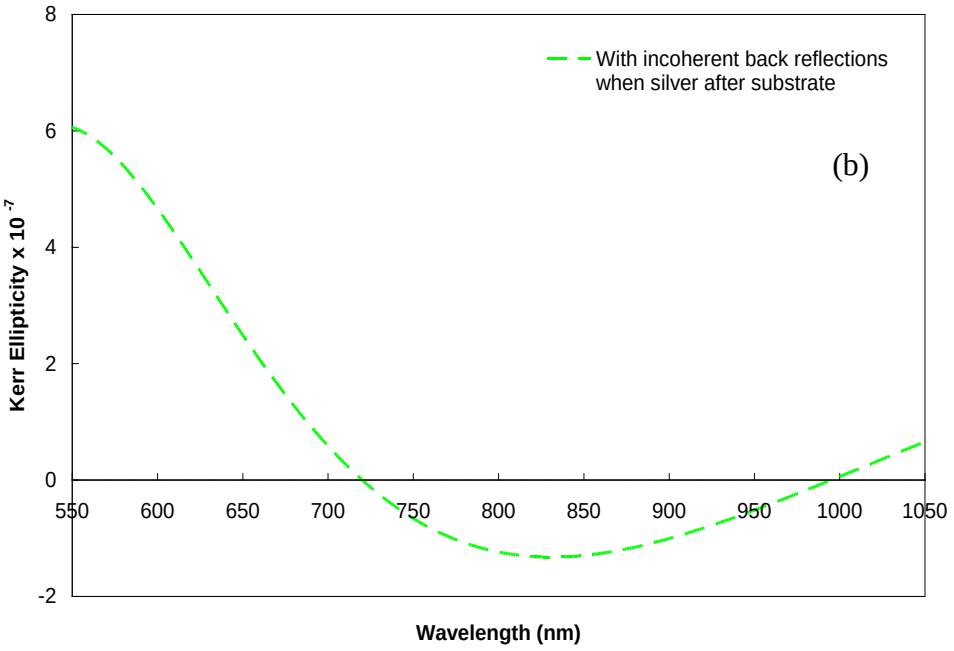

Figure 5.6: (a) Comparison with and without incoherent back reflections in Kerr ellipticity spectra for $Bi{:}YIG$ film and (b) the green spectrum is plotted in the magnified scale.

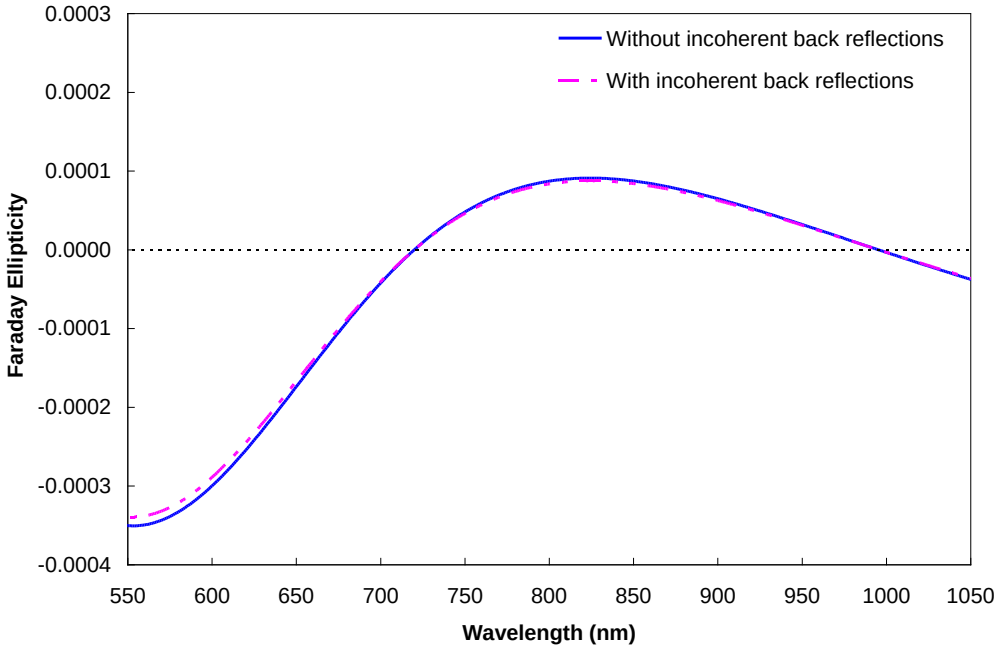

Figure 5.7: Comparison with and without incoherent back reflections in Faraday ellipticity spectra for $Bi{:}YIG$ film.

Turning now to another magneto-optical effect (rotation), we calculated Kerr rotation with incoherent back reflections using equation 5.22, supposing there was air after the substrate. The results are shown in figure 5.8. The pink curve is Kerr rotation with incoherent back reflections; and the blue curve is the Kerr rotation without incoherent back reflections for comparison. The effect of adding the incoherent back reflections in our calculations is clear in figure 5.8. As before, the green curve in figure 5.8 shows a significant change in Kerr rotation for incoherent back reflections for a structure with silver after the substrate. Similarly, Faraday rotations were calculated showing no considerable difference between both spectra with and without incoherent back reflections as seen in figure 5.9, for the same reason explained above.

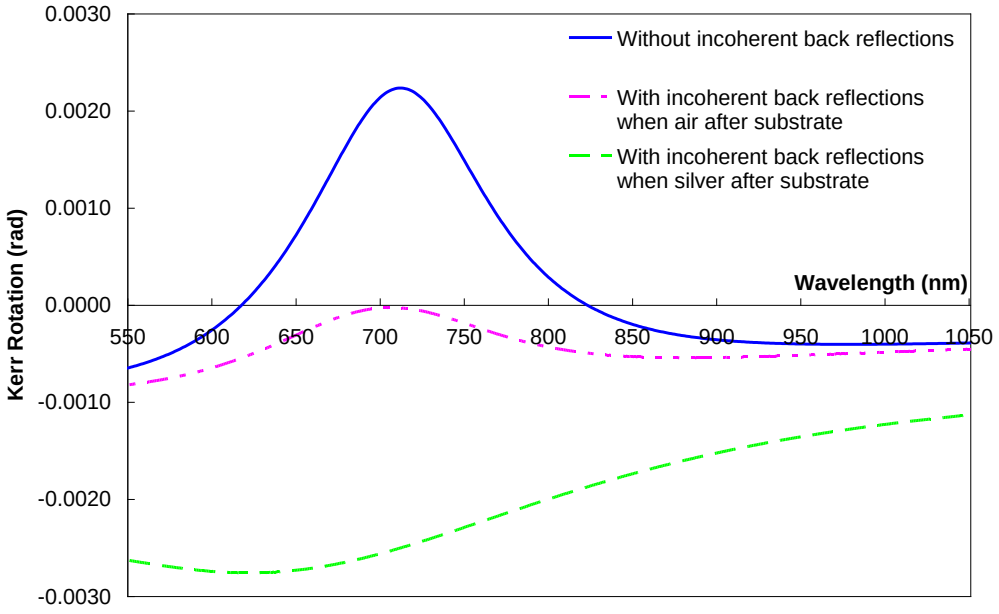

Figure 5.8: Comparison with and without incoherent back reflections in Kerr rotation spectra for $Bi{:}YIG$ film.

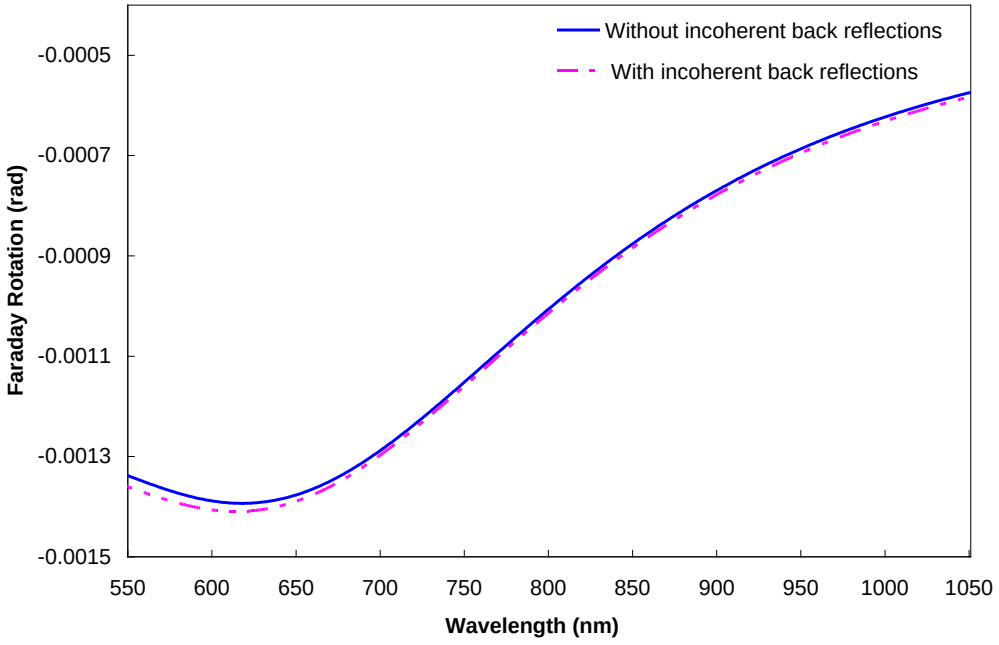

Figure 5.9: Comparison with and without incoherent back reflections in Faraday rotation spectra for $Bi{:}YIG$ film.

Lack of coherence between different reflections suggests state may not be fully polarised. Figure 5.10 shows the high degrees of polarisation for incoherent reflection that is calculated using equation 3.10, although the two reflections, the reflected light from the film and the reflected light from the first back reflection, are incoherent relative to each other. It is difficult to explain this result, but it might be the different reflections have similar polarisation states; just being incoherent does not necessary reduce degree of polarisation.

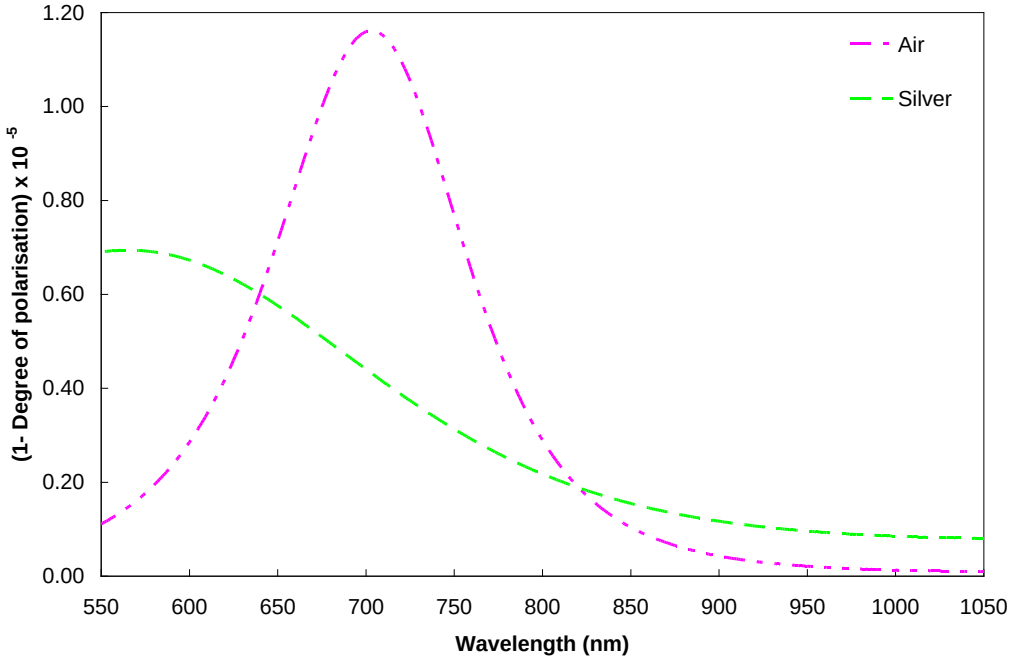

Figure 5.10: The degree of depolarisation for $Bi{:}YIG$ film with incoherent back reflections situation with air and silver after the substrate.

It may be interesting to investigate the changes in magneto-optical effects when using a thick film. Figure 5.11 shows Kerr rotation and ellipticity for a film thickness was set at ten times normal thickness, *i.e.*,10 $\left(\lambda/2\sqrt{\varepsilon_{xx}}\right)$. There are more fringes and an increase of magneto-optical values as more material now exists; for example, at 713

nm (where one peak of the ellipticity at that wavelength) the Kerr ellipticity is $\sim 9.3 \times 10^{-3}$ with a thick film compared with $\sim 1.5 \times 10^{-4}$ with the film thickness $\left(\lambda/2\sqrt{\varepsilon_{xx}}\right)$. At 720 *nm*, the Kerr rotation is $\sim -4.4 \times 10^{-4}\ rad$ with a thick film compared with $\sim -4.4 \times 10^{-5}\ rad$ with the film thickness $\left(\lambda/2\sqrt{\varepsilon_{xx}}\right)$. In general, the Kerr rotation increased approximately ten times.

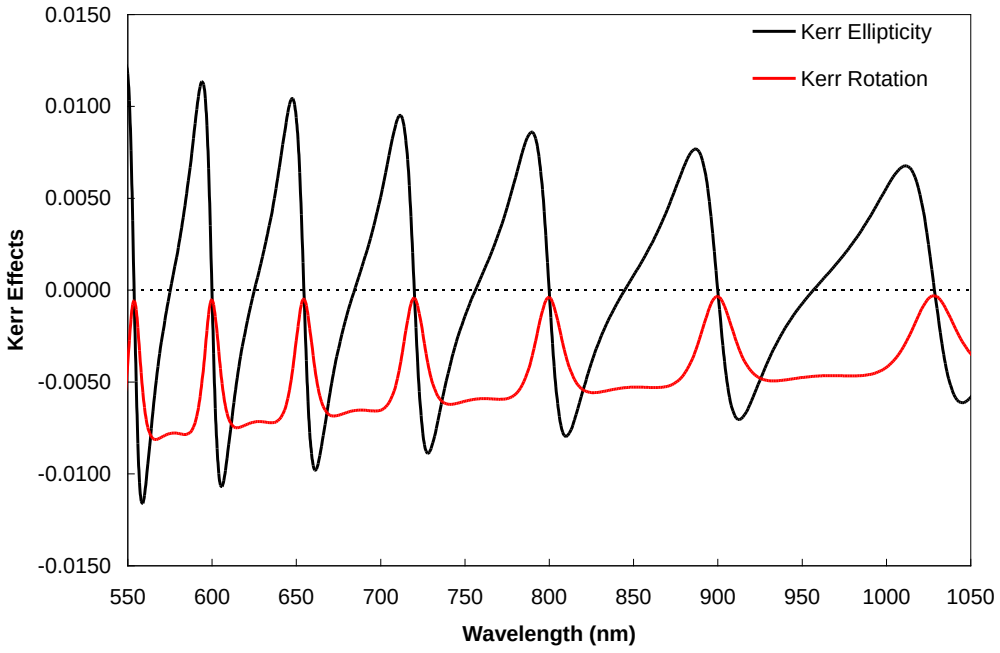

Figure 5.11: Kerr effects for $Bi{:}YIG$ film with incoherent back reflections when thickness is equal to 10 $(\lambda/2\sqrt{\varepsilon_{xx}})$, where $\lambda = 720\ nm$.

As mentioned in Chapter 4, a cavity structure enhances the magneto-optical effects. Here, the contribution effect of including the incoherent back reflections on the magneto-optical properties will be described. For the same cavity structure $(Ta_2O_5/SiO_2)^6\ /Bi{:}YIG/(SiO_2/Ta_2O_5)^6$, which was studied in Chapter 4 the Kerr ellipticity spectrum with incoherent back reflections was calculated and compared with that without incoherent back reflections, shown in figure 5.12-a. Similarly, in figure 5.12-b

the pink curve shows the Kerr rotation spectrum with incoherent back reflections, and the blue curve shows rotation without incoherent back reflections, for comparison. The maximum Kerr rotation presented in the cavity region, at 720 *nm* the maximum is ~0.380 *rad* without incoherent back reflections compared with ~0.139 *rad* with incoherent back reflections.

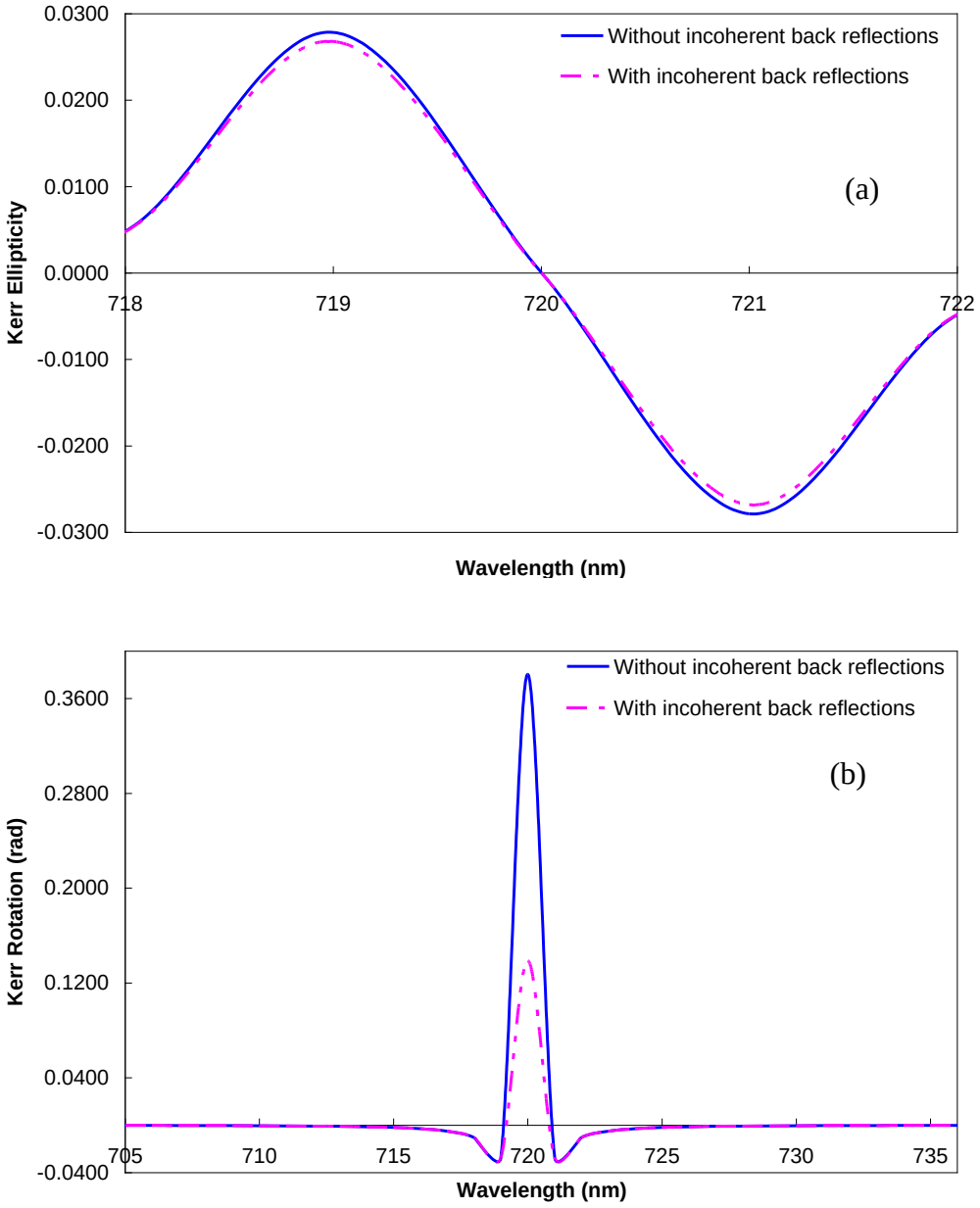

Figure 5.12: Kerr (a) ellipticity and (b) rotation spectra with and without incoherent back reflections for$(Ta_2O_5/SiO_2)^6\ /Bi{:}YIG/(SiO_2/Ta_2O_5)^6,$ using $\varepsilon_{xy} = -0.00369$.

In Chapter 4, we checked our calculations of the Faraday rotation spectrum for the cavity structure, $(SiO_2/TiO_2)^6\ /Co_6Ag_{94}/SiO_2$, which was taken from Dong *et al.* (2010) for both small and large ε_{xy} values. Here, we focus on $\varepsilon_{xy} = -1.2$, which gives much larger values of magneto-optical effects to consider the Kerr effects in both cases: with and without incoherent back reflections. The Kerr ellipticity spectrum with incoherent back reflections was calculated and compared with that without incoherent back reflections as shown in figure 5.13-a. In the cavity region, the figure shows a small effect on the Kerr ellipticity spectra with taken the contribution of incoherent back reflections from the substrate. Similarly, figure 5.13-b shows very little difference between the Kerr rotation with and without incoherent back reflections spectra, *i.e.*, the incoherent back reflections were not significant in this situation. A discontinuity or a jump (straight line) was seen from 625.7 *nm* to 625.8 *nm* and this may be of interest. We know the rotation in the terms of polar coordinates on the Poincaré sphere is the longitude. To explain the discontinuity, we plot the path of rotation on the Poincaré sphere as the point projections on the sphere describe the position of a polarisation state. As can be seen from 5.14, a smooth curve of the point projections means the polarised state moves smoothly around the sphere. For clarity, we plot the relation between S_1 and S_2; these Stokes' parameters are required to determine the rotation as given by equation 5.22. Figure 5.15 shows the longitude goes over the meridian line (the line has zero longitude conventionally) chosen for the branch cut as represented by the green dotted line on the figure. That means when the longitude crosses the meridian line, the jump (discontinuity) occurs. To modify this to a continuous spectrum, which has the same physical meaning, we added $-\pi$ to the points after the cut. This has no

physical consequence, because there is always an ambiguity in the inverse tangent function. The final continuous rotation spectrum is shown in figure 5.16.

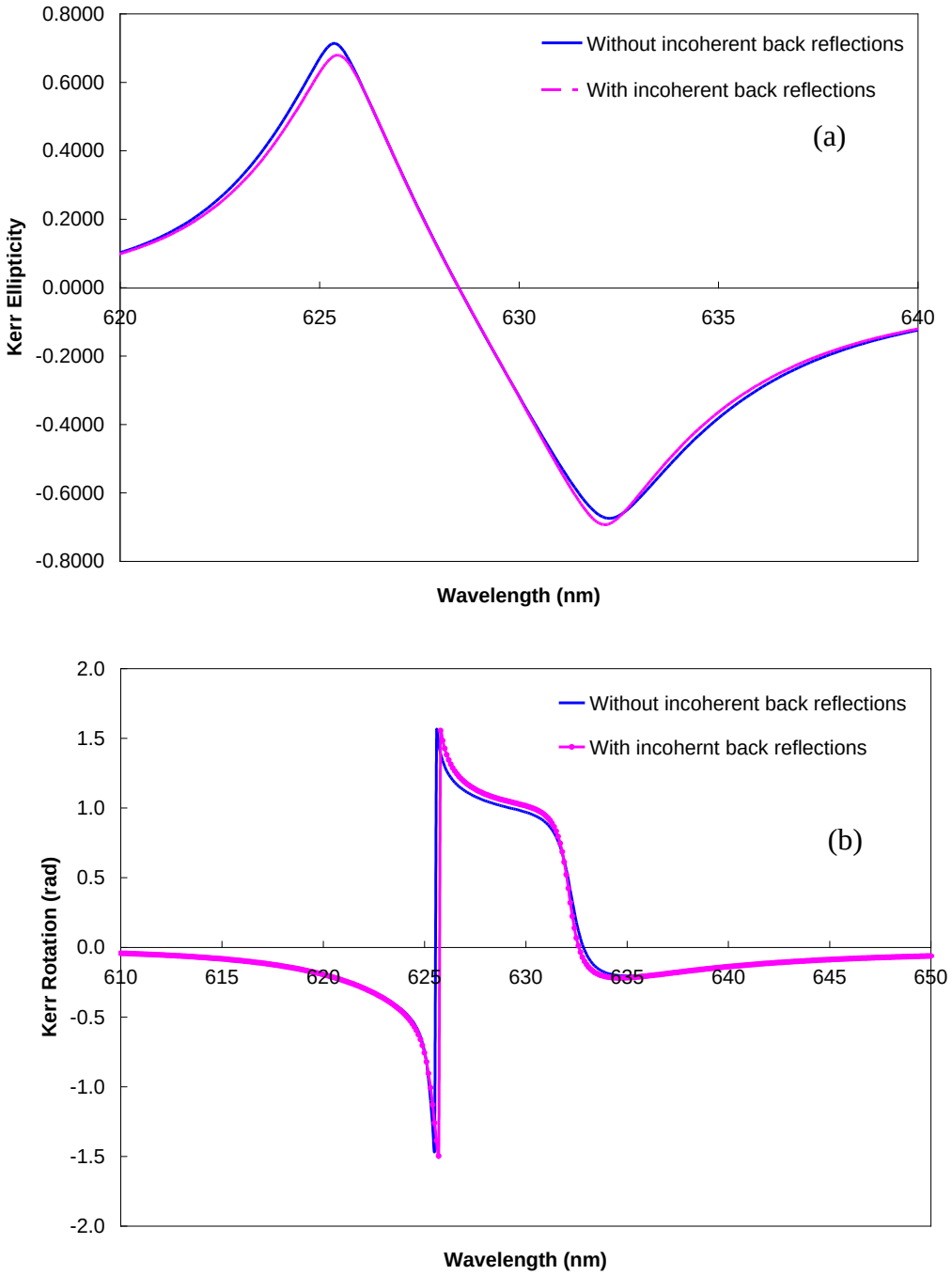

Figure 5.13: Kerr (a) ellipticity and (b) rotation spectra with and without incoherent back reflections for $(SiO_2/TiO_2)^6\ /Co_6Ag_{94}/SiO_2$, using $\varepsilon_{xy} = -1.2$, which gives much larger magneto-optical effects.

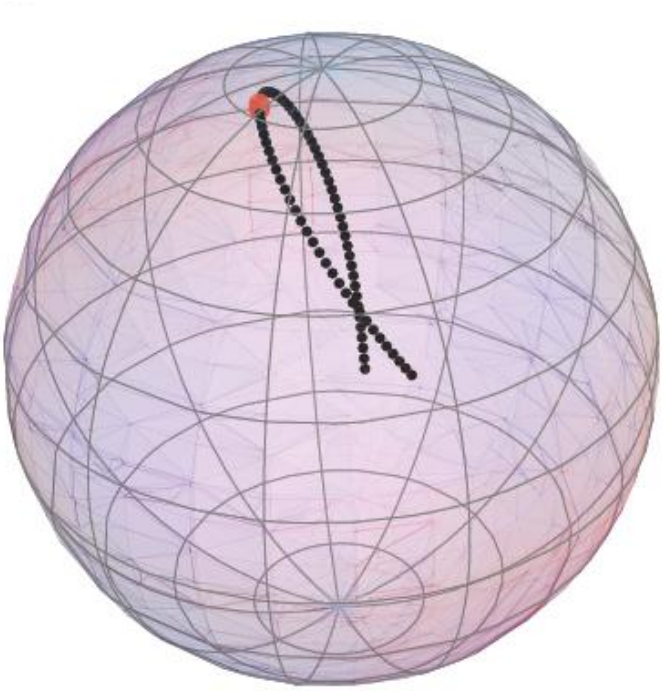

Figure 5.14: Visualisation of the path of rotation on the Poincaré sphere. The red points are the positions of wavelength where the jump occurs between 625.7 *nm* and 625.8 *nm*.

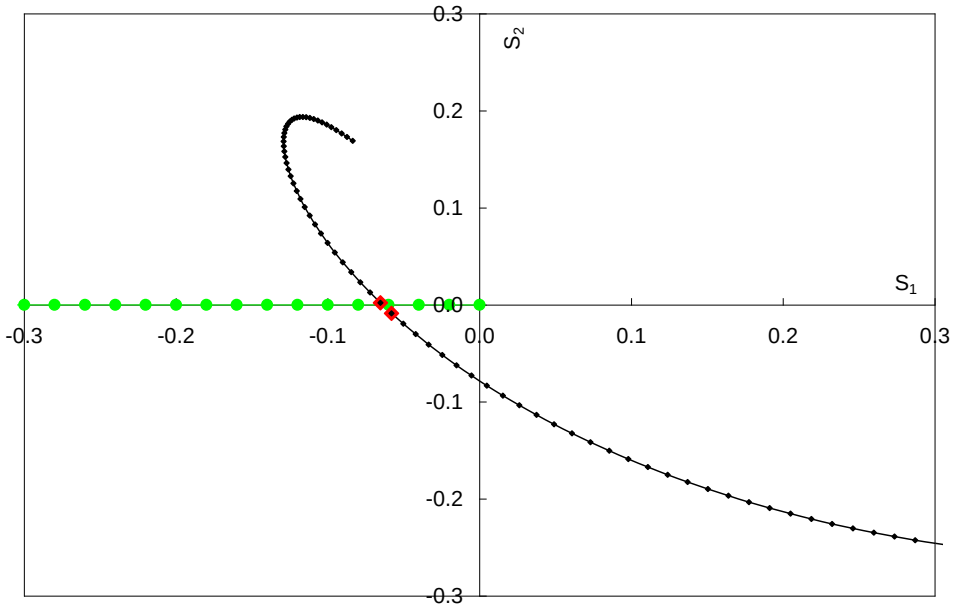

Figure 5.15: the relation between Stokes' parameters S_1 and S_2. The green dotted line refers arbitrarily to zero longitude. The red squares are the positions of wavelength where the jump occurs between 625.7 *nm* and 625.8 *nm*.

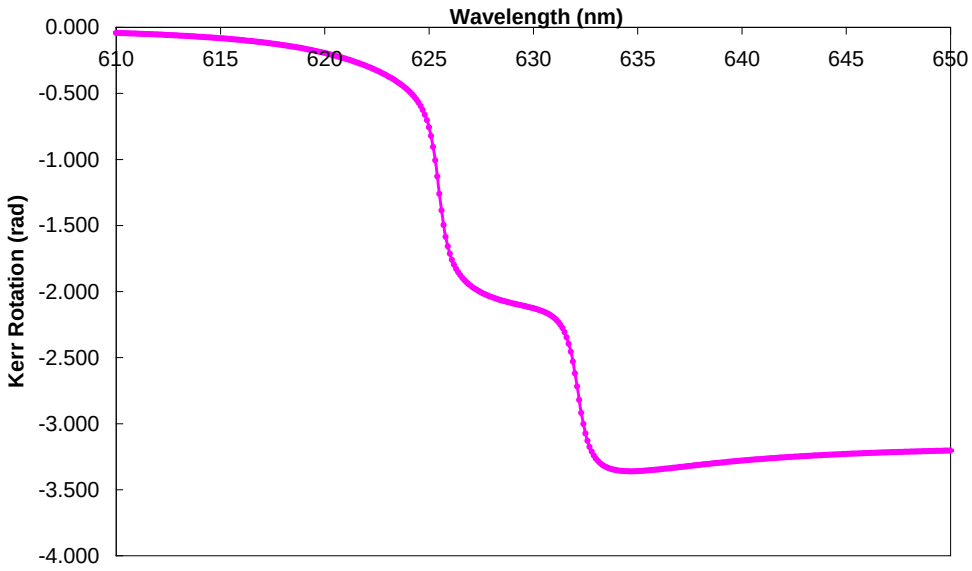

Figure 5.16: The modified Kerr rotation spectrum without incoherent back reflections for $(SiO_2/TiO_2)^6\ /Co_6Ag_{94}/SiO_2$, using $\varepsilon_{xy} = -1.2$.

As mentioned in section 5.2, Stokes' parameters can be found in terms of reflectivity expressions by using equations 5.11 for different polarised states and equation 5.23. Then we can find the expression of Kerr ellipticity in terms of the reflectivity amplitudes by using equations 5.21. In a different way, we can also find Kerr ellipticity expression in terms of the reflectivity amplitudes using equations 4.46 and 4.49 with help of equation 3.2. It should be pointed out that for a small magneto-optical constant, we can show analytically that Kerr ellipticity was identical using either Sato's (1981) definition in terms of left and right circularly polarised light, equation 3.2, or Born and Wolf's (1999) definition in terms of Stokes' parameters, equation 5.21, for both with and without incoherent back reflections. However, these definitions are not consistent for a large magneto-optical constant. By contrast, we can show that the Kerr

rotation without incoherent back reflections can be found by using Sato's (1981), equation 3.3 or Sakaguchi and Sugimoto's (1999) definitions, equation 3.5 (both require the phase information) or Born and Wolf's (1999) definition in terms of Stokes' parameters, which are given in terms of the reflectivity intensities, equation 5.22; all of them gave identical results. However, to compute Kerr rotation with incoherent back reflections, we can only use Born and Wolf's (1999) definition as explained in section 5.2. Born and Wolf's (1999) definitions for the magneto-optical effects in terms of Stokes' parameters are more general and suitable for both cases with and without incoherent back reflections of the substrate; the difference in both cases arises from different reflectivity expressions.

5.4 Conclusions

This study set out to determine the effect of the incoherent back reflections from a thick but finite transparent isotropic substrate on the magneto-optical properties of circularly birefringent structures. We have given a formula for the reflectivity and transmission, which can be used with the definition of Stokes' parameters to find the Kerr rotation and ellipticity spectra. The results of this investigation show the important contribution of incoherent back reflections from transparent isotropic substrate on the Kerr effects; therefore, the inclusion of incoherent back reflections is necessary in realistic situations to obtain accurate spectra.

CHAPTER 6

MODULATION METHOD

Spectra of the magneto-optics effects were studied previously when structures were placed on both finite and infinite substrates, *i.e.*, with and without incoherent back reflections. In this chapter Sato's modulation method will be investigated analytically for circularly birefringent materials. As seen in Chapter 5, the existence of the back reflections in substrate is very important and ignoring it gives significantly different results. We will hence, reanalyse Sato's method in the case of incoherent back reflections. We find that the method can still be applied in the case of the incoherent back reflections in the substrate, provided that the calculation of relevant parameters includes the incoherent reflections.

6.1 Introduction

Diverse experimental approaches have been used in measuring magneto-optical characteristics, for instance, the Faraday cell technique, used in a photoelectric ellipsometer device. This cell has a borosilicate crown glass rod wound with turns of wire. A current flows through the winding and a time-variant magnetic field is generated along the light path. The field in turn leads to a time-variant Faraday effect (Robinson, 1963). This Faraday cell method has a high sensitivity; however, it is restricted in wavelength span and is sensitive to stray magnetic fields. Moreover, a continuous spectrum is difficult to obtain. Another method uses mechanically rotating

birefringent plates instead of the Faraday cell but the last problem remains. A spinning analyser employs a continuously rotating analyser with the aim of intercepting the linear polarised light. The angle of the plane of polarisation of the incident wave is obtained directly from the phase of alternating current signal. It has a good sensitivity and is not affected by stray magnetic fields and a continuous spectral readout can be obtained. The measurement principle of magneto-optical effects using this spinning analyser and compensator is the linearly incident light on a magneto-optical active medium comes out from it as elliptical polarisation (Suits, 1971). A quarter wave plate placed in the optical path was required for those techniques in the Kerr ellipticity measurement; for every region of the wavelength, a suitable quarter wave plate should be chosen. That means an additional continuous readout problem could occur. This creates weakness in using those techniques (Sato, 1981). Therefore, Sato (1981) modified the equipment using a piezo-birefringent modulator.

At the start, an overview of the experimental modulation method carried out by Sato in 1981 and his analyses of this measurements may be useful to mention here. The author described the principle of the technique using the piezo-birefringent modulator to measure magneto-optical Kerr spectra. The incident light is transmitted across a polariser that is set at 45^{o}, and then passes through a modulator and experiences a periodically changing retardation, $\delta(t)$, so that

$$\boldsymbol{E} = \frac{E^{0}}{\sqrt{2}}\left(\hat{\mathbf{x}} + e^{i\delta(t)}\hat{\mathbf{y}}\right), \tag{6.1}$$

where E^{0} is the amplitude of the electric field, and $\hat{\mathbf{x}}$ and $\hat{\mathbf{y}}$ are unit vectors at x and y directions. The modulation is chosen to be:

$$\delta(t) = \delta_0 \sin \Omega t, \tag{6.2}$$

here δ_0 is the retardation amplitude and Ω is the modulation frequency. After that, the light is reflected by the sample and passes through an analyser at *x*-direction. This light can be described by the *x*-component of electric field in terms of the Fresnel reflection coefficients $\hat{r}_{\pm}$ for two circularly polarised lights as given by Sato (1981) as follows:

$$E_x = \frac{E^0}{2\sqrt{2}}\left\{\hat{r}_+\left(1 - i\, e^{i\,\delta}\right) + \hat{r}_-\left(1 + i\, e^{i\,\delta}\right)\right\}, \tag{6.3}$$

Finally, the intensity is detected using a photo-detector. This is defined as $\varepsilon|E_x|^2/4\pi$. Hence, equation 6.3 can be turned into intensity as:

$$I^{out} = \frac{\varepsilon(E^0)^2}{4\pi}\left\{R + \frac{\Delta R}{2}\sin\delta + R\sin\Delta\theta\cos\delta\right\}, \tag{6.4}$$

where R, ΔR and $\Delta\theta$ are defined as:

$$\begin{aligned} R &= \frac{1}{2}\left(R_{++} + R_{--}\right), \\ \Delta R &= R_{++} - R_{--}, \\ \Delta\theta &= \theta_+ - \theta_- . \end{aligned} \tag{6.5}$$

Ellipticity, χ, and the rotation, ψ, are defined as seen previously by Sato (1981) as:

$$\chi = \frac{1}{4}\left(\frac{\Delta R}{R}\right) = \frac{1}{2}\left(\frac{R_{++} - R_{--}}{R_{++} + R_{--}}\right), \tag{6.6}$$

$$\psi = -\frac{1}{2}\Delta\theta. \tag{6.7}$$

By substituting equation 6.2 into 6.4 and applying expansion expressions for $\sin\delta$ and $\cos\delta$, that means the result consists of three components: the direct current (dc) component which does not depend on frequency *i.e.*, a dc component *I*(0), an Ω-

component $I(\Omega)$ and a 2Ω component $I(2\Omega)$, where I is the intensity of light. The output intensity, equation 6.4, is written by Sato (1981) as the following equation:

$$I^{out} = I(0) + I(\Omega)\sin\Omega t + I(2\Omega)\cos 2\Omega t. \tag{6.8}$$

This equation represents the first terms of a Fourier series expansion of I^{out}. In the case of the setting analyser at *x*-direction, the $I(0)$, $I(\Omega)$ and $I(2\Omega)$ are obtained in terms of Bessel functions of integral order *n*, $J_n(\delta_0)$, as:

$$I(0) = I_0 R + I_0 J_0(\delta_0)\, R \sin\Delta\theta, \tag{6.9}$$

$$I(\Omega) = I_0\, J_1(\delta_0)\, \Delta R, \tag{6.10}$$

$$I(2\Omega) = 2I_0\, J_2(\delta_0)\, R \sin\Delta\theta. \tag{6.11}$$

I_0 is defined as $I_0 = \varepsilon(E^0)^2/8\pi$. It should be pointed out the actual values of the Bessel functions are not interesting in numerical calculations, but the importance of the Bessel functions is to determine only here the type of magneto-optic effects: Kerr ellipticity or Kerr rotation. By detecting the Ω and 2Ω components, the reflectance magneto-circular dichroism (RMCD), $\Delta R/R$, or ellipticity, χ, and the rotation, ψ, can be obtained, respectively, where the final results were given as the ratio of each modulated intensity to dc component, $I(\Omega)/I(0)$ and $I(2\Omega)/I(0)$. Considering the phase shift, $\Delta\theta$, is much smaller than one, leads to $J_0(\delta_0)\sin\Delta\theta$ can approximately be negligible compared with one, so the following equations are given:

$$\frac{I(\Omega)}{I(0)} = J_1(\delta_0)\,\frac{\Delta R}{R}, \tag{6.12}$$

$$\frac{I(2\Omega)}{I(0)} = J_2(\delta_0)\, 2\Delta\theta. \tag{6.13}$$

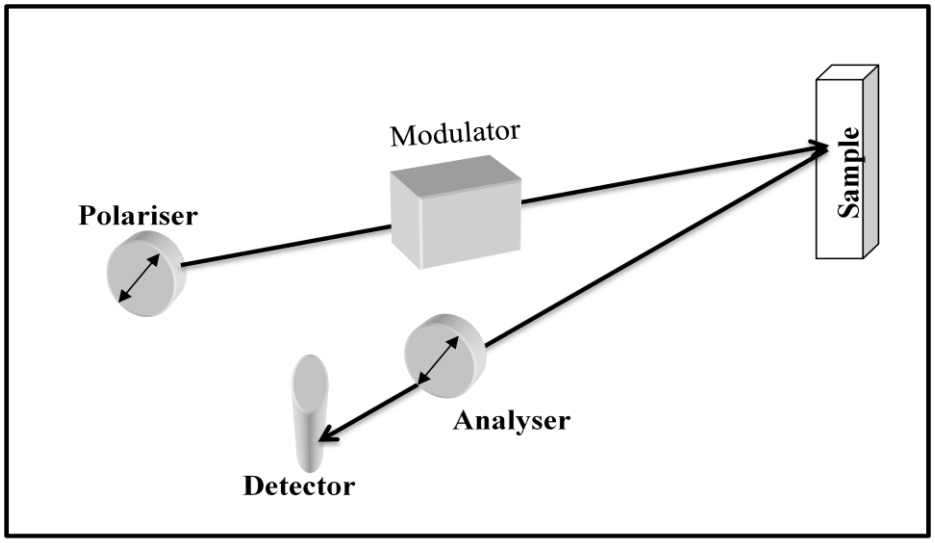

Figure 6.1: Schematic diagram of fundamental components in the measuring method**.** Adapted from Sato (1981).

6.2 Theory and calculations

In this section, we are going to calculate expressions for the Fourier components as in equations 6.9-6.11 using the general incoherent back reflection theory. We show analytically that ignoring the back reflections in the substrate, we get Sato's results. We show numerically that in the case of inclusion the back reflections the Fourier components can be expressed in Sato's form, but not been able to derive this analytically. Hence, the same procedures described by Sato (1981) were followed. Diagonal linearly polarised light emerges from the polariser. The outgoing light from the modulator can be written as in equation 6.1, which in the matrix notation (and by assuming $E^0 = 1$ for simplicity) can be rewritten as:

$$\boldsymbol{E} = \frac{1}{\sqrt{2}}\begin{pmatrix} 1 \\ e^{i\delta(t)} \end{pmatrix}. \tag{6.14}$$

After that, this light is reflected by the structure; and the outgoing reflected intensity can be obtained by using equation 5.11 in the case of modulated light instead of the linearly *x*-polarised incident light. It follows that, equation 5.11 becomes:

$$R_{\delta x} = \frac{1}{2}\begin{pmatrix}1 & e^{-i\delta(t)}\end{pmatrix}\left[\underline{r}^{\dagger}\underline{P_x}\,\underline{r} + \underline{t}^{\dagger}\left(\sum_{n=0}^{\infty}(\underline{r_b}^{\dagger}\,\underline{\tilde{r}}^{\dagger})^n\,\underline{r_b}^{\dagger}\,\underline{\tilde{t}}^{\dagger}\underline{P_x}\,\underline{\tilde{t}}\,\underline{r_b}\,(\underline{\tilde{r}}\,\underline{r_b})^n\right)\underline{t}\right]\begin{pmatrix}1\\ e^{i\delta(t)}\end{pmatrix}, \tag{6.15}$$

The following matrix was defined:

$$\underline{c} = \begin{pmatrix}c_{11} & c_{12}\\ c_{21} & c_{22}\end{pmatrix} = \left[\underline{r}^{\dagger}\underline{P_x}\,\underline{r} + \underline{t}^{\dagger}\left(\sum_{n=0}^{\infty}(\underline{r_b}^{\dagger}\,\underline{\tilde{r}}^{\dagger})^n\,\underline{r_b}^{\dagger}\,\underline{\tilde{t}}^{\dagger}\underline{P_x}\,\underline{\tilde{t}}\,\underline{r_b}\,(\underline{\tilde{r}}\,\underline{r_b})^n\right)\underline{t}\right]. \tag{6.16}$$

Then, equation 6.15 can be simplified as:

$$R_{\delta x} = \frac{1}{2}\begin{pmatrix}1 & e^{-i\delta(t)}\end{pmatrix}\begin{pmatrix}c_{11} & c_{12}\\ c_{21} & c_{22}\end{pmatrix}\begin{pmatrix}1\\ e^{i\delta(t)}\end{pmatrix},$$

$$= \frac{1}{2}\left[c_{11} + c_{22} + c_{12}e^{i\delta(t)} + c_{21}e^{-i\delta(t)}\right], \tag{6.17}$$

by substituting equation 6.2 into equation 6.17, we get:

$$R_{\delta x}(t) = \frac{1}{2}\left[c_{11} + c_{22} + c_{12}e^{i\delta_0 \sin\Omega t} + c_{21}e^{-i\delta_0 \sin\Omega t}\right]. \tag{6.18}$$

Equation 6.18 is periodic with a period $2\pi/\,\Omega$, so can be expanded as Fourier series, whose terms are Bessel functions. We calculate the first few term using the Wolfram Mathematica programme as the following:

$$a_0 = c_{11} + c_{22} + J_0(|\delta_0|)(c_{12} + c_{21}), \tag{6.19}$$

$$2\,b_1 = 2\,i\,J_1(\delta_0)(c_{12} - c_{21}), \tag{6.20}$$

$$2\,a_2 = 2\,J_2(|\delta_0|)(c_{12} + c_{21}). \tag{6.21}$$

Now, we are going to get Sato's results by concentrating just on a special case ignoring incoherent back reflections of substrate: this means $\underline{r_b} = 0$. The comparison between the last equations and equations 6.9-6.11 requires finding matrix elements: c_{11}, c_{12}, c_{21} and c_{22}. These can be found using equation 6.16 in the special case. The term $\underline{r}^{\dagger}\underline{P_x}\,\underline{r}$ is easy to calculate by substituting the previous definitions of $\underline{r}$ and $\underline{P_x}$ in Chapter 5, see equations 5.3 and 5.20.This gives:

$$\begin{pmatrix} c_{11} & c_{12} \\ c_{21} & c_{22} \end{pmatrix} = \underline{r}^{\dagger}\underline{P_x}\,\underline{r} = \begin{pmatrix} r_{xx}r_{xx}^{*} & r_{yx}r_{xx}^{*} \\ r_{xx}r_{yx}^{*} & r_{yx}r_{yx}^{*} \end{pmatrix}. \tag{6.22}$$

We substitute the expressions of the matrix elements c_{11}, c_{12}, c_{21} and c_{22} from 6.22 into equations 6.19-6.21. Since, for circular birefringent structures, $r_{xx} = r_{yy}$ and $r_{xy} = -r_{yx}$ (since $r_{+-} = r_{-+} = 0$ in equations 4.47 or 4.48), these equations can be rewritten as the following:

$$a_0 = r_{xx}r_{xx}^{*} + r_{xy}r_{xy}^{*} + J_0(|\delta_0|)\left(-r_{xy}r_{xx}^{*} - r_{xx}r_{xy}^{*}\right), \tag{6.23}$$

$$2\,b_1 = 2\,i\,J_1(\delta_0)\left(r_{xx}r_{xy}^{*} - r_{xy}r_{xx}^{*}\right), \tag{6.24}$$

$$2\,a_2 = 2\,J_2(|\delta_0|)\left(-r_{xy}r_{xx}^{*} - r_{xx}r_{xy}^{*}\right). \tag{6.25}$$

To rework the last three equations in terms of R, ΔR and $R\sin\Delta\theta$ as in equations 6.9-6.11, expressions for these quantities need to be found in terms of r_{xx} and r_{xy}. Starting from the definition of Sato (1981), see equation 6.5, R can be written in terms of r_{xx}, r_{xy}, r_{yx} and r_{yy} using equations 4.46 and 4.49 as:

$$R = \frac{1}{2}(|r_{++}|^2 + |r_{--}|^2)$$

$$= \frac{1}{4}(r_{xx}r_{xx}^* + r_{xx}r_{yy}^* + r_{yy}r_{xx}^* + r_{yy}r_{yy}^* + r_{xy}r_{xy}^* - r_{xy}r_{yx}^* - r_{yx}r_{xy}^* + r_{yx}r_{yx}^*), \quad (6.26)$$

For circular birefringent structures this can be simplified as:

$$R = r_{xx}r_{xx}^* + r_{xy}r_{xy}^*. \quad (6.27)$$

Following similar procedures ΔR is calculated as:

$$\Delta R = |r_{++}|^2 - |r_{--}|^2$$

$$= \frac{i}{2}(r_{xx}r_{xy}^* - r_{xx}r_{yx}^* + r_{yy}r_{xy}^* - r_{yy}r_{yx}^* - r_{xy}r_{xx}^* - r_{xy}r_{yy}^* + r_{yx}r_{xx}^* + r_{yx}r_{yy}^*),$$

$$= 2i(r_{xx}r_{xy}^* - r_{xy}r_{xx}^*). \quad (6.28)$$

Finally, let us work out $\sin\Delta\theta$:

$$\sin\Delta\theta = \sin(\theta_+ - \theta_-) = \frac{1}{|r_{++}||r_{-}|}[\mathrm{Im}(r_{++})\,\mathrm{Re}(r_{--}) - \mathrm{Im}(r_{--})\,\mathrm{Re}(r_{++})], \quad (6.29)$$

where Re and Im denote the real and the imaginary part of a complex number, respectively. Assuming $R \approx |r_{++}||r_{--}| \approx |r_{++}|^2 \approx |r_{--}|^2$, and using equations 4.46, 49, equation 6.29 can be rewritten as:

$$R\sin\Delta\theta = -2\left[\mathrm{Re}(r_{xx})\,\mathrm{Re}\left(r_{xy}\right) + \mathrm{Im}(r_{xx})\,\mathrm{Im}\left(r_{xy}\right)\right]. \quad (6.30)$$

Returning now to the terms $\left(-r_{xy}r_{xx}^* - r_{xx}r_{xy}^*\right)$ in equation 6.23 or 6.25 that can be rewritten in the following form:

$$-r_{xy}r_{xx}^* - r_{xx}r_{xy}^* = -2\left[\mathrm{Re}(r_{xx})\,\mathrm{Re}\left(r_{xy}\right) + \mathrm{Im}(r_{xx})\,\mathrm{Im}\left(r_{xy}\right)\right]. \quad (6.31)$$

Comparison between the last two equations gives:

$$R \sin\Delta\theta = -r_{xy}r_{xx}^{*} - r_{xx}r_{xy}^{*}. \quad (6.32)$$

Substituting equations 6.27, 6.28 and 6.32 into equations 6.23-6.25 then leads to equations 6.9-6.11, as required (with $I_0 = 1$).

We can also apply equations 6.19-6.21 in a more general case to find the magneto-optical effects for the situation which includes the effect of incoherent back reflections in the substrate. As including the incoherent back reflections is important in a realistic situation, this case was investigated numerically in this work. We get numerically same results, but not been able to drive this analytically.

6.3 Numerical Calculations

The modulated spectra were calculated for a simple circularly birefringent film, $Bi{:}YIG$, on a glass substrate ignoring absorption. Its parameters and the refractive index of glass substrate were taken from Kato *et al.*,(2003) as the following: $\varepsilon_{xx} = 5.59$; $\varepsilon_{xy} = -0.00369$; at $\lambda = 720\,nm$ with the film thickness equal to $\lambda/2\sqrt{\varepsilon_{xx}}$; and $n_s = 1.52$.

Figure 6.2 shows the unmodulated spectra of the first term of the Fourier series, *i.e.*, $I(0) = a_0$, by using equation 6.23 in both cases; with and without incoherent back reflections. This result gave an identical result to that produced using equation 6.9 in both cases when the phase shift, $\Delta\theta$, was much smaller than one. It should be pointed out, in this condition, equation 6.9 becomes the same as Sato's formula (1981) for *R*.

By comparing the pink and blue spectra, the effect of including incoherent back reflections in the substrate is shown clearly in the figure.

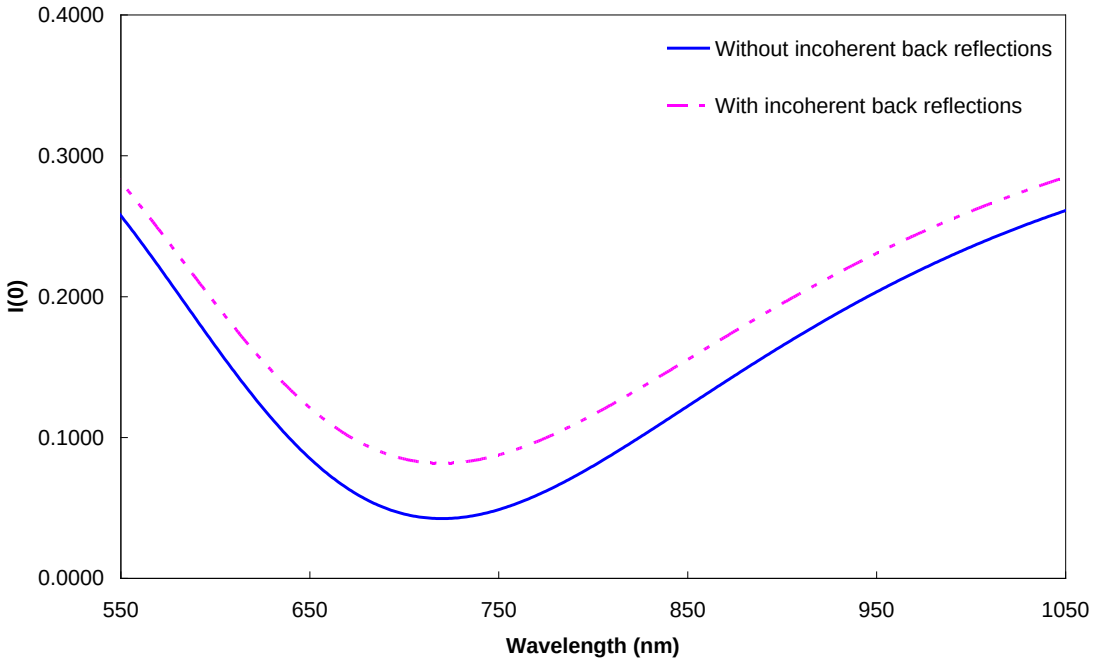

Figure 6.2: The unmodulated spectra both with and without incoherent back reflections using equation 6.23. The curves are identical to those obtained from Sato's method, equation 6.9 when $\Delta\theta$ is much smaller than one, in both cases.

By calculating $\frac{1}{4}\ (2b_1/a_0)$ and $\frac{-1}{2}(a_2/a_0)$ using equations 6.19-6.21, the magneto-optic effects: RMCD, $\Delta R/R$, or ellipticity, χ, and the rotation, ψ, can be determined. The Kerr ellipticity and rotation were found as shown in figures 6.3-a and -b, respectively both with and without incoherent back reflections. Both sets of spectra are indistinguishable from Sato's method. Figures 6.3-a and –b show clearly the effect on magneto-optical spectra of taking the incoherent back reflection within a transparent substrate into account. This effect is important in practical situations and ignoring it leads to wrong results in finding the off-diagonal components of the dielectric matrix, see equation 4.25. Hence, Sato's analysis is fine and works well, we just need to modify, R, ΔR and $R\ \sin\Delta\theta$ values to include the effects of incoherent back reflections in the substrate.

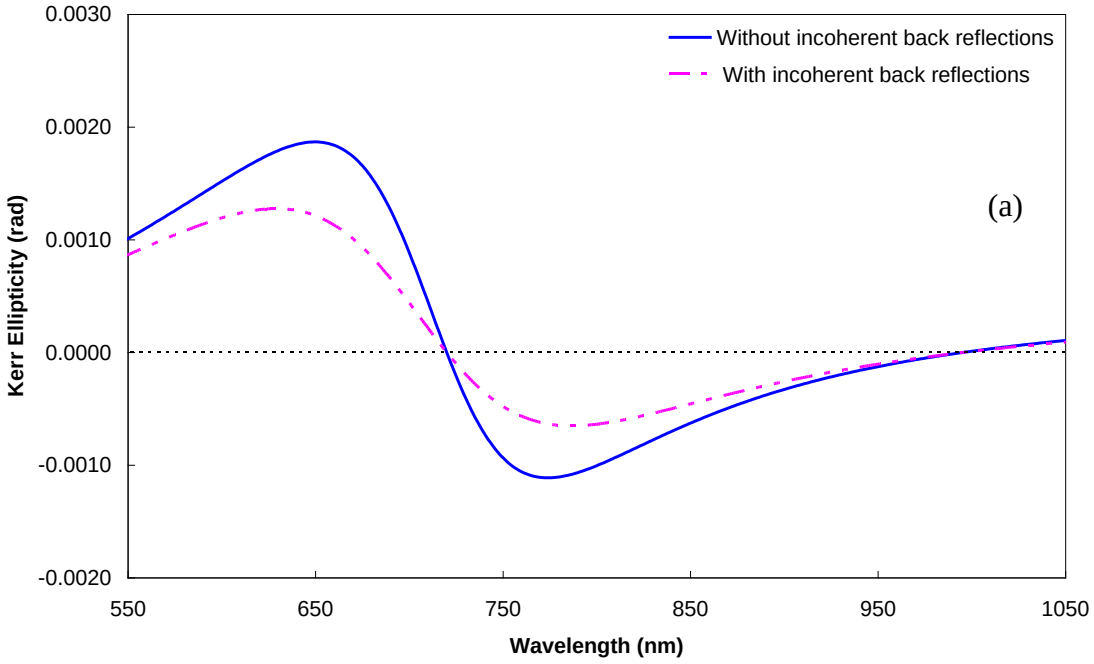

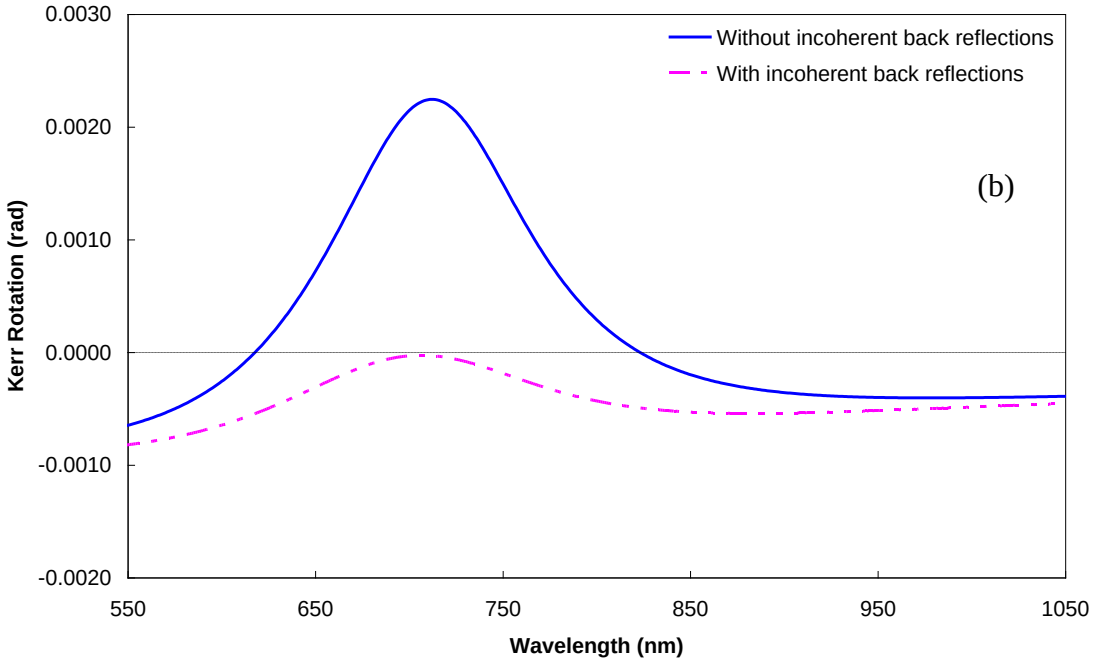

Figure 6.3: (a) Kerr ellipticity and (b) Kerr rotation spectra for $Bi{:}YIG$ film both with and without incoherent back reflections using equations 6.19- 6.21. The curves are identical to those obtained from Sato's method, *i.e.*, $\frac{1}{4}\times$ (equation 6.12) and equation 6.13, respectively in both cases.

6.4 Conclusions

At the start of this chapter, an overview of the experimental modulation method of Sato was given. The analytical calculations of Sato's modulation method were reanalysed including incoherent back reflections in the substrate, which is vital for a non-absorbing substrate in realistic cases to find the right ε_{xy} value. We have shown Sato's analysis works, with just R, ΔR and $R\sin\Delta\theta$ values needing to be adapted to include the effects of incoherent back reflections in the substrate. The formulae can then be used in both cases, with and without incoherent back reflections. We have only shown this for one set of parameters for the single layer, maybe it does not work so well if there is a significant reduction in the degree of polarisation.

CHAPTER 7

THEORETICAL ANALYSIS OF STRUCTURES ON A CIRCULARLY BIREFRINGENT SUBSTRATE

Chapter 5 has considered circularly birefringent films on a thick isotropic transparent substrate. One of the major issues in this chapter is the significance of using a thick circularly birefringent substrate instead of a thick isotropic one. This means both the simple film and the substrate are circularly birefringent media. Furthermore, exact and approximate analytical formulae for Faraday rotation will be derived for various cases: (1) a single circularly birefringent film with air on both sides; (2) a film on a circularly birefringent substrate; (3) a circularly birefringent cavity structure with Bragg mirrors on both sides. The measure of the effective number of light passes based on the Faraday rotation will be found.

7.1 Theory and calculations

The Faraday rotation of an extremely thin film in isolation is very difficult to determine experimentally. The following question is discussed in detail: can the Faraday rotation of a film on a circularly birefringent substrate be obtained by simply subtracting the rotation of the bare substrate from that of the whole structure? Let us consider a linearly incoming *x*-polarised wave incident normally on an arbitrary multilayer structure with circularly birefringent properties. Suppose this structure is also deposited on a thick circularly birefringent substrate.

We use the transfer matrix for a circularly birefringent structure, which was derived in Chapter 4 and modify the matrix treatment of incoherent multiple back reflections which was used in Chapter 5 in the case of a circularly birefringent multilayer structure on a transparent isotropic substrate. The rotation of the light going through the substrate, which will be considered in this analysis, is illustrated schematically in figure 7.1. The calculation requires changes in the expressions for the transmission and reflection coefficients of a circularly birefringent multilayer structure for waves propagating from air through the structure into the substrate and for waves propagating in the reverse direction. In addition, the rotation at the interface between the back of substrate and air will be calculated.

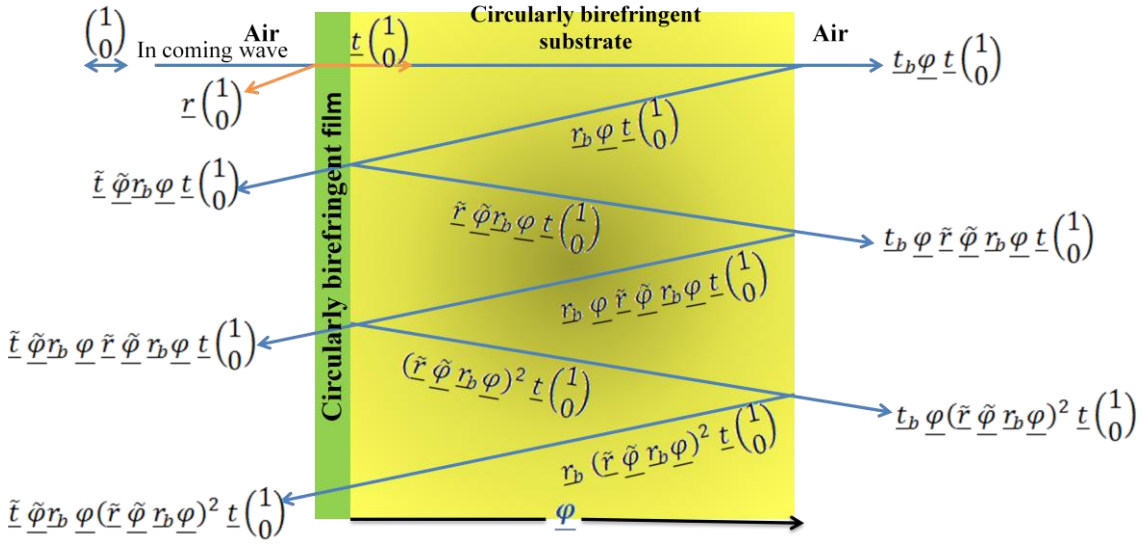

Figure 7.1: Schematic diagram of multiple incoherent reflections and transmission amplitudes in a thick circularly birefringent substrate. For clarity, the rays are drawn at small angles to the normal.

In general, the amplitude of the n^{th} reflection term can be written as

$$\underline{\tilde{t}}\,\underline{\tilde{\varphi}}\,\underline{r_b}\,\underline{\varphi}\,(\underline{\tilde{r}}\,\underline{\tilde{\varphi}}\,\underline{r_b}\,\underline{\varphi})^n\underline{t}\begin{pmatrix}1\\0\end{pmatrix}. \tag{7.1}$$

Similarly, the amplitude of the n^{th} transmission term can be written as

$$\underline{t_b}\,\underline{\varphi}\,(\underline{\tilde{r}}\,\underline{\tilde{\varphi}}\,\underline{r_b}\,\underline{\varphi})^n\underline{t}\begin{pmatrix}1\\0\end{pmatrix}, \tag{7.2}$$

where

$$\begin{aligned}
\underline{t} &= \begin{pmatrix} t_{xx} & t_{yx} \\ t_{xy} & t_{yy} \end{pmatrix}, \qquad \underline{r} = \begin{pmatrix} r_{xx} & r_{yx} \\ r_{xy} & r_{yy} \end{pmatrix}, \\
\underline{\tilde{t}} &= \begin{pmatrix} \tilde{t}_{xx} & \tilde{t}_{yx} \\ \tilde{t}_{xy} & \tilde{t}_{yy} \end{pmatrix}, \qquad \underline{\tilde{r}} = \begin{pmatrix} \tilde{r}_{xx} & \tilde{r}_{yx} \\ \tilde{r}_{xy} & \tilde{r}_{yy} \end{pmatrix}, \\
\underline{t_b} &= \begin{pmatrix} t^b_{xx} & t^b_{yx} \\ t^b_{xy} & t^b_{yy} \end{pmatrix}, \qquad \underline{r_b} = \begin{pmatrix} r^b_{xx} & r^b_{yx} \\ r^b_{xy} & r^b_{yy} \end{pmatrix}, \\
\underline{\varphi} &= \underline{\tilde{\varphi}} = \begin{pmatrix} \varphi_{11} & \varphi_{12} \\ \varphi_{21} & \varphi_{22} \end{pmatrix},
\end{aligned} \tag{7.3}$$

are the amplitude coefficient matrices used in figure 7.1. Here $\underline{t}$ and $\underline{r}$ are the amplitude coefficient matrices of transmission and reflection of the front of the multilayer structure, *i.e.*, wave travelling from air into the substrate going through the structure. $\underline{\tilde{t}}$ and $\underline{\tilde{r}}$ are the amplitude coefficient matrices of transmission and reflection for the opposite direction, *i.e.*, wave travelling from the substrate into air going through the structure. The first and second subscripts of the matrix elements refer to incoming and outgoing waves, respectively. $\underline{t_b}$ and $\underline{r_b}$ are the amplitude coefficient matrices of transmission and reflection of the back substrate, *i.e.*, wave travelling from the substrate into air. $\underline{\varphi}$ and $\underline{\tilde{\varphi}}$ are the rotation matrices in a thick circularly birefringent substrate for forward and reverse propagation directions, respectively. The calculations of all the matrix elements will be explained below.

Following this, the projection matrix, for example, $\underline{P_x}$, of linear *x*-polarisation is acted on amplitude expressions (7.1 and 7.2). To find the intensity in that projection, we take the modulus square and use the fact for any projection matrix, $\underline{P}^2 = \underline{P}$. We get the intensity in *x*-polarisation of the n^{th} reflection term as:

$$(1 \quad 0)\, \underline{t}^{\dagger}(\underline{\varphi}^{\dagger}\, \underline{r_b}^{\dagger}\, \underline{\tilde{\varphi}}^{\dagger}\, \underline{\tilde{r}}^{\dagger})^n\ \underline{\varphi}^{\dagger}\underline{r_b}^{\dagger}\, \underline{\tilde{\varphi}}^{\dagger}\, \underline{\tilde{t}}^{\dagger}\underline{P_x}\, \underline{\tilde{t}}\, \underline{\tilde{\varphi}}\, \underline{r_b}\, \underline{\varphi}\, (\underline{\tilde{r}}\, \underline{\tilde{\varphi}}\, \underline{r_b}\underline{\varphi})^n \underline{t} \begin{pmatrix} 1 \\ 0 \end{pmatrix}, \qquad (7.4)$$

Similarly, the intensity in *x*-polarisation of the n^{th} transmission term is:

$$(1 \quad 0)\, \underline{t}^{\dagger}\, (\underline{\varphi}^{\dagger}\underline{r_b}^{\dagger}\underline{\tilde{\varphi}}^{\dagger}\ \underline{\tilde{r}}^{\dagger})^n\ \underline{\varphi}^{\dagger}\underline{t_b}^{\dagger}\underline{P_x}\, \underline{t_b}\, \underline{\varphi}\, (\underline{\tilde{r}}\, \underline{\tilde{\varphi}}\, \underline{r_b}\underline{\varphi})^n\, \underline{t} \begin{pmatrix} 1 \\ 0 \end{pmatrix}. \qquad (7.5)$$

After that, we add the intensity of all different numbers of reflections to obtain a suitable formula for the total reflectivity and transmission intensities in *x*-polarisation. For outgoing *x*-polarised light, these total intensities are found as:

$$\begin{aligned} R_{xx} = (1 \quad 0) \Bigg[& \underline{r}^{\dagger}\underline{P_x}\, \underline{r} \\ & + \underline{t}^{\dagger} \left(\sum_{n=0}^{\infty} (\underline{\varphi}^{\dagger}\, \underline{r_b}^{\dagger}\, \underline{\tilde{\varphi}}^{\dagger}\, \underline{\tilde{r}}^{\dagger})^n\ \underline{\varphi}^{\dagger}\underline{r_b}^{\dagger}\, \underline{\tilde{\varphi}}^{\dagger}\, \underline{\tilde{t}}^{\dagger}\underline{P_x}\, \underline{\tilde{t}}\, \underline{\tilde{\varphi}}\, \underline{r_b}\, \underline{\varphi}\, (\underline{\tilde{r}}\, \underline{\tilde{\varphi}}\, \underline{r_b}\underline{\varphi})^n \right) \underline{t} \Bigg] \begin{pmatrix} 1 \\ 0 \end{pmatrix}, \end{aligned} \qquad (7.6)$$

$$T_{xx} = (1 \quad 0)\, \underline{t}^{\dagger} \left(\sum_{n=0}^{\infty} (\underline{\varphi}^{\dagger}\underline{r_b}^{\dagger}\underline{\tilde{\varphi}}^{\dagger}\ \underline{\tilde{r}}^{\dagger})^n\ \underline{\varphi}^{\dagger}\underline{t_b}^{\dagger}\underline{P_x}\, \underline{t_b}\, \underline{\varphi}\, (\underline{\tilde{r}}\, \underline{\tilde{\varphi}}\, \underline{r_b}\underline{\varphi})^n \right) \underline{t} \begin{pmatrix} 1 \\ 0 \end{pmatrix}. \qquad (7.7)$$

For different polarisation states, similar reflectivity and transmission expressions can be obtained just by changing the projection matrix: for outgoing y-linear polarised light, R_{xy}, outgoing a-linear diagonal polarised light at $+45^{\circ}$, R_{xa}, outgoing b-linear diagonal polarised light at -45°, R_{xb}, outgoing left circularly polarised light , R_{x+}, and outgoing right circularly polarised light , R_{x-},. These projection matrices are given in equation 5.20.

To study a circularly birefringent structure on circularly birefringent substrate as shown in figure 7.1 we need to consider waves propagating in forward direction from air into a circularly birefringent substrate going through a circularly birefringent structure and waves propagating in the reverse direction. We consider also the waves at the back of the substrate and air boundary and the rotation of light going through the substrate. As in Chapter 4, to calculate the reflectivities and transmissions we solve Maxwell's equations for electric and magnetic fields and apply the boundary conditions at interfaces between two media. The 4×4 transfer matrix of circularly birefringent film, which is derived in Chapter 4, is also used. The eigenvectors in the circularly birefringent substrate are circular; therefore, we need to convert them to linear polarised state as will be explained below; hence, in order to calculate the matrix elements in equation 7.3, the following calculations need to be considered.

7.1.1 Required calculations for the rotation going through the circularly birefringent substrate

As a consequence of using a thick circularly birefringent substrate, the rotation of light going through such a substrate needs to be considered. To obtain the rotation matrix for the substrate, $\underline{\varphi}$, we start from the general solution of Maxwell's equations for the electric field in terms of the circularly polarised eigenstates:

$$\boldsymbol{E}(z) = a\,(E_x^{0+}\hat{\mathbf{x}} + E_y^{0+}\hat{\mathbf{y}})e^{iq_s^{+}z} + b\,(E_x^{0-}\hat{\mathbf{x}} + E_y^{0-}\hat{\mathbf{y}})e^{iq_s^{-}z}, \tag{7.8}$$

where a and b are the amplitudes of $\boldsymbol{\sigma}^{+}$and $\boldsymbol{\sigma}^{-}$ waves. By substituting the eigenvector components, $E_x^{0\pm}$ and $E_y^{0\pm}$, from equation 4.35 into equation 7.8, then this equation can be rewritten as follows:

$$\boldsymbol{E}(z) = \left(a\, e^{iq_s^+ z} + b\, e^{iq_s^- z}\right)\hat{\mathbf{x}} - i\left(a\, e^{iq_s^+ z} - b\, e^{iq_s^- z}\right)\hat{\mathbf{y}}. \tag{7.9}$$

The initial field is obtained at *z=0*, as:

$$\begin{aligned} \boldsymbol{E}(0) &= (a+b)\hat{\mathbf{x}} - i(a-b)\hat{\mathbf{y}}, \\ &= E_x\,(0)\hat{\mathbf{x}} + E_y\,(0)\hat{\mathbf{y}}, \end{aligned} \tag{7.10}$$

from the last equation, *i.e.*, from E_x and E_y components, *a* and *b* can be found as:

$$\begin{aligned} a &= \frac{1}{2}\left(E_x(0) + i\,E_y(0)\right), \\ b &= \frac{1}{2}\left(E_x(0) - i\,E_y(0)\right). \end{aligned} \tag{7.11}$$

Substituting these amplitudes waves *a* and *b* in equation 7.9 when the substrate thickness $z = h_s$ leads to:

$$\left.\begin{aligned} E_x(h_s) &= e^{\frac{i\,(q_s^+ + q_s^-)\,h_s}{2}}\left[\cos\varphi\;\; E_x(0) - \sin\varphi\;\; E_y(0)\right], \\ E_y(h_s) &= e^{\frac{i\,(q_s^+ + q_s^-)\,h_s}{2}}\left[\sin\varphi\;\; E_x(0) + \cos\varphi\;\; E_y(0)\right], \end{aligned}\right\} \tag{7.12}$$

where the rotation angle for substrate is $\varphi = h_s(q_s^+ - q_s^-)/2$. The last equations can be rewritten in the matrix form as the following:

$$\begin{pmatrix} E_x(h_s) \\ E_y(h_s) \end{pmatrix} = e^{\frac{i\,(q_s^+ + q_s^-)\,h_s}{2}} \begin{pmatrix} \cos\varphi & -\sin\varphi \\ \sin\varphi & \cos\varphi \end{pmatrix} \begin{pmatrix} E_x(0) \\ E_y(0) \end{pmatrix}, \tag{7.13}$$

neglecting $e^{\frac{i\,(q_s^+ + q_s^-)\,h_s}{2}}$ as the total phase is not interesting in the case of incoherent treatment, the rotation matrix, $\underline{\varphi}$, is given by:

$$\underline{\varphi} = \begin{pmatrix} \cos\varphi & -\sin\varphi \\ \sin\varphi & \cos\varphi \end{pmatrix} \tag{7.14}$$

7.1.2 Required calculations for the forward propagation direction

To calculate the elements of the amplitude coefficient matrices of transmission and reflection for wave travelling from air into the substrate going through the structure, the solutions of Maxwell's equations in the air for electric and magnetic field for both polarisations are given by:

$$\left.\begin{aligned} E_x\,(z) &= ae^{iq_0 z} + be^{-iq_0 z}, \\ B_y\,(z) &= f_0\left(ae^{iq_0 z} - be^{-iq_0 z}\right), \\ E_y\,(z) &= a'\,e^{iq_0 z} + b'\,e^{-iq_0 z}, \\ B_x\,(z) &= -f_0\left(a'e^{iq_0 z} - b'e^{-iq_0 z}\right), \end{aligned}\right\} \tag{7.15}$$

where f_0 is defined by $f_0 = q_0/\omega$. a and a' are the amplitudes of the incoming waves. b and b' are the amplitudes of outgoing waves. The solutions of Maxwell's equations in the circularly birefringent substrate are:

$$\left.\begin{aligned} E_x\,(z) &= l\,E_x^{0+}e^{iq_s^+ z} + g\,E_x^{0-}e^{iq_s^- z}, \\ B_y\,(z) &= f_s^+ l\,E_x^{0+}e^{iq_s^+ z} + f_s^- g\,E_x^{0-}e^{iq_s^- z}, \\ E_y\,(z) &= l\,E_y^{0+}e^{iq_s^+ z} + gE_y^{0-}e^{iq_s^- z}, \\ B_x\,(z) &= -f_s^+ l\,E_y^{0+}e^{iq_s^+ z} - f_s^- g\,E_y^{0-}e^{iq_s^- z}, \end{aligned}\right\} \tag{7.16}$$

where $f_s^{\pm}$ are given by $f_s^{\pm} = q_s^{\pm}/\omega$. l and g are the amplitudes of the outgoing waves. Choosing the incoming wave to be linearly *x*-polarised at *z=0*, and substituting the eigenvector components, $E_x^{0\pm}$ and $E_y^{0\pm}$, from equation 4.35 into equation 7.16. We obtain the amplitudes of the forward and backward waves as the following: the incident amplitude for linearly incoming *x*-polarised wave $E_{0x}^{in} = a = 1$ and $E_{0y}^{in} = a' = 0$. The

outgoing amplitude for linearly *x*-polarised wave $E_{0x}^{out} = b = r_{xx}$ and $l + g = t_{xx}$. The outgoing *y*-polarised wave $E_y^{out} = b' = r_{xy}$ and $l - g = it_{xy}$. Using the transfer matrix to relate the fields at either side of the structure, we get for linearly incoming *x*-polarised wave:

$$\begin{pmatrix} t_{xx} \\ \frac{1}{2}\left(f_s^+\left(t_{xx} + it_{xy}\right) + f_s^-\left(t_{xx} - it_{xy}\right)\right) \\ it_{xy} \\ \frac{i}{2}\left(f_s^+\left(t_{xx} + it_{xy}\right) - f_s^-\left(t_{xx} - it_{xy}\right)\right) \end{pmatrix} = M \begin{pmatrix} 1 + r_{xx} \\ f_0(1 - r_{xx}) \\ r_{xy} \\ f_0 r_{xy} \end{pmatrix}, \tag{7.17}$$

where M is the 4×4 transfer matrix of circularly birefringent structure for a forward direction. Solving simultaneous equations in 7.17 gives r_{xx}, r_{xy}, t_{xx} and t_{xy}. Similarly, by setting the incoming wave to be y-polarised we get:

$$\begin{pmatrix} t_{yx} \\ \frac{1}{2}\left(f_s^+\left(t_{yx} + it_{yy}\right) + f_s^-\left(t_{yx} - it_{yy}\right)\right) \\ it_{yy} \\ \frac{i}{2}\left(f_s^+\left(t_{yx} + it_{yy}\right) - f_s^-\left(t_{yx} - it_{yy}\right)\right) \end{pmatrix} = M \begin{pmatrix} r_{yx} \\ -f_0 r_{yx} \\ 1 + r_{yy} \\ -f_0(1 - r_{yy}) \end{pmatrix}, \tag{7.18}$$

solving simultaneous equations in 7.18 gives r_{yy}, r_{yx}, t_{yy} and t_{yx}.

7.1.3 Required calculations for the reverse propagation direction

To calculate the elements of the amplitude coefficient matrices of transmission and reflection of the reverse direction, *i.e.*, wave travelling from the circularly birefringent substrate into air going through the structure, the solutions of Maxwell's equations in this substrate for electric and magnetic field for both polarisations are given by:

$$\left.\begin{aligned} E_x\,(z) &= aE_x^{0+}e^{iq_s^+z} + cE_x^{0+}e^{-iq_s^+z} + bE_x^{0-}e^{iq_s^-z} + dE_x^{0-}e^{-iq_s^-z}, \\ B_y\,(z) &= f_s^+\left(aE_x^{0+}e^{iq_s^+z} - cE_x^{0+}e^{-iq_s^+z}\right) + f_s^-\left(bE_x^{0-}e^{iq_s^-z} - dE_x^{0-}e^{-iq_s^-z}\right), \\ E_y\,(z) &= aE_y^{0+}e^{iq_s^+z} + cE_y^{0+}e^{-iq_s^+z} + bE_y^{0-}e^{iq_s^-z} + dE_y^{0-}e^{-iq_s^-z}, \\ B_x\,(z) &= -f_s^+\left(aE_y^{0+}e^{iq_s^+z} - cE_y^{0+}e^{-iq_s^+z}\right) - f_s^-\left(bE_y^{0-}e^{iq_s^-z} - dE_y^{0-}e^{-iq_s^-z}\right), \end{aligned}\right\} \quad (7.19)$$

here a, b are the amplitudes of incoming waves, c, d are the amplitudes of outgoing waves. The solutions of Maxwell's equations in the air are:

$$\left.\begin{aligned} E_x\,(z) &= l\,e^{iq_0z}, \\ B_y\,(z) &= f_0\,l\,e^{iq_0z}, \\ E_y\,(z) &= l'\,e^{iq_0z}, \\ B_x\,(z) &= -f_0\,l'\,e^{iq_0z}, \end{aligned}\right\} \quad (7.20)$$

where l and l' are the amplitudes of outgoing waves. Choosing the incoming wave to be linearly x-polarised at $z=0$, and substituting the eigenvector components, $E_x^{0\pm}$ and $E_y^{0\pm}$, from equation 4.35 into equation 7.19. We obtain the amplitude of incoming waves as $E_{0x}^{in} = a + b = 1$ and $E_{0y}^{in} = a - b = 0$. The amplitude of outgoing waves $E_{0x}^{out} = c + d = \tilde{r}_{xx}$ and $l = \tilde{t}_{xx}$, similarly $E_{0y}^{out} = -i(c - d) = \tilde{r}_{xy}$ and $l' = \tilde{t}_{xy}$. Using the transfer matrix to relate the fields at either side of the structure, gives for linearly incoming x-polarised wave:

$$\begin{pmatrix} \tilde{t}_{xx} \\ f_0\,\tilde{t}_{xx} \\ \tilde{t}_{xy} \\ -f_0\,\tilde{t}_{xy} \end{pmatrix} = \widetilde{M} \begin{pmatrix} 1 + \tilde{r}_{xx} \\ \frac{1}{2}\left(f_s^+\left(1 - \tilde{r}_{xx} - i\tilde{r}_{xy}\right) + f_s^-\left(1 - \tilde{r}_{xx} + i\tilde{r}_{xy}\right)\right) \\ \tilde{r}_{xy} \\ \frac{i}{2}\left(f_s^+\left(1 - \tilde{r}_{xx} - i\tilde{r}_{xy}\right) - f_s^-\left(1 - \tilde{r}_{xx} + i\tilde{r}_{xy}\right)\right) \end{pmatrix}. \quad (7.21)$$

where $\widetilde{M}$ is the 4×4 transfer matrix of circularly birefringent structure for a reverse direction. Solving simultaneous equations in 7.21 gives $\tilde{r}_{xx}, \tilde{r}_{xy}, \tilde{t}_{xx}$ and $\tilde{t}_{xy}$. In a similar way, by setting linearly incoming y-polarised wave we get:

$$\begin{pmatrix} \tilde{t}_{yx} \\ f_0\,\tilde{t}_{yx} \\ \tilde{t}_{yy} \\ -f_0\,\tilde{t}_{yy} \end{pmatrix} = \widetilde{M} \begin{pmatrix} \tilde{r}_{yx} \\ \frac{-i}{2}\left(f_s^{+}\left(i\,\tilde{r}_{yx} - \tilde{r}_{yy} - 1\right) + f_s^{-}\left(i\,\tilde{r}_{yx} + \tilde{r}_{yy} + 1\right)\right) \\ 1 + \tilde{r}_{yy} \\ \frac{1}{2}\left(f_s^{+}\left(i\tilde{r}_{yx} - \tilde{r}_{yy} - 1\right) - f_s^{-}\left(i\tilde{r}_{yx} + \tilde{r}_{yy} + 1\right)\right) \end{pmatrix}, \tag{7.22}$$

solving equation 7.22 gives $\tilde{r}_{yy}, \tilde{r}_{yx}, \tilde{t}_{yy}$ and $\tilde{t}_{yx}$.

7.1.4 Required calculations at circularly birefringent substrate-air interface

To calculate the elements of the amplitude coefficient matrices of transmission and reflection of the back substrate, *i.e.,* at the interface between the substrate and air, we could just follow the same procedures discussed in section 7.1.3 but now, the transfer matrix is a unit matrix because there is only one interface. Here, we solve Maxwell's equations for electric and magnetic fields, which are as in equations 7.19 and 7.20, then apply the boundary conditions at that interface. This gives:

$$t_{xx}^{b} = t_{yy}^{b} = \frac{2\,q_s^{+}\,q_s^{-} + q_0\,(q_s^{+} + q_s^{-})}{(q_0 + q_s^{+})\,(q_0 + q_s^{-})}, \tag{7.23}$$

$$r_{xx}^{b} = r_{yy}^{b} = \frac{q_s^{+}\,q_s^{-} - q_0^{2}}{(q_0 + q_s^{+})\,(q_0 + q_s^{-})}, \tag{7.24}$$

$$t_{xy}^{b} = r_{xy}^{b} = t_{yx}^{b} = r_{yx}^{b} = \frac{-i\,q_0(q_s^{+} - q_s^{-})}{(q_0 + q_s^{+})\,(q_0 + q_s^{-})}. \tag{7.25}$$

A further check for equations 7.23 and 7.24 is the case of an isotropic transparent substrate, *i.e.,* when $q_s^{+} = q_s^{-} = q_s$. This leads to Fresnel's equations, equation 5.6. Also, from equation 7.25, t_{xy}^{b}, r_{xy}^{b}, t_{yx}^{b}, r_{yx}^{b}, all become equal to zero. The Faraday

rotation going from the back of the substrate to air can be obtained directly by applying the equations 7.23 and 7.25 in equation 3.5 in transmission. As can be seen, there is no rotation if $q_s^{\pm}$ are real, *i.e.*, there is no absorption in the substrate. However, to find the Faraday rotation going from the back of the substrate to air, we just assume the circularly birefringent substrate is absorption medium with the complex reflective indices defined as $\tilde{n}_s^{\pm} = n_s^{\pm} + i\kappa_s^{\pm},$ in a similar way to equation 4.24. Here the real part is $n_s^{\pm}$. The extinction coefficients $\kappa_s^{\pm}$ are given by $\kappa_s^{\pm} = \lambda\, \alpha^{\pm}/4\pi$ in terms of absorption coefficients of substrate $\alpha^{\pm}$ as defined for isotropic media by Pedrotti and Pedrotti (1993). To obtain a rotation formula, equations 7.23 and 7.25 are applied in terms of n_0 and $\tilde{n}_s^{\pm}$ in equation 3.5 for transmission. In order to simplify the calculations, the difference is always small in $n_s^- - n_s^+$ and in $\kappa_s^- - \kappa_s^+$ so, we can put $n_s^{\pm}$ equal to average refractive index of substrate n_s and similarly for $\kappa_s^{\pm} = \kappa_s$. We only concentrated on the actual value when there is subtraction as in $n_s^- - n_s^+$ and in $\kappa_s^- - \kappa_s^+$. The expression of the Faraday rotation going from the back of the substrate to air is found as:

$$\psi \approx \mathrm{Re}\left(t_{xy}^b / t_{xx}^b\right) \approx \frac{1}{2}\mathrm{Re}\left[\frac{n_0\left(\kappa_s^- - \kappa_s^+ + i\,(n_s^- - n_s^+)\right)}{(\kappa_s - i\,n_s)(\kappa_s - i\,(n_s + n_0)}\right]. \qquad (7.26)$$

That means any circularly birefringent substrate with absorption property has some rotation even if the absorption is the same for the two different circular polarisations, *i.e.*, the difference between absorption coefficients is equal to zero.

7.2 Results and Discussion

Ignoring absorption for simplicity, a structure $EuFeO_3/Bi{:}YIG$ was studied. It consisted of circularly birefringent thin film Eu orthoferric, $EuFeO_3$, and this film was

deposited on a circularly birefringent thick substrate, $Bi{:}YIG$. The film parameters were taken from Kahn *et al.* (1996) as $\varepsilon_{xx} = 6.980$. In addition, from the graph given by the authors, an off diagonal element was taken as an approximate value; $\varepsilon_{xy} \approx 0.011$ at $\lambda = 442.8\,nm$, at this wavelength, the film thickness was equal to $\lambda/2\sqrt{\varepsilon_{xx}}$. Substrate parameters were taken from Kato *et al.*,(2003) as the following: $\varepsilon_{xx} = 5.59$; $\varepsilon_{xy} = -0.00369$; at $\lambda = 720\,nm$ and its thickness was set as $0.5\,mm$. In this calculation, we used those parameters, which correspond to different wavelength values for the film and substrate because those are available realistic parameters.

To determine the Faraday rotation, equation 5.22 was used with equation 7.7 in different polarisation states for a single pass of substrate, *i.e.*, $n = 0$ in equation 7.7. The Faraday rotation spectrum was firstly calculated for the whole structure as shown by the blue curve in figure 7.2. The Faraday rotation for the substrate alone was also calculated, using $\varphi = h_s\,(q_s^+ - q_s^-)/2$, but on this scale it is indistinguishable from the curve for the whole structure. The green spectrum shows the small differences between the Faraday values of the whole structure and substrate alone. This differences spectrum was calculated by subtracting the Faraday values of the circularly birefringent substrate from those of the whole structure. To compare with the green curve, the Faraday rotation for the single pass of the film alone was calculated as represented by the pink curve. As can be seen, the rotation of the film is very small. The differences spectrum did not give the same Faraday rotation as that rotation was calculated for the single pass in the film alone; this was perhaps not expected experimentally. The effect of the multiple reflections inside the film produced this result. So, as a consequence of this last numerical result, the following theories will be considered analytically below.

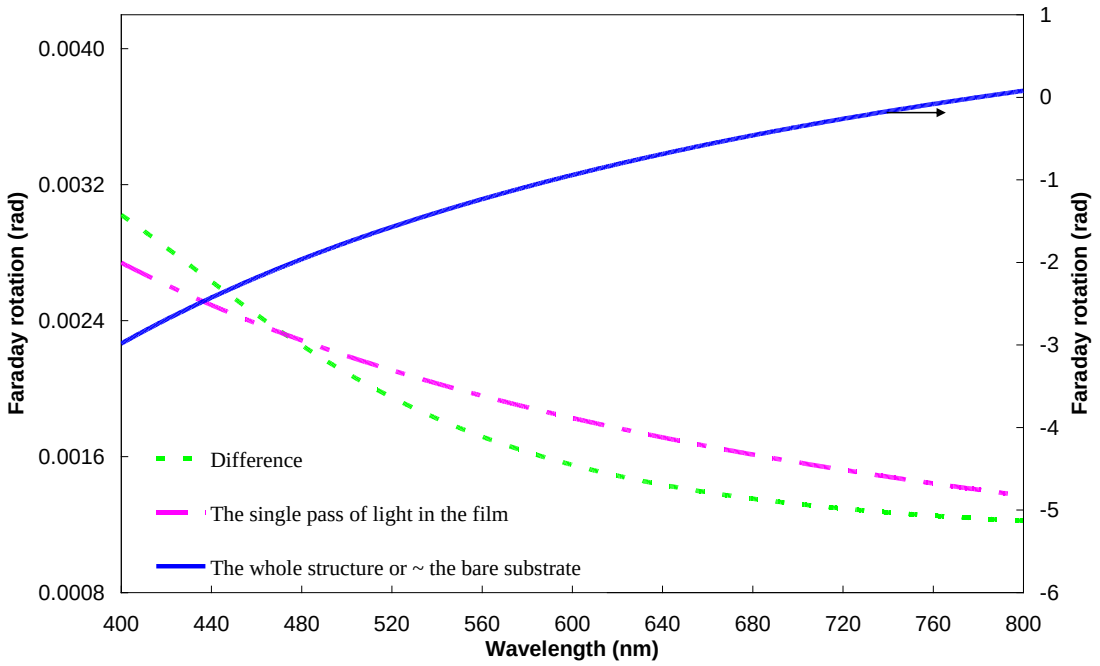

Figure 7.2: Numerical Faraday rotation spectra for the whole structure, $EuFeO_3/Bi{:}YIG$; for a thick substrate, $Bi{:}YIG$; for differences between the spectra of the whole structure and substrate alone and finally for the single pass in a thin film, $EuFeO_3$.

7.3 Faraday rotation theory of simple film with air on both sides

Multiple reflection and transmission beam problems through two parallel plates, the thin film, have been studied in many optics books, for example, Smith *et al.*, (2007), Born and Wolf (1999) and Pedrotti and Pedrotti (1993). In general, the total transmitted amplitude, E_0^t, of N transmissions terms, is the sum of a geometric series (see figure 7.3) and given for an isotropic film as:

$$E_0^t = E_0^i\, t\, \tilde{t}\, e^{i\delta/2}\left(1 + \tilde{r}^2 e^{i\delta} + \tilde{r}^4\, e^{2i\delta} + \cdots + (\tilde{r}^2\, e^{i\delta})^{N-1}\right),$$

$$= E_0^i\, t\, \tilde{t}\, e^{i\delta/2} \sum_{N=1}^{\infty} (\tilde{r}^2\, e^{i\delta})^{N-1}, \qquad (7.27)$$

where E_0^i is the amplitude of incident wave. t and $\tilde{t}$ are the amplitude coefficients of transmission from air to a film and from a film to air, respectively. r and $\tilde{r}$ are the amplitude coefficients of reflection out and in the film, respectively. δ represents the phase difference between successive reflected beams (2 passes through film). If $N \to \infty$, hence $\tilde{r}^{2N}$ becomes zero, the transmitted amplitude of the isotropic thin film is given by:

$$E_0^t = E_0^i \frac{t\,\tilde{t}\,e^{i\delta/2}}{1-\tilde{r}^2\,e^{i\delta}} \tag{7.28}$$

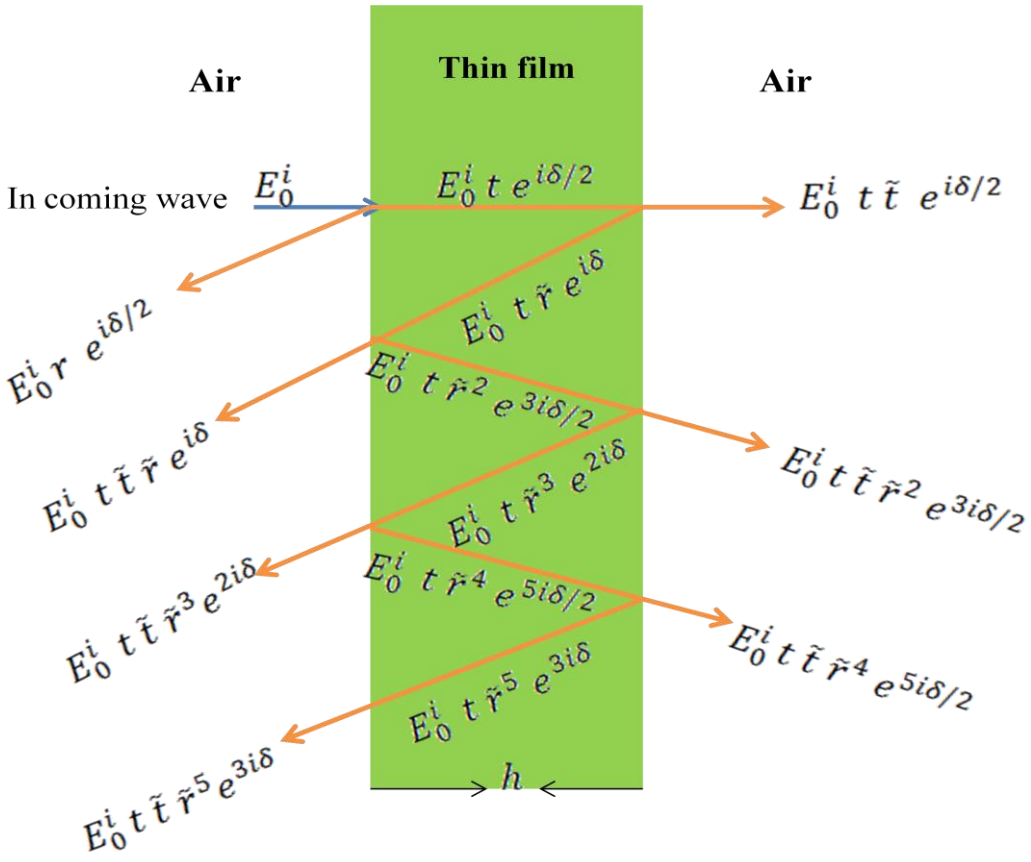

Figure 7.3: Schematic diagram of multiple passes in a simple film with air on both sides. For symbols see the text. For clarity, the rays are drawn at small angles to the normal. Adapted from Pedrotti and Pedrotti (1993).

7.3.1 Exact formula of Faraday rotation

The multiple transmission beam problem through an isotropic film was explained above. Here we will study this problem when a circularly birefringent film is used instead of an isotropic film. As a result of the properties of the film, we can separate the above problem into two circular polarisation problems as there is no mixing between the two. Let us consider a linearly polarised incoming wave incident normally on a simple circularly birefringent film, which has air on both sides as shown by figure 7.3. Now this film has two refractive indices, $n^{\pm}$, so equation 7.28 can be modified as the pair of equations as:

$$\left.\begin{aligned} E_0^{t_+} &= E_0^{i_+}\,\frac{t_+\,\tilde{t}_+\,e^{i\delta^+/2}}{1-\tilde{r}_+^2\,e^{i\delta^+}}, \qquad (a)\\ E_0^{t_-} &= E_0^{i_-}\,\frac{t_-\,\tilde{t}_-\,e^{i\delta^-/2}}{1-\tilde{r}_-^2\,e^{i\delta^-}}, \qquad (b) \end{aligned}\right\} \tag{7.29}$$

It should be pointed out in this derivation, we deal with the incident amplitude for linearly incoming *x*-polarised wave and can express this as equal amplitudes for the two circular polarisations, *i.e.*, $(E_0^{i_+} = E_0^{i_-} = E_{0x}^{i}/\sqrt{2} = E_0^{i})$. Fresnel's equations at normal incidence are used to calculate $t_{\pm}, \tilde{t}_{\pm}$ and $\tilde{r}_{\pm}$ as follows:

$$t_{\pm} = \frac{2n_0}{n^{\pm}+n_0}, \qquad \tilde{t}_{\pm} = \frac{2n^{\pm}}{n^{\pm}+n_0}, \qquad \tilde{r}_{\pm} = \frac{n^{\pm}-n_0}{n^{\pm}+n_0}. \tag{7.30}$$

$\delta^{\pm}$ indicate there are two phase differences given at normal incidence by:

$$\delta^{\pm} = 2\,q^{\pm}h = 2\,q_o n^{\pm}\,h, \tag{7.31}$$

in which h is the film thickness, $q^{\pm}$ are the two wave-vector values of a circularly birefringent film and q_o is the wave-vector value of the air. Then the Faraday rotation, ψ, of the thin film can be found exactly by using Sato's definition (1981) as:

$$\psi = -\frac{1}{2}(\theta_+ - \theta_-), \tag{7.32}$$

where the phases $\theta_{\pm}$ of the complex number, $E_0^{t_\pm} = \left|E_0^{t_\pm}\right| e^{\theta_\pm}$, are $Arg\{ E_0^{t_\pm}\}$.

The difference between these phases here should be a Faraday rotation so equation 7.32 can be rewritten in argument of a complex number as:

$$\psi = \frac{1}{2} Arg\left\{\frac{E_0^{t-}}{E_0^{t+}}\right\} = \frac{1}{2} Arg\left\{\frac{t_- \tilde{t}_- e^{i\delta^-/2}(1 - \tilde{r}_+^2 e^{i\delta^+})}{t_+ \tilde{t}_+ e^{i\delta^+/2}(1 - \tilde{r}_-^2 e^{i\delta^-})}\right\}. \tag{7.33}$$

7.3.2 Approximate formula of Faraday

Now, as we know, the difference between two circular refractive indices is small for a real material, so we use this to deduce an approximate formula for Faraday rotation of the circularly birefringent thin film which has air on both sides. We write:

$$n^{\pm} = n \pm \Delta, \tag{7.34}$$

where n is the average refractive index of the film and 2Δ is the small difference between two circular refractive indices. The comparison between this definition (equation 7.34) and the definition in terms of two circularly polarised lights (see equation 4.34 and 4.35) gives $\Delta = -\varepsilon_{xy}/2\,n$. Substituting equation 7.34 into equation 7.31, gives:

$$\delta^{\pm} = 2\, q_0 (n \pm \Delta) h. \tag{7.35}$$

In order to find analytically the approximate formula of Faraday rotation, we calculate $\frac{t_-\,\tilde{t}_-}{t_+\,\tilde{t}_+}$ using equation 7.30, 7.34 and Binominal expansion to first order in $\left(\frac{\Delta}{n}\right)$, to get:

$$\frac{t_-\,\tilde{t}_-}{t_+\,\tilde{t}_+} = \frac{n^-}{n^+}\left(\frac{n_0+n^+}{n_0+n^-}\right)^2 \approx 1 - \frac{2\Delta}{n} + \frac{4\Delta}{n_0+n} \tag{7.36}$$

Also, applying equation 7.35 in $e^{i\delta^{\pm}/2}$ of equation 7.33 and using Taylor and Binominal expansions to first order in Δ, gives:

$$\frac{e^{i\delta^-/2}}{e^{i\delta^+/2}} \approx 1 - 2\,i\,q_o h\,\Delta. \tag{7.37}$$

Besides that, $\frac{1-\tilde{r}_+^2\,e^{i\delta^+}}{1-\tilde{r}_-^2\,e^{i\delta^-}}$ need to be found; by using equations 7.30, 7.34, Binominal expansion and the same procedures on $e^{i\delta^{\pm}}$, we obtain:

$$\frac{1-\tilde{r}_+^2\,e^{i\delta^+}}{1-\tilde{r}_-^2\,e^{i\delta^-}} \approx 1 - \frac{4\,\tilde{r}\,e^{i\,\delta_o}\,\Delta}{1-\tilde{r}^2 e^{i\,\delta_o}}\left(i\,q_0\tilde{r}\,h + \frac{2\,n_0}{(n_0+n)^2}\right). \tag{7.38}$$

where

$$\tilde{r} = \frac{n-n_0}{n+n_0}, \qquad \text{and} \qquad \delta_0 = 2\,n\,q_0\,h. \tag{7.39}$$

By multiplying equations 7.36, 7.37 and 7.38 with some algebra, we get:

$$\begin{aligned}\frac{E_0^{t_-}}{E_0^{t_+}} &= \frac{t_-\,\tilde{t}_-\,e^{i\delta^-/2}(\,1-\tilde{r}_+^2\,e^{i\delta^+})}{t_+\,\tilde{t}_+\,e^{i\delta^+/2}(\,1-\tilde{r}_-^2\,e^{i\delta^-})} \\ &\approx 1 + 2\,\Delta\left[\left(\frac{\tilde{r}}{n}\right) - \frac{2\,\tilde{r}\,e^{i\,\delta_o}}{1-\tilde{r}^2 e^{i\,\delta_o}}\left(i\,q_0\tilde{r}\,h + \frac{2\,n_0}{(n_0+n)^2}\right) - i\,q_o h\right].\end{aligned} \tag{7.40}$$

We define $\frac{E_0^{t_-}}{E_0^{t_+}} = 1 + z,$ from the geometry for a complex number z, θ is given as:

$$\theta = \tan^{-1}\frac{\mathrm{Im}(z)}{1+\mathrm{Re}(z)} \approx \mathrm{Im}(z), \tag{7.41}$$

the approximation is good for small *z*.

Hence, the Faraday rotation is just the imaginary part of that complex number. By taking only the imaginary part of equation 7.40, the required approximate formula for the Faraday rotation is found as:

$$\psi_{Appx} = \mathrm{Im}\left[\frac{-e^{i\,\delta_o}}{1-\tilde{r}^2 e^{i\,\delta_o}}\left(\frac{4\,\tilde{r}\,n_0}{(n_0+n)^2} + 2\,i\,q_0\,\tilde{r}^2\,h\right) - i\,q_o h\right]\Delta. \tag{7.42}$$

Here the superscript $Appx$ refers to approximate value. This can be rewritten as the following:

$$\psi_{Appx} = \frac{-\Delta}{\left(1-\widetilde{\mathrm{R}}\right)^2\left(1+\frac{4\,\widetilde{\mathrm{R}}}{\left(1-\widetilde{\mathrm{R}}\right)^2}\sin^2\frac{\delta_o}{2}\right)}\left[\frac{4\sqrt{\widetilde{R}}\,n_0}{(n_0+n)^2}\,\sin\,\delta_o + 2\,\widetilde{\mathrm{R}}\left(\cos\,\delta_o - \widetilde{\mathrm{R}}\right)q_0\,h\right] - q_o h\,\Delta, \tag{7.43}$$

where $\widetilde{\mathrm{R}}$ is the reflectivity in the film and defined by $\widetilde{\mathrm{R}} = |\tilde{r}\,|^2$, $\frac{4\,\widetilde{\mathrm{R}}}{\left(1-\widetilde{\mathrm{R}}\right)^2}$ represents the finesse coefficient, *FC*. As given in Hecht (2002), this coefficient is related to the finesse quantity $\mathcal{F}$, as $\mathcal{F} = \pi\sqrt{FC}/2 = \pi\sqrt{\widetilde{\mathrm{R}}}\,/\left(1-\widetilde{\mathrm{R}}\right)$. The resolving power or the quality factor of resonator is $Q = \mathcal{F}\,\lambda_0/FSR$, where λ_0 is the wavelength on resonance and FSR refers to free spectral range, defined as the wavelength difference at which fringes of different order overlap (Hecht, 2002). The finesse can be considered as the number of lines of a diffraction grating which give the same resolution as the Fabry-

Perot, so it represents a measure of the effective number of passes of the light through the film (Born and Wolf, 1999).

Applying the resonance condition for a maximum transmission, which is $\frac{\delta_o}{2} = m\,\pi$, where m is an integer leads to $\cos\,\delta_o = 1$ and $\sin\,\delta_o = 0$. The last equation then becomes:

$$\psi_{Res} = -2\,q_0\,h\,\frac{\tilde{R}}{(1-\tilde{R})}\,\Delta - \,q_o h\,\Delta. \tag{7.44}$$

Here the superscript Res refers to resonance value. $q_o h\,\Delta$ is the contribution of the Faraday rotation from the first pass of light through the film and $\frac{\tilde{R}}{(1-\tilde{R})}$ is a measure of the effective number of double passes based on the Faraday rotation. The Fabry-Perot, Faraday measures for the effective number of passes are different. However, for a high reflectivity, $\tilde{R} \approx 1$, the difference between $\sqrt{\tilde{\mathrm{R}}}$ and $\tilde{\mathrm{R}}$ is negligible so both are proportional to $1/(1-\tilde{R})$. So, as $\tilde{R}$ approaches one, the behaviour is very similar.

7.4 Results and Discussion

The Faraday rotation of the thin film, $EuFeO_3$, which had air on both sides was calculated using the exact analytical formula (equation 7.33), as shown by the black curve in figure 7.4. The exact and approximate Faraday spectra of the film with air on both sides are indistinguishable on this scale. The black curve also shows the numerical result for this film.

The disagreement between exact and approximate analytical formulae starts noticeably at about $\varepsilon_{xy} = 1.7$, *i.e.*, the difference becomes obvious when the ε_{xy} value is much larger, at least 1.7 hundreds of times of practical value of ε_{xy} as shown by figure 7.5. For $\varepsilon_{xy} \approx 0.011$ (the real used value), the fraction of the difference value (*i.e.* the difference between approximate and exact analytical rotations) to exact value is $\approx 1.14 \times 10^{-6}$. The evidence from this calculation shows this approximate formula is very good for any realistic material.

The effect by having the multiple passes through the film is also shown in figure 7.4; as the black curve shows the Faraday rotation spectrum for the multiple passes through the film and the pink curve shows that for a single pass through the film. Clearly, from the figure the black curve for the film with air on both sides disagrees with 'difference' curve in figure 7.2. As can also be seen from figure 7.4 the resonance case occurred at about $\lambda = 443\, nm$, as shown by the red point. It should be pointed out this is not a transmission peak. This is a Faraday rotation, which depends on the phase difference for the two circularly polarised lights. This probably occurs where the phase variation is maximum, which may not necessary corresponded to the transmission peak. The following theory, *i.e.*, Faraday rotation theory of a simple film on a circularly birefringent substrate will be considered analytically below.

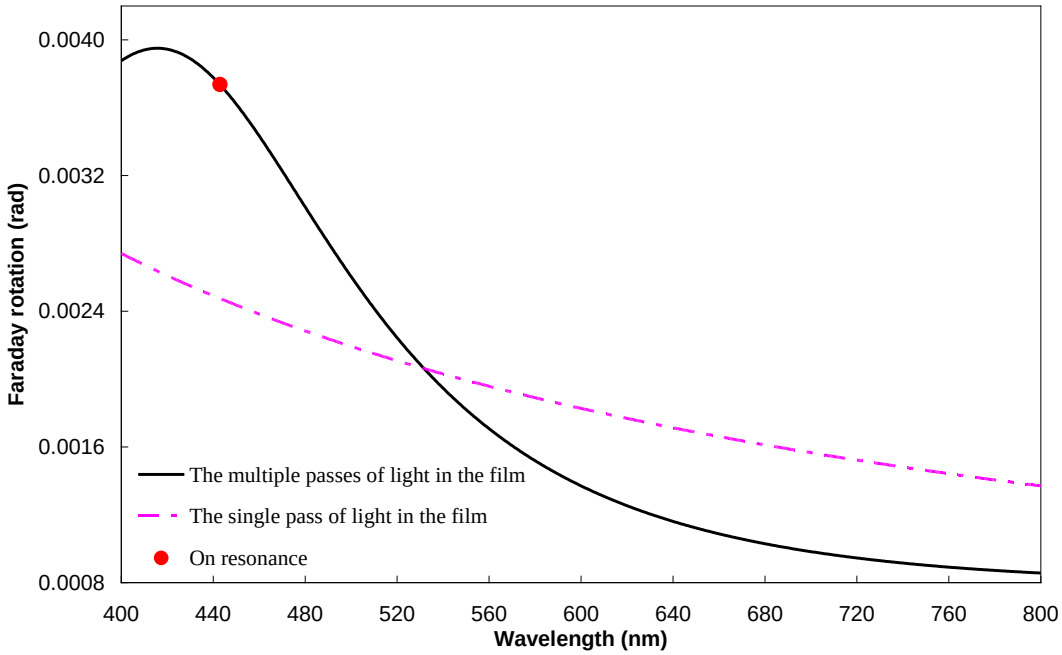

Figure7.4: The exact, approximate analytical Faraday rotation results and the numerical result, for a thin film, $EuFeO_3$ with air on both sides and has the multiple passes, are shown by the black curve. The single pass of light in the film is shown by the pink curve. The red point indicates Faraday rotation on resonance.

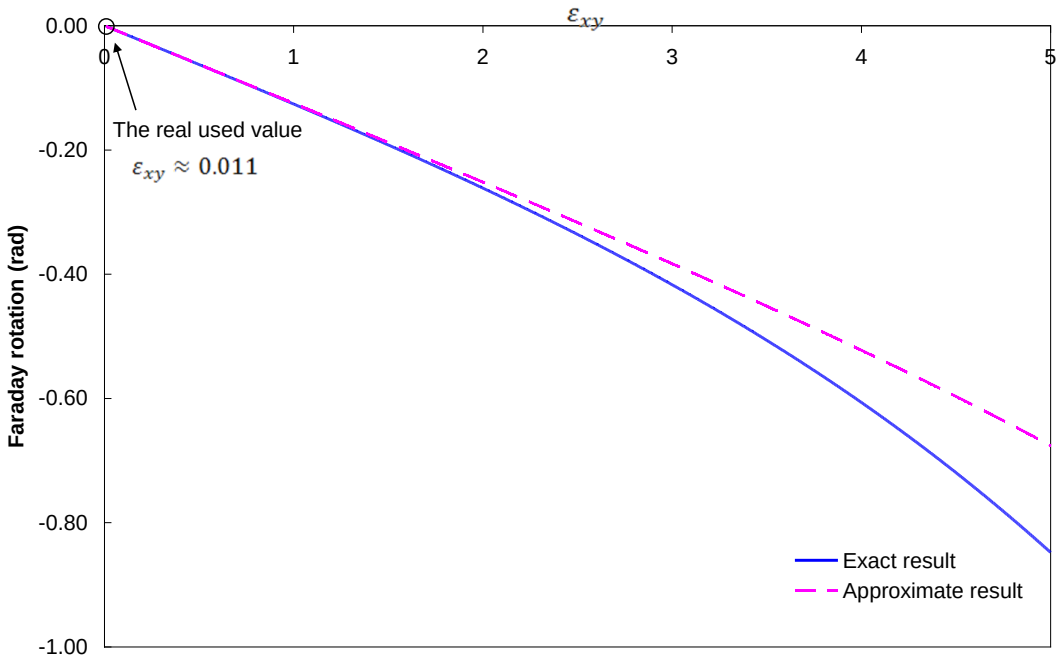

Figure7.5: Faraday rotations against the ε_{xy} values for a thin film, $EuFeO_3$ with air on both sides at $\lambda = 600\ nm$.

7.5 Faraday rotation theory of a simple film on a circularly birefringent substrate

In section 7.3, the Faraday rotation was investigated analytically for a simple circularly birefringent film, which had air on both sides. This section will consider analytically the Faraday rotation for a simple circularly birefringent film on a circularly birefringent substrate. We will derive exact and approximate analytical formulae for the Faraday rotation when a film is placed on a circularly birefringent substrate.

7.5.1 Exact formula of Faraday rotation

Let us now assume the light is incident at a normal direction on a simple circularly birefringent film. This film has two refractive indices, $n^{\pm}$, and is deposited on a circularly birefringent substrate which also has two refractive indices, $n_s^{\pm}$. This means the film has air on one side and circularly birefringent medium on another side, so this is a more general result for a simple film. From figure 7.6 and as above, the same procedures were followed; the transmitted amplitudes of this film are given by:

$$\left.\begin{aligned} E_0^{t_+} &= E_0^{i_+}\ \frac{t_1^+\ t_2^+\ e^{i\delta^+/2}}{1-\tilde{r}_1^+ r_2^+\ \ e^{i\delta^+}}, \qquad (a)\\ E_0^{t_-} &= E_0^{i_-}\ \frac{t_1^-\ t_2^-\ e^{i\delta^-/2}}{1-\tilde{r}_1^- r_2^-\ e^{i\delta^-}}, \qquad (b) \end{aligned}\right\} \tag{7.45}$$

As mentioned above ($E_0^{i_+} = E_0^{i_-} = E_{0x}^i/\sqrt{2} = E_0^i$) and $\delta^{\pm}$ is defined by equation 7.35. $t_1^{\pm}$ and $t_2^{\pm}$ are the amplitude coefficients of transmission from air to a film and from a film to a substrate, respectively. At the first interface, $r_1^{\pm}$ and $\tilde{r}_1^{\pm}$ are the amplitude coefficients of reflection out and in the film, respectively. At the second interface, $r_2^{\pm}$

and $\tilde{r}_2^{\pm}$ are the amplitude coefficients of reflection in and out the film, respectively. Fresnel's equations are used to calculate $t_{1,2}^{\pm}$, $\tilde{r}_1^{\pm}$ and $r_2^{\pm}$ as follows:

$$t_1^{\pm} = \frac{2n_0}{n^{\pm} + n_0}, \quad t_2^{\pm} = \frac{2n^{\pm}}{n^{\pm} + n_s^{\pm}}, \quad \tilde{r}_1^{\pm} = \frac{n^{\pm} - n_0}{n^{\pm} + n_0}, \quad r_2^{\pm} = \frac{n^{\pm} - n_s^{\pm}}{n^{\pm} + n_s^{\pm}}. \qquad (7.46)$$

Finally, the exact Faraday rotation, ψ, of this film is computed by using equation 7.33.

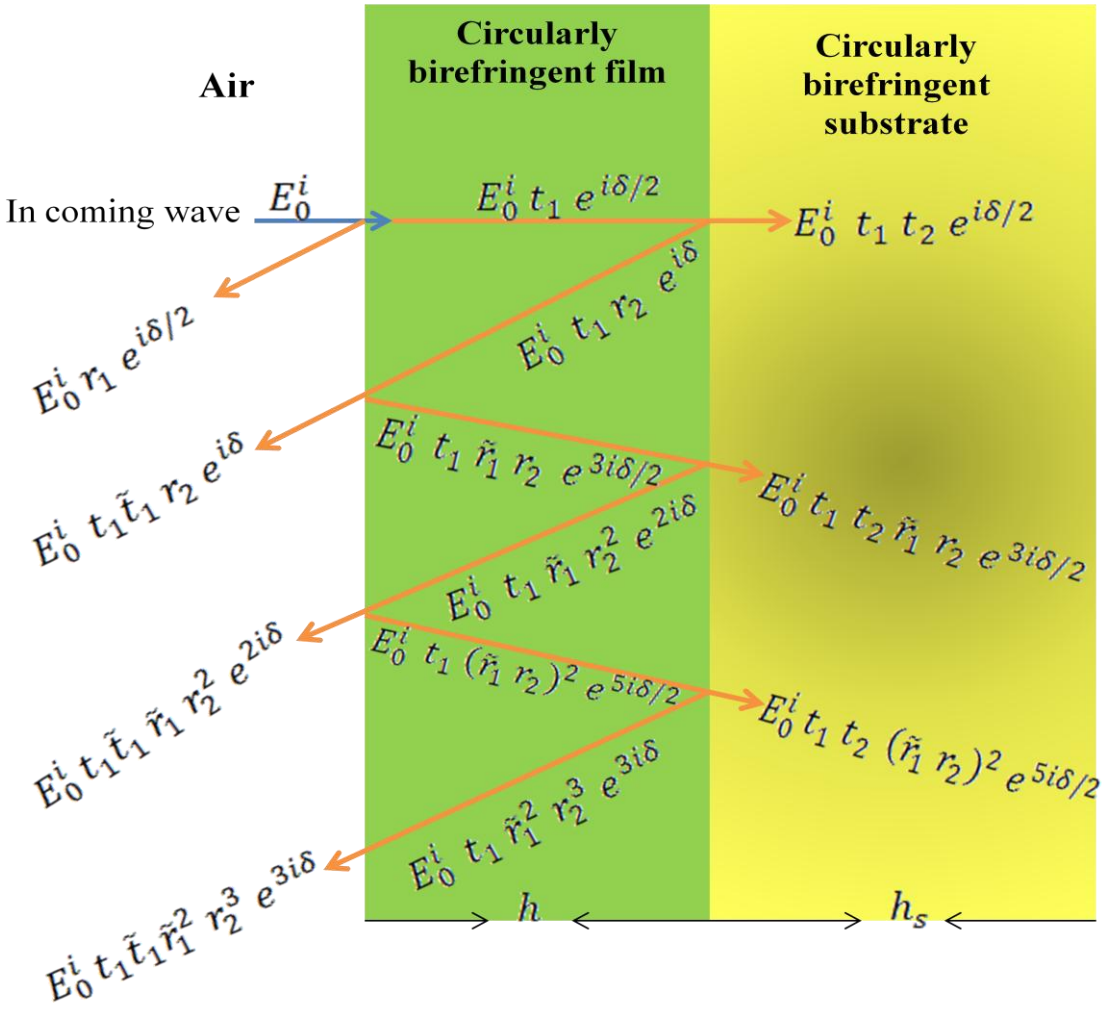

Figure7.6: Schematic diagram of multiple passes inside a simple circularly birefringent film deposited on a circularly birefringent substrate. For symbols see the text. For clarity, the rays are drawn at small angles to the normal.

7.5.2 Approximate formula of Faraday rotation

The same procedures were followed, as explained in section 7.3.2. Some further assumptions have to be included to derive an approximate formula of Faraday rotation for a circularly birefringent thin film on a circularly birefringent substrate. First, for the film which has an average refractive index, n, equation 7.34 was supposed as before. Second, for the circularly birefringent substrate that has an average refractive index, n_s, we assume:

$$n_s^{\pm} = n_s \pm \Delta_s, \tag{7.47}$$

where $2\Delta_s$ is the small difference between two circular refractive indices in the substrate.

As mentioned previously, the Faraday rotation can be rewritten in argument of a complex number as given by equation 7.33. Hence, substituting equation 7.45 into equation 7.33 (in this case) to find the analytical approximate formula of Faraday rotation gives:

$$\psi = \frac{1}{2} Arg \left\{ \frac{t_1^- \, t_2^- e^{i\delta^-/2} (1 - \tilde{r}_1^+ \, r_2^+ \, e^{i\delta^+})}{t_1^+ \, t_2^+ \, e^{i\delta^+/2} (1 - \tilde{r}_1^- \, r_2^- \, e^{i\delta^-})} \right\}. \tag{7.48}$$

Then using equation 7.46 to find $\frac{t_1^- \, t_2^-}{t_1^+ \, t_2^+}$ and in a similar way, substituting equation 7.34 and 7.47 with applying Binominal expansion to first order in Δ and Δ_s gives:

$$\begin{aligned} \frac{t_1^- \, t_2^-}{t_1^+ \, t_2^+} &= \frac{n^-}{n^+} \left(\frac{n_0 + n^+}{n_0 + n^-} \right) \left(\frac{n_s^+ + n^+}{n_s^- + n^-} \right) \\ &\approx 1 + 2\,\Delta \left(\frac{1}{n_0 + n} + \frac{1}{n_s + n} - \frac{1}{n} \right) + \frac{2\,\Delta_s}{n_s + n}. \end{aligned} \tag{7.49}$$

From the foregoing $\frac{e^{i\delta^-/2}}{e^{i\delta^+/2}}$ is given by equation 7.37. To find $\frac{1-\tilde{r}_1^+ r_2^+ e^{i\delta^+}}{1-\tilde{r}_1^- r_2^- e^{i\delta^-}}$, equations 7.34 and 7.47 were substituted into equation 7.46 for $\tilde{r}_1^{\pm}$ and $r_2^{\pm}$. In addition, we use Binominal expansion and do the same procedures on $e^{i\delta^{\pm}}$, we get:

$$\frac{1-\tilde{r}_1^+ r_2^+ e^{i\delta^+}}{1-\tilde{r}_1^- r_2^- e^{i\delta^-}} \approx 1+\frac{2\, e^{i\delta_0}}{1-\tilde{r}_1 r_2 e^{i\delta_0}} \left[\left(\frac{\tilde{r}_1(r_2-1)}{n_s+n}+\frac{r_2(\tilde{r}_1-1)}{n_0+n}-2\, i\, q_o\, h\, \tilde{r}_1 r_2\right)\Delta+\frac{\tilde{r}_1(r_2+1)\Delta_s}{n_s+n}\right]. \tag{7.50}$$

where δ_o is defined as given by equation 7.39. $\tilde{r}_1$ and r_2 are the reflection coefficients inside the film as shown in figure 7.6 and defined by the following equations:

$$\tilde{r}_1=\frac{n-n_0}{n+n_0}, \qquad r_2=\frac{n-n_s}{n+n_s}. \tag{7.51}$$

By multiplying equations 7.49, 7.37 and 7.50 with some algebra which include taking the common factors and ignoring both $\Delta\Delta_s$ terms and higher orders in Δ and Δ_s, we get:

$$\frac{E_0^{t-}}{E_0^{t+}}=\frac{t_1^-\, t_2^- e^{i\delta^-/2}\left(1-\tilde{r}_1^+ r_2^+ e^{i\delta^+}\right)}{t_1^+\, t_2^+\, e^{i\delta^+/2}(1-\tilde{r}_1^- r_2^- e^{i\delta^-})} \approx 1+2\,\Delta\left[2\left(\frac{1}{n_0+n}+\frac{1}{n_s+n}-\frac{1}{n}\right)-i\, q_o h + \frac{e^{i\delta_0}}{1-\tilde{r}_1 r_2 e^{i\delta_0}}\left(\frac{\tilde{r}_1(r_2-1)}{n_s+n}+\frac{r_2(\tilde{r}_1-1)}{n_0+n}-2\, i\, q_o\, h\, \tilde{r}_1 r_2\right)\right] + 2\,\Delta_s\left[\frac{1}{n_s+n}+\frac{e^{i\delta_0}}{1-\tilde{r}_1 r_2 e^{i\delta_0}}\left(\frac{\tilde{r}_1(r_2+1)}{n_s+n}\right)\right]. \tag{7.52}$$

By using equation 7.48 and 7.52 then taking the imaginary part as explained above, we find:

$$\psi_{Appx} = \mathrm{Im}\left[\left(\frac{e^{i\delta_0}}{1-\tilde{r}_1 r_2 e^{i\delta_0}}\left(\frac{\tilde{r}_1(r_2-1)}{n_s+n}+\frac{r_2(\tilde{r}_1-1)}{n_0+n}-2\,i\,q_o\,h\,\tilde{r}_1 r_2\right)\right.\right.$$
$$\left.\left.-\,i\,q_o h\right)\Delta+\frac{e^{i\delta_0}\,\Delta_s}{1-\tilde{r}_1 r_2 e^{i\delta_0}}\left(\frac{\tilde{r}_1(r_2+1)}{n_s+n}\right)\right]. \tag{7.53}$$

Then the approximate formula of Faraday rotation is given by the following equation:

$$\psi_{Appx} = \frac{-\Delta}{\left(1-\sqrt{\widetilde{\mathrm{R}}_1\mathrm{R}_2}\right)^2\left(1+\frac{4\sqrt{\widetilde{\mathrm{R}}_1\mathrm{R}_2}}{\left(1-\sqrt{\widetilde{\mathrm{R}}_1\mathrm{R}_2}\right)^2}\sin^2\frac{\delta_o}{2}\right)}\left[\frac{\sqrt{\mathrm{R}_2}\left(1-\sqrt{\widetilde{\mathrm{R}}_1}\right)}{(n_0+n)}\sin\,\delta_o\right.$$
$$\left.+\,2\sqrt{\widetilde{\mathrm{R}}_1\mathrm{R}_2}\,\left(\cos\,\delta_o-\sqrt{\widetilde{\mathrm{R}}_1\mathrm{R}_2}\right)\,q_0\,h\right]-\,q_o h\,\Delta$$
$$-\frac{\sqrt{\widetilde{\mathrm{R}}_1}\,\left[\left(1-\sqrt{\mathrm{R}_2}\right)\Delta-\left(1+\sqrt{\mathrm{R}_2}\right)\Delta_s\right]\sin\,\delta_o}{(n_s+n)\,\left(1-\sqrt{\widetilde{\mathrm{R}}_1\mathrm{R}_2}\right)^2\left(1+\frac{4\sqrt{\widetilde{\mathrm{R}}_1\mathrm{R}_2}}{\left(1-\sqrt{\widetilde{\mathrm{R}}_1\mathrm{R}_2}\right)^2}\sin^2\frac{\delta_o}{2}\right)}. \tag{7.54}$$

Where $\tilde{R}_1$ and R_2 are the reflectivities inside the film and defined by $\tilde{R}_1 = |\tilde{r}_1|^2$ and $R_2 = |r_2|^2$. In this equation, $\frac{4\sqrt{\widetilde{\mathrm{R}}_1\mathrm{R}_2}}{\left(1-\sqrt{\widetilde{\mathrm{R}}_1\mathrm{R}_2}\right)^2}$ represents the finesse coefficient, *FC*, in a general case. $q_o h\,\Delta$ is the contribution of Faraday rotation from the first pass of light in the film. The other terms result from multiple passes through the film. It should be pointed out in a special case; air as substrate leads to $\Delta_s = 0$, $n_s = n_0$ and $\tilde{R}_1 = R_2 = \widetilde{\mathrm{R}}$. Hence equation 7.54 returns back to equation 7.43. On resonance equation 7.54 becomes:

$$\psi_{Res} = -2\,q_0\,h\,\frac{\sqrt{\widetilde{\mathrm{R}}_1\mathrm{R}_2}}{(1-\sqrt{\widetilde{\mathrm{R}}_1\mathrm{R}_2})}\,\Delta-\,q_o h\,\Delta, \tag{7.55}$$

It should be pointed out the calculations here were made to find the Faraday rotation contribution from the film only. This is what are trying to compare to the difference between the substrate alone and the whole structure. In other words, the calculations did not include the rotation going through the substrate or at the substrate-air interface. To find the total Faraday rotation for the whole structure, those last two rotations must be added to equation 7.55.

7.6 Results and Discussion

The Faraday rotation of the thin film, $EuFeO_3$, on a circularly birefringent substrate, $Bi{:}YIG$, was calculated using the exact analytical formula (see equation 7.33 and 7.45). This result corresponds to the difference between the Faraday rotation of the whole structure and that of the substrate alone and agrees exactly with 'difference' curve, see figure 7.7.

As in section 7.4, the Faraday rotation was also calculated using approximate analytical formula (equation 7.54) and at $\varepsilon_{xy} \approx 0.011$ (the real used value). Excellent agreements were found between the Faraday rotation calculated using the exact analytical formula and the rotation calculated from using the approximate analytical formula. Clearly, those agreements demonstrated the approximate formula is good for any realistic material.

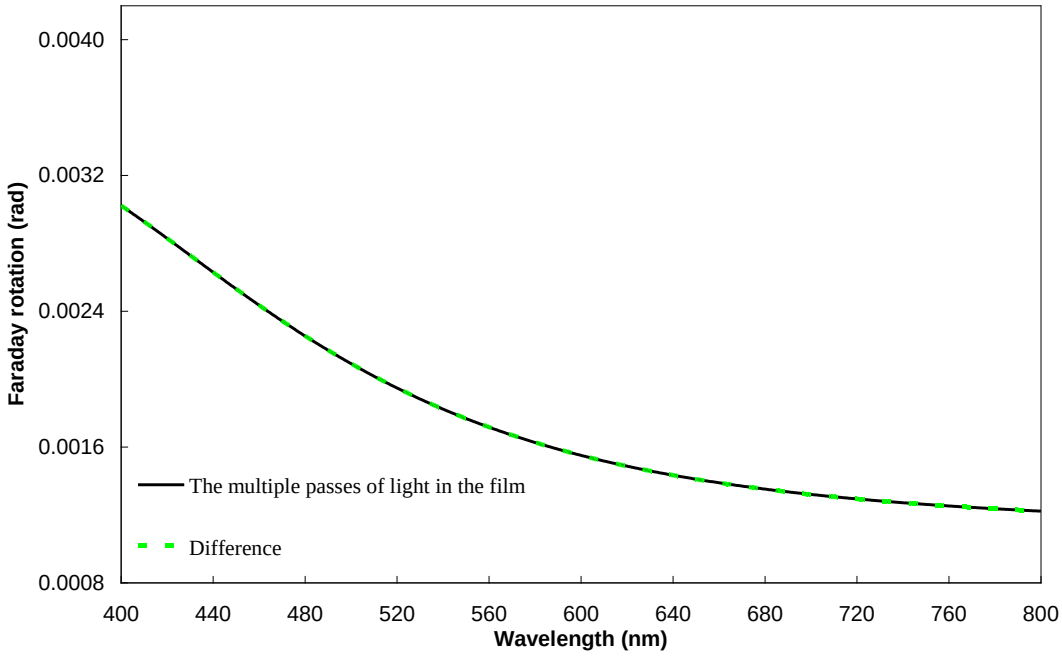

Figure7.7: The exact, approximate analytical Faraday rotation results and the numerical result, for a thin film, $EuFeO_3$ on a circularly birefringent substrate and has the multiple passes, are shown by the black curve. The difference between the spectra of the whole structure and substrate alone is shown by the green curve.

7.7 Faraday rotation theory of a circularly birefringent cavity

In section 7.5, an analytical Faraday rotation formula was deduced for a simple circularly birefringent film deposited on circularly birefringent substrate. The film had different media on both sides. In this section, to deduce a more general formula for the Faraday rotation, the following structure will be investigated. The structure consists of a circularly birefringent cavity which has quarter-wave stacks, Bragg mirrors, on each side of the cavity. This structure is placed on a transparent isotropic substrate as shown in figure 7.8.

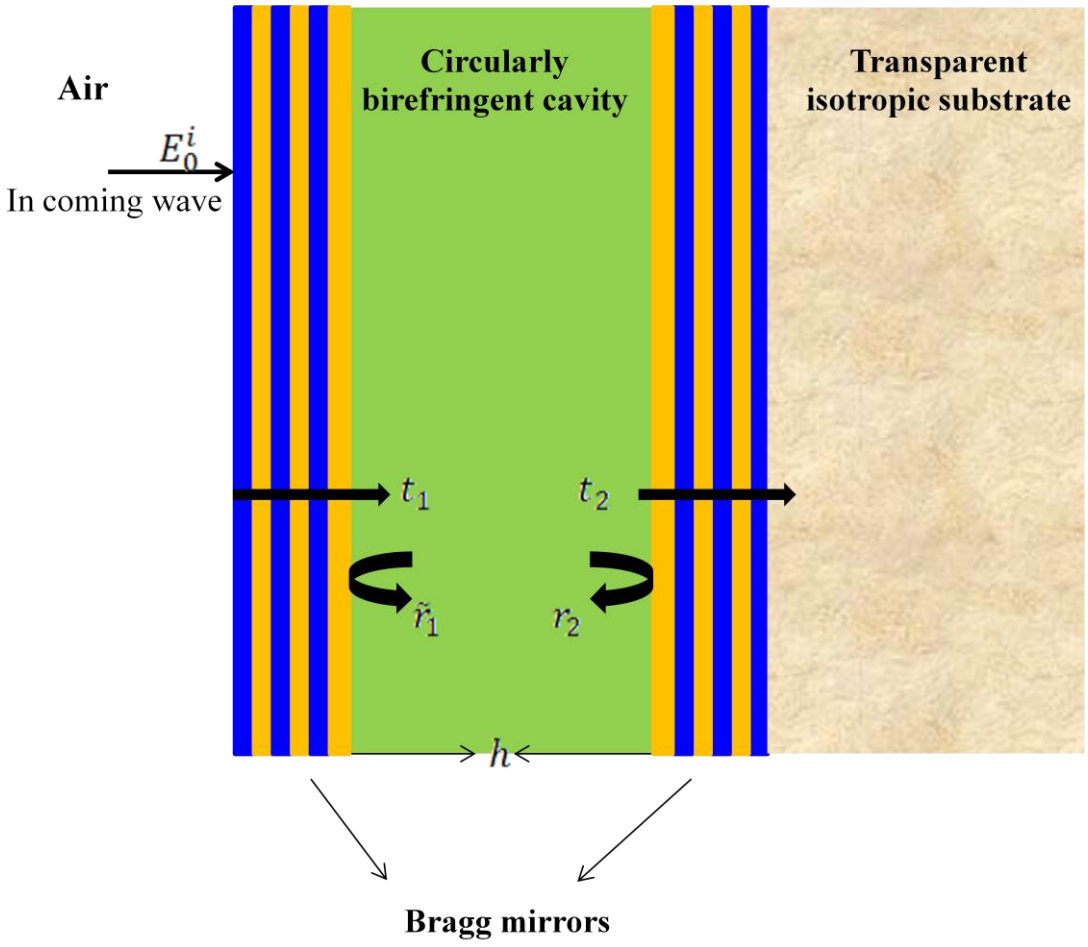

Figure7.8: Schematic diagram of a circularly birefringent cavity structure on a transparent isotropic substrate. Here, *h* is the cavity thickness.

7.7.1 Exact formula of Faraday rotation

In this section, a circularly birefringent cavity structure will be considered. The structure consists of a circularly birefringent cavity with an average refractive index *n* and a thickness *h*. The structure also has quarter-wave stacks, Bragg mirrors, on each side of the cavity. Further, it is placed on a transparent isotropic substrate as depicted in figure 7.8. We consider a beam of light incident on a cavity structure at a normal direction. As seen above, the transmitted amplitudes of the cavity are given by equation 7.45. As a consequence of the Bragg mirrors in this structure, the T-matrix matrix is used to calculate $t_{1,2}^{\pm}$, $\tilde{r}_1^{\pm}$ and $r_2^{\pm}$ instead of Fresnel's equations. By recalling the reflectivity and transmission coefficients from Chapter 4 as calculated by equations 4.22 and 4. 23, we get:

$$
\begin{aligned}
t_1^{\pm} &= \frac{2n_o\,(m_{11}^{(1)}m_{22}^{(1)} - m_{12}^{(1)}m_{21}^{(1)})}{n^{\pm}m_{11}^{(1)} - n^{\pm}\,n_o m_{12}^{(1)} - m_{21}^{(1)} + n_o m_{22}^{(1)}},\\
\tilde{r}_1^{\pm} &= \frac{-n_o\tilde{m}_{11}^{(1)} - n_o n^{\pm}\,\tilde{m}_{12}^{(1)} + \tilde{m}_{21}^{(1)} + n^{\pm}\tilde{m}_{22}^{(1)}}{n_o\tilde{m}_{11}^{(1)} - n_o n^{\pm}\,\tilde{m}_{12}^{(1)} - \tilde{m}_{21}^{(1)} + n^{\pm}\tilde{m}_{22}^{(1)}},\\
t_2^{\pm} &= \frac{2n^{\pm}\,(m_{11}^{(2)}m_{22}^{(2)} - m_{12}^{(2)}m_{21}^{(2)})}{n_s m_{11}^{(2)} - n^{\pm}\,n_s m_{12}^{(2)} - m_{21}^{(2)} + n^{\pm}m_{22}^{(2)}},\\
r_2^{\pm} &= \frac{-n_s m_{11}^{(2)} - n^{\pm}\,n_s m_{12}^{(2)} + m_{21}^{(2)} + n^{\pm}m_{22}^{(2)}}{n_s m_{11}^{(2)} - n^{\pm}\,n_s m_{12}^{(2)} - m_{21}^{(2)} + n^{\pm}m_{22}^{(2)}},
\end{aligned}
\tag{7.56}
$$

where the subscript indices of *m* and $\tilde{m}$ refer to the matrix elements. $m^{(1),(2)}$ are the matrix elements for forward propagation direction through the first and second Bragg mirrors, respectively. $\tilde{m}^{(1)}$ is the matrix element for reversed propagation direction

through the first Bragg mirror. Then, the Faraday rotation, ψ, of cavity structure can be obtained exactly using equation 7.45 and rotation definition is given by equation 7.33.

7.7.2 Approximate formula of Faraday rotation

Starting from equation 7.48, using equation 7.56, and following the same procedure discussed previously, gives:

$$\frac{t_1^- \, t_2^-}{t_1^+ \, t_2^+} \approx 1 + 2\,\Delta \left(\frac{1}{n + \dfrac{n_o m_{22}^{(1)} - m_{21}^{(1)}}{m_{11}^{(1)} - n_o m_{12}^{(1)}}} + \frac{1}{n + \dfrac{n_s m_{11}^{(2)} - m_{21}^{(2)}}{m_{22}^{(2)} - n_s m_{12}^{(2)}}} - \frac{1}{n} \right). \tag{7.57}$$

$$\frac{1 - \tilde{r}_1^+ \, r_2^+ \, e^{i\delta^+}}{1 - \tilde{r}_1^- r_2^- \, e^{i\delta^-}} \approx 1 - \frac{2\Delta \, e^{i\delta_0}}{1 - \tilde{r}_{\,1} \, r_2 e^{i\delta_0}} \left[\frac{-\tilde{r}_1 \, (r_2 - 1) \left(m_{22}^{(2)} - n_s m_{12}^{(2)} \right)}{n_s m_{11}^{(2)} - n_s n \, m_{12}^{(2)} - m_{21}^{(2)} + n \, m_{22}^{(2)}} \right. \tag{7.58}$$

$$\left. \frac{-r_2 \;\; (\tilde{r}_1 - 1) \left(\tilde{m}_{22}^{(1)} - n_o \tilde{m}_{12}^{(1)} \right)}{n_o \tilde{m}_{11}^{(1)} - n_o n \, \tilde{m}_{12}^{(1)} - \tilde{m}_{21}^{(1)} + n \, \tilde{m}_{22}^{(1)}} + \; 2 \, i \;\; q_o \, h \, \tilde{r}_1 r_2 \right],$$

where δ_o is given by equation 7.39. $\tilde{r}_1$ and r_2 are defined for a non-circularly birefringent cavity with refractive index n by the following equations:

$$\tilde{r}_1 = \frac{-n_o \tilde{m}_{11}^{(1)} - n_o n \, \tilde{m}_{12}^{(1)} + \tilde{m}_{21}^{(1)} + n \, \tilde{m}_{22}^{(1)}}{n_o \tilde{m}_{11}^{(1)} - n_o n \, \tilde{m}_{12}^{(1)} - \tilde{m}_{21}^{(1)} + n \, \tilde{m}_{22}^{(1)}},$$

$$r_2 = \frac{-n_s m_{11}^{(2)} - n_s n \, m_{12}^{(2)} + m_{21}^{(2)} + n \, m_{22}^{(2)}}{n_s m_{11}^{(2)} - n_s n \, m_{12}^{(2)} - m_{21}^{(2)} + n \, m_{22}^{(2)}}, \tag{7.59}$$

Here $\tilde{r}_1$ and r_2 are complex numbers because the T-matrix is a complex matrix as noted in Chapter 4. As above, $\frac{e^{i\delta^-/2}}{e^{i\delta^+/2}}$ is given by equation 7.37. Multiplying equations 7.57, 7.37 and 7.58 gives a complex number. The imaginary part of this complex number is not a simple expression, as in the above calculations. Hence, we leave the approximate formula of Faraday rotation as:

$$\psi_{Appx} = \frac{1}{2}\mathrm{Im}\left\{1 + 2\,\Delta\left[\left(\frac{1}{n + \frac{n_o m_{22}^{(1)} - m_{21}^{(1)}}{m_{11}^{(1)} - n_o m_{12}^{(1)}}} + \frac{1}{n + \frac{n_s m_{11}^{(2)} - m_{21}^{(2)}}{m_{22}^{(2)} - n_s m_{12}^{(2)}}} - \frac{1}{n}\right) - i\,q_o h\right.\right.$$

$$+ \frac{e^{i\delta_0}}{1 - r_1 r_2 e^{i\delta_0}}\left(\frac{\tilde{r}_1\,(r_2 - 1)\left(m_{22}^{(2)} - n_s m_{12}^{(2)}\right)}{n_s m_{11}^{(2)} - n_s n\, m_{12}^{(2)} - m_{21}^{(2)} + n\, m_{22}^{(2)}}\right. \qquad (7.60)$$

$$\left.\left.\left. + \frac{r_2\ (\tilde{r}_1 - 1)\left(\widetilde{m}_{22}^{(1)} - n_o \widetilde{m}_{12}^{(1)}\right)}{n_o \widetilde{m}_{11}^{(1)} - n_o n\, \widetilde{m}_{12}^{(1)} - \widetilde{m}_{21}^{(1)} + n\, \widetilde{m}_{22}^{(1)}} - 2\,i\ q_o\, h\, \tilde{r}_1 r_2\right)\right]\right\}.$$

However, the study of Faraday rotation on the resonance is an interesting case as will be seen. We assume the mirrors and cavity have the same resonance condition and the mirrors are identical. Applying the resonance condition in the cavity, which means $\frac{\delta_o}{2} = m\,\pi$, leads to $e^{i\delta_0} = 1$. In addition, substituting the wavelength, λ, from equation 1.1, *i.e.*, $\lambda = 4\,n_l h_l$ into $q_l = 2\,\pi\,n_l/\lambda$ gives a resonance condition in Bragg mirrors, $q_l h_l = \pi/2$, where h_l, n_l and q_l are the thickness, the refractive index and the wave-vector value of the layer *l*. Then, applying this resonance condition in the Bragg

mirrors leads to $\cos q_l h_l = 0$ and $\sin q_l h_l = 1$. According to that, the T-matrix in equation 4.21 for the first layer, $l = 1$, becomes:

$$M = \begin{pmatrix} 0 & \frac{i}{n_1} \\ i\ n_1 & 0 \end{pmatrix}. \tag{7.61}$$

So, for $\mathbb{N}$ bilayers the T-matrix can be expressed for the first Bragg mirrors as follows:

$$M^{(1)} = \begin{pmatrix} \left(\frac{-n_1}{n_2}\right)^{\mathbb{N}} & 0 \\ 0 & \left(\frac{-n_2}{n_1}\right)^{\mathbb{N}} \end{pmatrix}, \tag{7.62}$$

For the reverse of first Bragg mirrors and the second Bragg mirrors as:

$$\widetilde{M}^{(1)} = M^{(2)} = \begin{pmatrix} \left(\frac{-n_2}{n_1}\right)^{\mathbb{N}} & 0 \\ 0 & \left(\frac{-n_1}{n_2}\right)^{\mathbb{N}} \end{pmatrix}. \tag{7.63}$$

Clearly, the elements of the last two matrices are now real if there is no absorption, as in our case. Substituting these matrices elements in the expressions for $\tilde{r}_1$ and r_2, equation 7.59, gives:

$$\begin{aligned} \tilde{r}_1 &= \frac{n\,(n_1)^{2\,\mathbb{N}} - n_0 (n_2)^{2\,\mathbb{N}}}{n\,(n_1)^{2\,\mathbb{N}} + n_0 (n_2)^{2\,\mathbb{N}}} \\ r_2 &= \frac{n\,(n_1)^{2\,\mathbb{N}} - n_s (n_2)^{2\,\mathbb{N}}}{n\,(n_1)^{2\,\mathbb{N}} + n_s (n_2)^{2\,\mathbb{N}}} \end{aligned} \tag{7.64}$$

Finally, the approximate formula of Faraday rotation on the resonance is given by the following expression:

$$\psi_{Res} = -2\, q_0\, h\, \Delta \frac{\tilde{r}_1\, r_2}{1 - \tilde{r}_1\, r_2} - \, q_o h\, \Delta, \tag{7.65}$$

since $\tilde{r}_1$ and r_2 are real, this has the same form as equation 7.55.

7.8 Results and Discussion

A cavity structure $(Ta_2O_5/SiO_2)^6\ /Bi{:}YIG/(SiO_2/Ta_2O_5)^6$ was taken from Kato *et al.*,(2003). This structure consists of a circularly birefringent thin film, $Bi{:}YIG$, with dielectric Bragg mirrors, on each side of the film. Ignoring absorption, the parameters of the film, the parameters of dielectric layers and the refractive index of glass substrate were taken from Kato *et al.*,(2003) as the following: for $Bi{:}YIG$, $\varepsilon_{xx} = 5.59$; $\varepsilon_{xy} = -0.00369$; at $\lambda = 720\, nm$ and its thickness was equal to $\lambda/2\sqrt{\varepsilon_{xx}}$. The refractive indices for the isotropic materials were taken as $n_1 = n_{Ta_2O_5} = 2.18$, and $n_2 = n_{SiO_2} = 1.47$ for Ta_2O_5 and for SiO_2 dielectric layers, respectively at $\lambda = 720\, nm$ and their thicknesses were equal to $\lambda/4n_{1,2}$. The refractive index of the glass substrate was $n_s = 1.52$. The Faraday rotation of this cavity structure was calculated using the exact and approximate analytical formula as shown by one curve only (the black curve) in figure 7.9, because they are indistinguishable on this scale. So, the approximate formula worked well.

The resonance occurred at wavelength $\lambda \approx 720\, nm$ as can be seen by the red point in figure7.9. From the comparison, this wavelength agrees with the resonance wavelength for the cavity structure given by Kato *et al.*,(2003). However, we obtained a different Faraday rotation value as that found by Kato *et al.*,(2003). This result may be explained as absorption in the structure was neglected in this work.

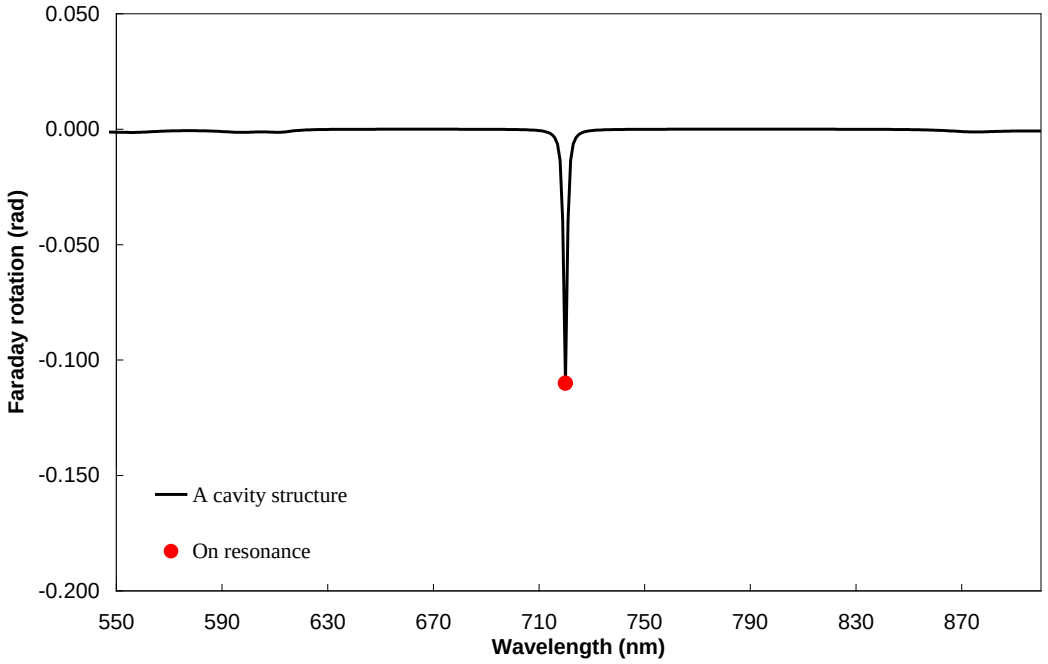

Figure7.9: Numerical spectrum and analytical Faraday rotation spectra for a cavity structure $(Ta_2O_5/SiO_2)^6\ /Bi{:}YIG/(SiO_2/Ta_2O_5)^6$ are shown by the same black curve. The red point indicates Faraday rotation on resonance.

7.9 Conclusions

Total reflectivity and transmission were calculated for a circularly birefringent film deposited on a thick circularly birefringent substrate. In addition, a formula for Faraday rotation was derived exactly and approximately for different situations: a single circularly birefringent film with air on both sides; the film on a circularly birefringent substrate; and a circularly birefringent cavity structure. The results of this analytical study show that the approximate formulae worked excellently for any realistic material. These analytical formulae enhance our numerical calculations. The measure of the effective number of double passes based on the Faraday rotation was found. We can use

the Faraday rotation as o'clock, which accounts how much time photons spent in the film. Because we can get from the Faraday rotation, the effective distance (*i.e.*, number of passes multiplies by the actual thickness of the material) and then divide this effective distance by the speed of the medium to find the time. In general, it seems that the value of Faraday rotation on resonance could be found straightforwardly. Returning to the question posed at the beginning of this chapter, regarding the difference between the Faraday rotation of the whole structure and that of the substrate alone, we have given a formula for the difference, but it is not the simple rotation for the film, because of multiple reflections in the film.

CHAPTER 8

CONCLUSIONS

8.1 Summary

In the field of photonic nanostructures, computational techniques are required in a number of problems. These include photonic band analysis, calculation of reflection or transmission spectra, and emission spectra. Moreover, the problems can be handled by computer methods using the experimental data. The knowledge of various properties of the structure enables us to understand it, since the spectra of the structure are found to be one of the important sources. From the magneto-optical spectra, the value of dielectric constants can be obtained.

This thesis describes theoretical modelling of magneto-photonic structures using the transfer matrix, which is developed here for circularly birefringent materials. The work is useful in analysing real experimental magneto-optic data, and in the creation of novel structures which make use of the sensitivities of the optical properties of photonic crystals to minute differences in the refractive indices.

We started from Maxwell's equations to derive the 4×4 transfer matrix for circularly birefringent structures. The matrix was used to compute optical and magneto-optical properties at normal incidence of light for a structure on an infinite thickness substrate. We modelled both a simple circularly birefringent film and a circularly birefringent cavity structure. This work has confirmed previous studies showing that the cavity structure enhanced magneto-optical effects.

We next considered the effects of incoherent reflections within a finite thickness substrate. The incoherent reflections can arise for a number of reasons, for example, a slight wedge in the substrate or the finite angular resolution of measurements. We first investigated the effect of inclusion multiple incoherent back reflections within an isotropic transparent substrate. The results showed a significant contribution of these reflections to the magneto-optical Kerr rotation from a thin film. Since the measurements of this sort are used to obtain the values of magneto-optical constants of the material, it is important that the incoherent reflections are taken into account in analysing the experiments.

The present investigation found that both Sato's definition and the definition in terms of Stokes' parameters gave the same Kerr ellipticity result for both coherent and incoherent back reflections situations for a small magneto-optical constant. However, for a large magneto-optical constant the Kerr ellipticity resulting from these definitions was not the same. With either a small or large value of magneto-optical constant, the Kerr rotation results were the same from the definitions of Sato's (1981) or Sakaguchi and Sugimoto's (1999) or the definition in terms of Stokes' parameters in the case of ignoring the incoherent back reflections. On the other hand, when incoherent back reflections are included, the definition of rotation in terms of Stokes' parameters is the only way to proceed, since other definitions depend on phase information. In general, therefore, it seems that the definition of magneto-optical effects in terms of Stokes' parameters is the only one, which is universally applicable.

The total reflectivity and transmission expressions were also found for a circularly birefringent film deposited on a thick circularly birefringent substrate. We

also gave a formula for the difference between the Faraday rotation of the whole structure and that of the substrate alone. As a result of multiple reflections, this does not display the simple Faraday rotation of the film that has air on both sides.

Exact and approximate analytical formulae for the Faraday rotation were derived for several different cases: first, a single circularly birefringent film with air on both sides; second, a film on a circularly birefringent substrate; and finally a circularly birefringent cavity structure. The results show that the approximate formulae derived for a small ε_{xy}, work well in any real medium. The analytical results agree with our numerical calculations. The approximate formulae were used to derive an expression for the effective number of light passes through the film.

We used our model to re-analyse Sato's modulation method for determining magneto-optical spectra. Our study showed that the expressions given by Sato still work in the presence of incoherent back reflections

8.1 Outlook to the Future

This work might be extended in the following points:

Within the current framework, it would be straightforward to add absorption; we did not do it here for simplicity and because the effects are strongest without absorption.

The code is written so it would be easy to change from simple circular birefringent materials to those which are linearly birefringent or mixture of the two by changing the eigenvector components to appropriate one for the material used.

Some changes will be needed for the treatment of the circularly birefringent materials when the light is incident at a finite angle (non-normal incidence), for example, a wave vectors need to be changed.

This work could provide basis for modifying treatments of two- and three-dimensional photonic structures.

APPENDIX A

Both rotation definitions of Sato (1981) and Sakaguchi and Sugimoto (1999) are, in fact, identical, as is proven analytically here

We start from the trigonometric identity for $\tan\Delta\theta$. This is given as:

$$\tan\Delta\theta = \tan(\theta_+ - \theta_-) = \frac{\tan\theta_+ - \tan\theta_-}{1 + \tan\theta_+ \tan\theta_-}, \tag{A.1}$$

Substituting $\tan\theta_\pm$ from the complex reflectivity coefficients give:

$$\tan\theta_\pm = \frac{\mathrm{Im}(r_{\pm\pm})}{\mathrm{Re}(r_{\pm\pm})}, \tag{A.2}$$

Then, by applying the relationships for circular birefringent structures between r_{++}, r_{--}, and $r_{xx,}r_{xy,}$ *i.e.*, equations 4.46, 49 and it can be shown that:

$$\psi = -\frac{1}{2}\Delta\theta = \frac{1}{2}\tan^{-1}\left(\frac{2\ \mathrm{Re}\left(\frac{r_{xy}}{r_{xx}}\right)}{1 - \left[\frac{r_{xy}}{r_{xx}}\right]^2}\right). \tag{A.3}$$

REFRENCES

Akahane, Y., Asano, T., Song, B.S., and Noda, S. (2003a). 'High-Q Photonic Nanocavity in A Two-Dimensional Photonic Crystal'. *Nature* **425**, 944-947.

Akahane, Y., Asano, T., Song, B.S., and Noda, S. (2003b). 'Investigation of High-Q Channel Drop Filters Using Donor-Type Defects in Two-Dimensional Photonic Crystal Slabs'. *Applied Physics Letters* **83**, 1512-1514.

Akahane, Y., Asano, T., Song, B.S., and Noda, S. (2005). 'Fine-Tuned High-Q Photonic-Crystal Nanocavity'. *Optics Express* **13**, 1202-1214.

Astratov, V.N., Stevenson, R.M., Culshaw, I.S., Whittaker, D.M., Skolnick, M.S., Krauss, T.F., and De La Rue, R.M. (2000a). 'Heavy Photon Dispersions in Photonic Crystal Waveguides'. *Applied Physics Letters* **77**, 178-180.

Astratov, V.N., Stevenson, R.M., Culshaw, I.S., Whittaker, D.M., Skolnick, M.S., Krauss, T.F., and De la Rue, R.M. (2000b). 'Reflectivity Studies of Photonic Band Structure Effects in Two-Dimensional Air/Semiconductor Lattices'. *Physica Status Solidi a-Applied Research* **178**, 565-569.

Berenger, J.P. (1994). 'A perfectly Matched Layer for The Absorption of Electromagnetic-Waves'. *Journal of Computational Physics* **114**, 185-200.

Berreman, D.W. (1972). 'Optics in Stratified and Anisotropic Media - 4X4-Matrix Formulation'. *Journal of the Optical Society of America* **62**, 502-510.

Born, M., and Wolf, E. (1999). 'Principles of optics : Electromagnetic Theory of Propagation, Interference and Diffraction of Light ', 7th, expanded edition, Cambridge University Press, Cambridge.

Chen, S., and Li, X. (2003). The Application of Multiple Scattering Theory (Mst) In Calculating The Deuterium Flux Permeating The Pd Thin Film. In in Tenth International Conference on Cold Fusion Cambridge, MA: LENR-CANRorg This paper was presented at the 10th International Conference on Cold Fusion It may be different from the version published by World Scientific, Inc (2003) in the official Proceedings of the conference, http://wwwlenr-canrorg/acrobat/ChenStheapplicapdf , accessed on 19/09/2013.

Daraei, A., Tahraoui, A., Sanvitto, D., Timpson, J.A., Fry, P.W., Hopkinson, M., Guimaraes, P.S.S., Vinck, H., Whittaker, D.M., Skolnick, M.S., *et al.* (2006). 'Control of Polarized Single Quantum Dot Emission in High-Quality-Factor Microcavity Pillars'. *Applied Physics Letters* **88**, 0511131-0511133.

Dong, L., Jiang, H., Chen, H., and Shi, Y. (2010). 'Enhancement of Faraday rotation effect in heterostructures with magneto-optical metals'. *Journal of Applied Physics* **107**, 093101.

Fan, S.H., Johnson, S.G., Joannopoulos, J.D., Manolatou, C., and Haus, H.A. (2001). 'Waveguide Branches in Photonic Crystals'. *Journal of the Optical Society of America B-Optical Physics* **18**, 162-165.

Finazzi, M., Duo, L., and Ciccacci, F. (2009). 'Magnetic properties of interfaces and multilayers based on thin antiferromagnetic oxide films'. *Surface Science Reports* **64**, 139-167.

Gao, X., Woollam, J.A., Kirby, R.D., Sellmyer, D.J., Tanaka, C.T., Nowak, J., and Moodera, J.S. (1999). 'Dielectric tensor for magneto-optic NiMnSb'. *Physical Review B* **59**, 9965-9971.

Gedney, S.D. (1996). 'An Anisotropic Perfectly Matched Layer- Absorbing Medium for the Truncation of FDTD Lattices '. *IEEE Transactions on Antennas and Propagation* **44**, 1630-1639.

Gérard, J.M., Sermage, B., Gayral, B., Legrand, B., Costard, E., and Thierry-Mieg, V. (1998). 'Enhanced Spontaneous Emission by Quantum Boxes in a Monolithic Optical Microcavity'. *Physical Review Letters* **81**, 1110-1113.

Hamrle, J., Blomeier, S., Gaier, O., Hillebrands, B., Schneider, H., Jakob, G., Postava, K., and Felser, C. (2007). 'Huge Quadratic Magneto-Optical Kerr Effect and Magnetization Reversal in the Co2FeSi Heusler Compound'. *Journal of Physics D-Applied Physics* **40**, 1563-1569.

Harbecke, B. (1986). 'Coherent and Incoherent Reflection and Transmission of Multilayer Structures '. *Applied Physics B-Photophysics and Laser Chemistry* **39**, 165-170.

Hecht, E. (2002). 'Optics', 4th; International edition, Addison-Wesley, San Francisco

Inoue, M., Uchida, H., Nishimura, K., and Lim, P.B. (2006). 'Magnetophotonic Crystals - A novel Magneto-Optic Material with Artificial Periodic Structures'. *Journal of Materials Chemistry* **16**, 678-684.

Joannopoulos, J.D., John, S.G., Winn, J.N., and Meade, R.D. (2008). 'Photonic Crystals : Molding the Flow of Light ', Second edition, Princeton University Press, Princeton

Joannopoulos, J.D., Villeneuve, P.R., and Fan, S.H. (1997). 'Photonic crystals: Putting A New Twist on Light'. *Nature* **386**, 143-149.

John, S. (1987). 'Strong Localization of Photons in Certain Disordered Dielectric SuperlattIices'. *Physical Review Letters* **58**, 2486-2489.

Johnson, S.G., and Joannopoulos, J.D. (2002). 'Photonic crystals : The Road from Theory to Practice', Kluwer Academic Publishers, Boston.

Johnson, S.G., and Joannopoulos, J.D. (2003). Introduction to Photonic Crystals: Bloch's Theorem, Band Diagrams, and Gaps (But No Defects), http://ab-initio.mit.edu/photons/tutorial/ ,accessed on 22/12/2009.

Johs, B., French, R.H., Kalk, F.D., McGahan, W.A., and Woollam, J.A. (1994). 'Optical Analysis of Complex Multilayer Structures Using Multiple Data Types ', Vol 2253.

Kahl, S., and Grishin, A.M. (2004). 'Enhanced Faraday rotation in all-garnet magneto-optical photonic crystal'. *Applied Physics Letters* **84**, 1438-1440.

Kahn, F.J., Pershan, P.S., and Remeika, J.P. (1969). 'Ultraviolet Magneto-Optical Properties of Single-Crystal Orthoferrites, Garnets, and Other Ferric Oxide Compounds'. *Physical Review* **186**, 891-918.

Kato, H., Matsushita, T., Takayama, A., Egawa, M., Nishimura, K., and Inoue, M. (2003). 'Theoretical Analysis of Optical and Magneto-Optical Properties of One-Dimensional Magnetophotonic Crystals'. *Journal of Applied Physics* **93**, 3906-3911.

Katsidis, C.C., and Siapkas, D.I. (2002). 'General Transfer-Matrix Method for Optical Multilayer Systems with Coherent, Partially Coherent, and Incoherent Interference'. *Applied Optics* **41**, 3978-3987.

Labilloy, D., Benisty, H., Weisbuch, C., Smith, C.J.M., Krauss, T.F., Houdr, eacute, R., and Oesterle, U. (1999). 'Finely Resolved Transmission Spectra and Band Structure of Two-Dimensional Photonic Crystals Using Emission from InAs Quantum Dots'. *Physical Review B* **59**, 1649.

Lekner, J. (1991). 'Reflection and Refraction by Uniaxial Crystals'. *Journal of Physics-Condensed Matter* **3**, 6121-6133.

Lin, S.Y., Chow, E., Hietala, V., Villeneuve, P.R., and Joannopoulos, J.D. (1998). 'Experimental Demonstration of Guiding and Bending of Electromagnetic Waves in a Photonic Crystal'. *Science* **282**, 274-276.

Lourtioz, J.-M., Benisty, H., Berger, V., Ge'rard, J.-M., Maystre, D., and Tchelnokov, A. (2008). 'Photonic Crystals: Towards Nanoscale Photonic Devices ', Second edition, Springer, Berlin

Mansuripur, M. (2009). 'Classical Optics and Its Applications ', Second edition edition, Cambridge University Pree, Cambridge.

McPhedran, R.C., Nicorovici, N.A., McKenzie, D.R., Rouse, G.W., Botten, L.C., Welch, V., Parker, A.R., Wohlgennant, M., and Vardeny, V. (2003). 'Structural Colours Through Photonic Crystals'. *Physica B-Condensed Matter* **338**, 182-185.

Mekis, A., Chen, J.C., Kurland, I., Fan, S.H., Villeneuve, P.R., and Joannopoulos, J.D. (1996). 'High Transmission Through Sharp Bends in Photonic Crystal Waveguides'. *Physical Review Letters* **77**, 3787-3790.

Novotny, L., and Hecht, B. (2006). 'Principles of Nano-Optics', first edition, Cambridge University Press, Cambridge.

Orfanidis, S.J. (2008). 'Electromagnetic Waves and Antennas ', http://www.ece.rutgers.edu/~orfanidi/ewa/ch04.pdf , accessed on 5/03/2012.

Palik, E.D. (1998). 'Handbook of Optical Constants of Solids', Academic Press an imprint of elsevier, San Diego, London.

Parker, A.R., McPhedran, R.C., McKenzie, D.R., Botten, L.C., and Nicorovici, N.A.P. (2001). 'Photonic Engineering - Aphrodite's Iridescence'. *Nature* **409**, 36-37.

Pedrotti, F.L., and Pedrotti, L.S. (1993). 'Introduction to Optics', Second edition, Prentice Hall, Englewood Cliffs, New Jersey.

Pershan, P.S. (1967). 'Magneto-Optical Effects'. *Journal of Applied Physics* **38**, 1482-1490.

Plum, E., Liu, X.X., Fedotov, V.A., Chen, Y., Tsai, D.P., and Zheludev, N.I. (2009). 'Metamaterials: optical activity without chirality'. *Phys Rev Lett* **102**, 113902.

Reim, W., and Schoenes, J. (1990). 'Ferromagnetic Materials: a hand Book on the Properties of Magnetically Ordered Substances: Magneto-optical spectroscopy of f-Electron systems', Vol 5, Elsevier Science Publishers B. V., edited by E. P. Wohlfarth and K. H. J. Buschow, North-Holland.

Robinson, C.C. (1963). 'Longitudinal Kerr Magneto-Optic Effect In Thin Films of Iron, Nickel, and Permalloy'. *Journal of the Optical Society of America* **53**, 681-687.

Sakaguchi, S., and Sugimoto, N. (1999). 'Multilayer films composed of periodic magneto-optical and dielectric layers for use as Faraday rotators'. *Optics Communications* **162**, 64-70.

Sanvitto, D., Daraei, A., Tahraoui, A., Hopkinson, M., Fry, P.W., Whittaker, D.M., and Skolnick, M.S. (2005). 'Observation of Ultrahigh Quality Factor in A Semiconductor Microcavity'. *Applied Physics Letters* **86**, 1911091-1911093.

Sato, K. (1981). 'Measurement of Magneto- optical Kerr Effect Using Piezo-birefringent Modulator'. *Japanese Journal of Applied Physics* **20**, 2403-2409.

Smith, F.G., King, T.A., and Wilkins, D. (2007). 'Optics and Photonics: An introduction ', Second edition, John Wiley & Sons,Ltd, England.

Smith, G.S. (1997). 'An Introduction to Classical electromagnetic Radiatiion
', Cambridge University Press, Cambridge.

Stokes, G.G. (1852). 'On the Composition and Resolution of Strams of Polarizd Light from Different Sources'. *Transaction/ Cambridg Philosophical Society* **9**, 399.

Suits, F. (1992). 'Poincaré Sphere Interpretation of Kerr-Effect Measurements Using a Photoelastic Modulator'. *Ieee Transactions on Magnetics* **28**, 2976-2978.

Suits, J.C. (1971). 'Magneto-Optical Rotation and Ellipticity Measurements with a Spining Analyzer'. *Review of Scientific Instruments* **42**, 19-22.

Swanepoel, R. (1983). 'Determination of The Thickness and Optical-Constants of Amorphous-Silcon'. *Journal of Physics E-Scientific Instruments* **16**, 1214-1222.

Tayeb, G., Gralak, B., and Enoch, S. (2003). 'Structural Colors in Nature and Butterfly-Wing Modeling'. *Optics and Photonics News* **14**, 438-443.

VanDrent, W.P., and Suzuki, T. (1997). 'Ultra-Violet Range Magneto-Optic Study of FCC-Co and Co/Pt Multilayers'. *Journal of Magnetism and Magnetic Materials* **175**, 53-62.

Villeneuve, P.R., Fan, S.H., and Joannopoulos, J.D. (1996). 'Microcavities in Photonic Crystals: Mode Symmetry, Tunability, and Coupling Efficiency'. *Physical Review B* **54**, 7837-7842.

Wang, S.Y., Zheng, W.M., Qian, D.L., Zhang, R.J., Zheng, Y.X., Zhou, S.M., Yang, Y.M., Li, B.Y., and Chen, L.Y. (1999). 'Study of the Kerr Effect of Co_xAg_{100-x} Granular Films'. *Journal of Applied Physics* **85**, 5121-5123.

Wang, X., Zhang, X.G., Yu, Q., and Harmon, B.N. (1993). 'Multiple-scattering theory for electromagnetic waves'. *Physical Review B* **47**, 4161.

Whittaker, D.M., and Culshaw, I.S. (1999). 'Scattering-Matrix Treatment of Patterned Multilayer Photonic Structures'. *Physical Review B* **60**, 2610-2618.

Whittaker, D.M., and Gehring, G.A. (2010). 'Role of Incoherent Substrate Reflections in Photonic Crystal Spectroscopy'. *arXiv:10123677v1 [PhysicsOptics]*, 1-8.

Yablonovitch, E. (1987). 'Inhibited Spontaneous Emission in Solids-State Physics and Electronics'. *Physical Review Letters* **58**, 2059-2062.

Yablonovitch, E. (2001). 'Photonic Crystals: Semiconductors of Light'. *Scientific American, Inc* **285**, 47-51, 54-45.

Yariv, A., and Yeh, P. (1977). 'Electromagnetic Proppagation in Periodic Stratified Media. 2. Birefringence, Phase Matching, and X-Ray Lasers'. *Journal of the Optical Society of America* **67**, 438-448.

Yee, K. (1966). 'Numerical Solution of Initial Boundary Value Problems Involving Maxwell's Equations in Isotropic Media'. *Antennas and Propagation, IEEE Transactions on* **14**, 302-307.

Yeh, P. (1979). 'Electromagnetic Propagation in Birefringent Layered Media .'. *Journal of the Optical Society of America* **69**, 742-756.

Yeh, P., Yariv, A., and Hong, C.S. (1977). 'Electromagnetic Proppagation in Periodic Stratified Media .1. General Theory'. *Journal of the Optical Society of America* **67**, 423-438.

Yonekura, J., Ikeda, M., and Baba, T. (1999). 'Analysis of Finite 2-D Photonic Crystals of Columns and Lightwave Devices Using The Scattering Matrix Method'. *Journal of Lightwave Technology* **17**, 1500-1508.

Zhang, W.Y., Chan, C.T., and Sheng, P. (2001). 'Multiple Scattering Theory and its Application to Photonic Band Gap Systems Consisting of Coated Spheres'. *Opt Express* **8**, 203-208.